Fatigue crack growth in Selective Laser Melted Ti-6Al-4V

What is the influence of an off-axis build direction

J. Michielssen

Technische Universiteit Delft

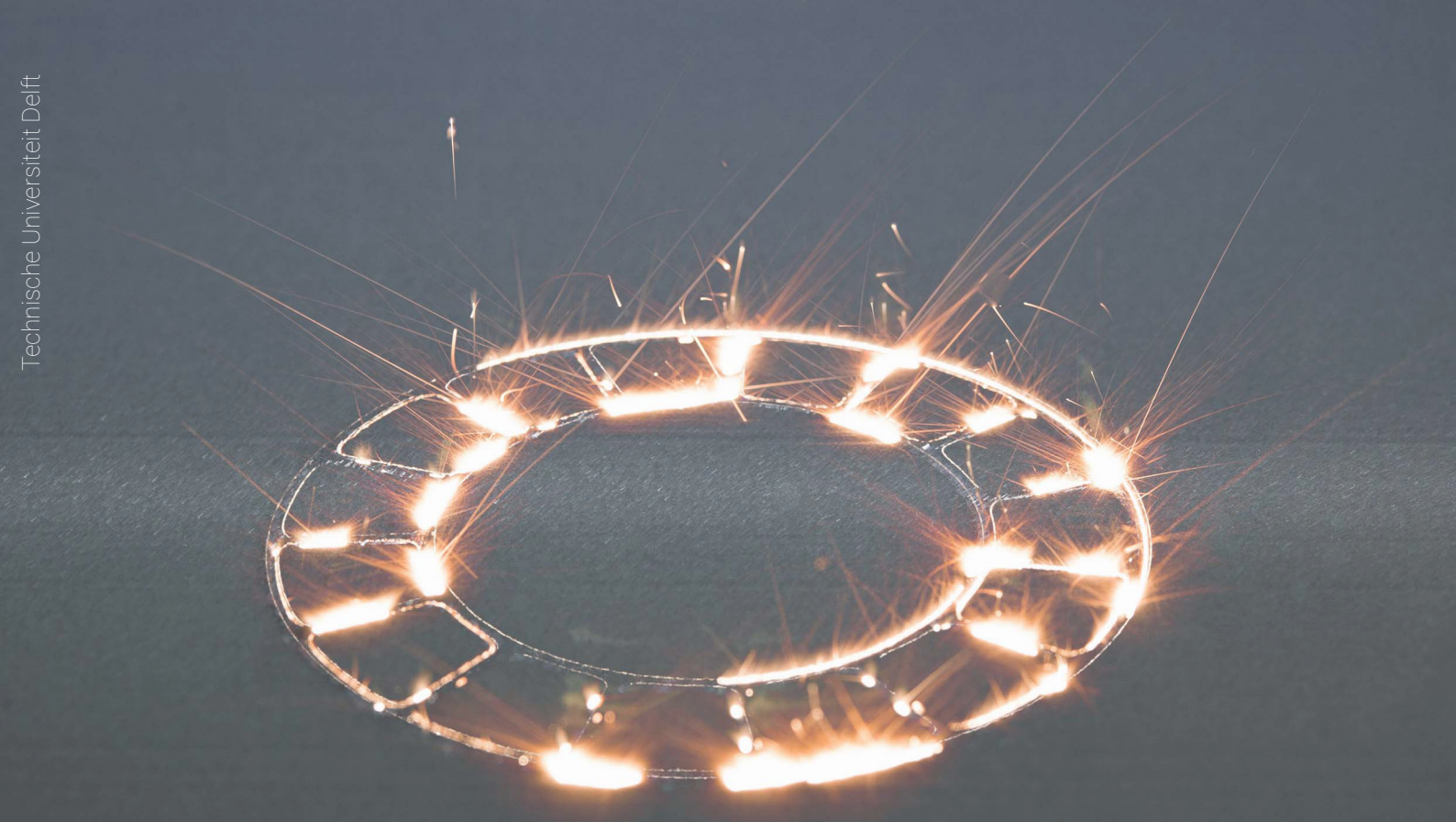

TU Delft

Fatigue crack growth in Selective Laser Melted Ti-6Al-4V

What is the influence of an off-axis build direction

by

J. Michielssen

to obtain the degree of Master of Science
at the Delft University of Technology,
to be publicly defended on Tuesday 21 February 2017 at 13:30.

Student number:	4111877	
Project duration:	4 April 2016 – 21 February 2017	
Thesis committee:	Dr. C. D. Rans,	TU Delft, supervisor
	Dr. ir. R. C. Alderliesten,	TU Delft
	Dr. ir. B. F. Lopes dos Santos,	TU Delft

TU Delft

Acknowledgements

With this thesis, I will end my career as a student in Delft. Seven years ago, moving from Belgium to the Netherlands did not seem as a large step in my life. Nevertheless, this turned out to a bit different. Being a student in Delft, changed my view and changed me into the person I am today. My student life in Delft has been the perfect combination of studying interesting and challenging subjects together with enjoying your time as a student and getting to know a lot of great people. Nevertheless, everything has an end as well as my time in Delft.

First of all, I would like to thank my supervisor, Calvin Rans, for the support and motivation provided throughout the entire thesis process. By discussing my results and showing me the bigger picture, Calvin found a way to keep me motivated to finish this project as good as possible. Before the start of this thesis, I made the decision that the choice of supervisor would be more important than the subject of my thesis. With Calvin as a supervisor, I am very happy I made this choice. Next, I am grateful to the NLR for providing my the specimens and answering all my questions regarding the processing details. Furthermore, I want to thank the exam committee, Rene Alderliesten and Bruno Lopes dos Santos, for their time and expertise to asses my work.

Secondly, I am deeply grateful the staff of the Aerospace Structures and Materials Laboratory, in particular Gertjan Mulder and Frans Oostrum. To obtain the results showed in my thesis, many experiments had to be performed. As I did not have any experience in experimental research, they helped me many times with their own expertise.

I would like to show my appreciations to my fellow students. Tijs, Robert and Philippe, thank you for all the in depth discussions about my thesis and good chats in the Aerospace Structures and Materials Laboratory. Furthermore, I would like to thank my room mates of 2.44 for their advice in performing this master thesis and good working atmosphere.

Finally, special thanks to Myrthe, my parents and brothers and sisters for their support during my entire lifetime.

Jef Michielssen
February 10, 2017

Summary

Throughout the years, additive manufacturing has gained a lot of interest from all different industries. The new way of building up a part, instead of removing material, offers a lot of new possibilities for engineers and designers. Selective Laser Melting (SLM) is one of these new techniques which could mean a breakthrough in the aerospace industry. Due to its specific manufacturing process, SLM is able to print Ti-6Al-4V while maintaining good mechanical properties. However, before SLM parts can be used in service, certification of the material is required.

Literature suggests that SLM material properties depend on the production parameters used. For certifying a part, this means that besides the geometry, SLM manufacturing parameters should also be taken into account. Throughout the past years, some research has been done in this field. Experiments showed that the damage tolerance principle is the preferred certification approach, due to the presence of internal defects. The damage tolerance approach is based on understanding the crack propagation properties of a material. Therefore, the effect of the manufacturing parameters on the crack propagation rate for SLM materials should be understood. A literature review revealed a knowledge gap concerning the effect of the print orientation and the effect of different heat treatments on the crack propagation properties. A thorough understanding is required before further steps can be taken in the certification process of SLM Ti-6Al-4V parts.

The aim of this thesis is to investigate the effect of a varying build orientation and different heat treatment on the crack propagation properties of SLM Ti-6Al-4V. Crack propagation rates will be measured for five different build orientation and two heat treatments, by performing fatigue tests. This data should provide sufficient information to draw conclusions relevant for future certification process.

To gather data, fatigue tests were performed at the faculty of Aerospace Engineering. A constant cyclic load allows a crack to propagate through a Ti-6Al-4V specimen. To skip the crack initiation phase, single edge notch specimens were used. Ten unique types of specimens were tested by combining five different build orientation (0°, 30°, 45°, 60° and 90°) with two different heat treatments (Stress relieved and Hot Isostatic Pressing). Throughout the experiment, the crack propagation rate was measured in three different ways (Extensometer, Visual Inspection, Striation counting). Three measurement approaches were used to validate the measured data and function as a backup if one would malfunction. As a second research objective, the crack propagation direction was measured using the pictures taken during the fatigue tests. To explain differences in the crack propagation properties, additional data was gathered by a DIC analysis, fractography and a microstructural analysis.

In the end, similar crack propagation rates were measured for all specimens. Although, small differences were seen in the microstructure and DIC analysis, they did not seem to change the crack propagation rate. This observation led to the conclusion that the crack propagation rate is not influenced by a change in build orientation or a change in heat treatment. On the other hand, the measured crack paths showed some differences. Small crack deflections were found for 30° - SR and 45° & 60° - HIP, while all other specimens had cracks propagating in a direction normal to the applied stress. As only off-axis specimens showed repetitive crack deflections, it can be concluded that the anisotropic microstructure is causing this behaviour. However, no conclusive explanation could be given based on the data gathered in this experiment. It is expected that different mechanisms caused the crack deviations as it happened in both heat treatments but for different orientations. Further research in this specific field in needed to explain the measured behaviour.

This research showed promising results for the future certification process. As the crack propagation rate is not influenced by the build orientation or heat treatment, the current certification process might be suitable for SLM Ti-6Al-4V. The crack deflections are relative small, which means that they may be negligible when designing or certifying the part. However, it is still interesting to investigate this effect in more detail. Being able to steer the crack by printing it in different way might be useful in future applications or change certification processes.

Contents

List of Figures

List of Tables

Acronyms

AB	As-built
AM	Additive Manufacturing
CMOD	Crack Mouth Opening Displacement
DIC	Digital Image Correlation
FEM	Finite Element Method
HIP	Hot Isostatic Pressing
HT	Heat Treatment
SLM	Selective Laser Melting
SR	Stress relieved

Symbols

a	Crack length [m]
h	Height - Distance between initial crack and clamp [m]
w	Width of the specimen [m]
$\frac{da}{dN}$	Crack propagation rate [m/cycle]
ΔK	Stress intensity factor [MPa$\sqrt{m}$]
α	Layer orientation with respect to horizontal line [°]
β	Geometry term in stress intensity factor [-]
δ	Crack mouth opening displacement [m]
ϵ	Angle between layer orientation and columnar grain direction [°]
σ	Applied stress [MPa]
θ	Columnar grain direction with respect to horizontal line [°]

1 Introduction

Throughout the years, industry has constantly been looking for new possibilities to make more complex parts with better mechanical properties. Driven by weight and cost savings, a lot of research has been done to come up with new manufacturing techniques.

Additive Manufacturing (AM) is one of these new manufacturing ideas which may result in a new industrial revolution. Additive Manufacturing is based on the idea that a part is created by adding material to create its final shape. This is completely different from the current techniques where material is removed from bulk. By building a part layer by layer, instead of removing material, more complex shapes can be created. For over the past 20 years, a lot of research has been done in the field of Additive Manufacturing. This makes it, the most rapid developing manufacturing process [8]. Not only the manufacturing process makes Additive Manufacturing unique. Also for designers, a lot of new areas can be discovered. With an unlimited freedom in geometric designs, engineers can rethink the way they design structures and create more efficient parts than ever before.

As a leading sector in innovation, the aerospace industry has a lot of interest in this new manufacturing technique. In particular, techniques which are able to create metallic parts may be interesting. Four major advantages for the aerospace industry can be found when using Additive Manufacturing [9];

- **Lightweight:** For an industry driven by weight reduction, AM can give some new solutions. For example, honeycomb structure can be printed from light but strong materials as titanium.
- **Complex geometries:** Aerospace applications often have multiple functions which results in complex geometries. Using AM, new geometries can be created which can not be built with the current techniques.
- **Economics:** Low production costs may be achieved with AM, as there is no need for many different expensive tooling techniques. Furthermore, molds and dies do not have to be fabricated to create parts. Since the part is printed in its final shape, there is no or less waste material.
- **Digital spare parts:** All aircraft part drawings can be stored in the computer and only printed if needed. This can be useful when taking into account the lifetime of an aircraft (20-50 years or longer).

Additive Manufacturing can bring a real revolution to the aerospace sector. Currently, different techniques exist which can print titanium parts. Within aerospace sector, there is a lot of interest in printing titanium, as it is a high performance material with good corrosion resistance [10]. Ti-6Al-4V is the most popular commercial titanium type, which is common used for critical parts as landing gear, airframe and engine parts [11][12]. However, titanium is hard to machine due to it high hardness properties. Creating a complex geometry using titanium may be expensive and difficult, if not impossible. Additive manufacturing can change this, as it allows complex geometries to be made of Ti-6Al-4V, which may result many new opportunities.

Selective Laser Melting (SLM) is such a promising additive manufacturing technique, which is able to create titanium parts. The SLM process is a powder bed fusion process which consist out of three phases. These phases are repeated until the product is finished. First, a bed of titanium powder is spread over the support base of the SLM machine. When the powder is evenly distributed, a high energy laser will melt the powder at predefined locations. By melting and naturally cooling of the powder, a semi part is created. Then, when the laser has covered all locations, the base will be lowered and the process will be repeated. A graphical presentation of this process can be seen in Figure 1.1.

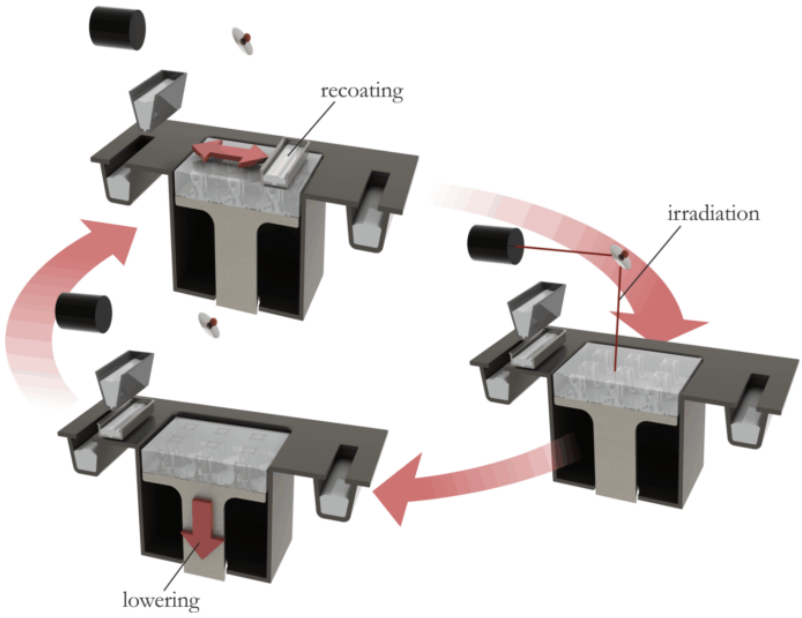

Figure 1.1: Selective Laser Melting process [1]

Titanium reacts well to the high temperature changes during the SLM process, resulting in good mechanical properties. This makes it an interesting material to investigate. Nevertheless, previous research [13] has shown that changing the process parameters (scanning velocity, laser energy, scanning directions,...) gives a change in the material properties and its mechanical properties.

In order to use a SLM part in industry and to ensure safety, parts should be certified according to certain regulations. Due to the changing material and mechanical properties with changing process parameters, certification of a SLM part is still a challenge.

This thesis looks into the certification of SLM structures, finds a knowledge gap and fills this gap by conclusions drawn based on experiments.

This report consists of several chapters. First, the present certification methods are discussed and the possibilities to apply them for SLM structures. In order to do this, a detailed look into the SLM material is provided. A knowledge gap is identified which should be filled before SLM structures can be certificated. All of this is discussed in Chapter 2, 'Literature review', which is concluded with some research questions. Chapter 3, 'Methodology', describes the practical implementation of the research approach. This chapter describes the test set-up in detail. All results gathered during the experiment are shown in Chapter 4, 'Results'. These results are analysed and discussion in Chapter 5. Finally, conclusions will be drawn based on the results. These conclusions and their impact on the future certification methods are given in Chapter 6, 'Conclusions'.

2

Literature review

Many aerospace structures have been certified over the past years. For current materials and production techniques, well-known certification methods can be used to improve the safety and efficiency of structures.

At this moment, industry is looking into new production opportunities where Additive Manufacturing will be used to create structures. Creating parts by adding material instead of removing it, can have lot of advantages in the upcoming years. However, there are still some barriers which should be crossed. One of them, is the certification of these new structures.

This chapter summarises current certification methods and how to use these for SLM structures. First, current certification techniques are explained. Then, the SLM material is investigated in more detail. Material properties, as well as the effect of input parameters, will be discussed. Finally, both sections will be combined in a search for a SLM suited certification method. This chapter is concluded by stating a knowledge gap. Identifying and solving this lack of knowledge is crucial before one could start thinking about certification of SLM structures.

2.1. Certification of aerospace structures

For many years, people have been using tools and structures to make their lives easier. However, many of these structures tend to fail after a certain period. Failure is often caused by overloading the structure or due to fatigue of the structure. The latter is a phenomenon that was first investigated in the 19th century. Some serious fatigue accidents resulted in the first investigations in this field [14]. Repetitive loading and unloading of a structure initiates cracks which eventually grow and can lead to failure. To cope with this material degradation and ensure safety, certification of structures was a necessity.

Certification is based on understanding the behaviour of a structure in all different kind of loading conditions and environments. Scientists have tried to understand all physical aspects of fatigue and have tried to understand and predict them. The large amount of factors, influencing the fatigue life, makes it hard to come up with physical models. This is why, up to now, certification is done based on empirical models and databases.

Many tests have been done over the years, for different materials and different types of structures. These tests have resulted in large material databases and empirical equations. By using them, one can predict fatigue failure in an accurate way. Predicting fatigue life is all about understanding the influences of two categories namely, material behaviour and geometrical influence. One can only certify a structure, if information is provided on the material properties and geometry of the structure.

Knowledge about the material properties is needed to predict the materials behaviour. Due to a difference in microstructure, different materials can act differently for similar loading conditions. Anisotropy of a material can cause a difference in material failure when loaded in a different direction.

Geometry can also change the way cracks are propagating through the structure. Sharp edges and holes increase the stress locally and therefore initiate cracks more easily. Crack propagation, on the other hand, can also be affected by a change in the stress distribution due to the presence of a thickness difference, holes or other geometrical features. All sort of combinations of these features will change the fatigue life of a structure.

A combination of geometry and material properties is required to certify a certain structure.

Luckily, most metals are isotropic which means that they behave equal in all loading directions. This simplifies the certification drastically, since material properties do not depend on loading direction. With large material databases and empirical formulas, for different geometries, certification has been done in the past years. Traditionally, three different certification methods are used in industry; Safe life, Fail safe and Damage Tolerance [14]. Each of them following a different approach to certify a structure. The techniques and their approaches are listed below.

- **Safe Life**
  The safe life principle is based on the idea that a part or structure should be able to survive a predefined lifetime. In order to do this, a SN-curve for a part is created by testing the parts for different loading magnitudes. As a result, a graph is created which gives the fatigue life (number of cycles) over a range of applied amplitude stresses.
- **Fail safe**
  Fail safe is a redundant system approach. This principle is based on multiple load paths. When one of the load paths would fail a secondary load path is able to cope with the predicted loads. This means that a structure would not fail as a whole when one load path fails.
- **Damage Tolerance**
  The damage tolerance approach is based on crack propagation and the material's resistance to it. In a damage tolerance approach initial damage in the material is considered. By understanding how a crack will propagate, in terms of rate and direction, an ideal inspection method and interval can be defined. Therefore, all cracks will be found and repaired before they become critical.

Each of these principles can be applied for SLM structures. Nevertheless, they all have their disadvantages. Safe Life will prevent structures from failing however, this means that the structure might already be replaced while it can still withstand many more cycles. Furthermore, to create a proper SN-curve a large test phase is needed which is time and cost inefficient. Fail safe can be inefficient in terms of performance to weight ratio. Having a secondary load path, which can carry all the loads, will make the structure heavier which is in general unwanted in the aerospace industry. Besides that, inspections are still needed to see if a load path failed. Damage tolerance requires a lot of knowledge about the crack propagation properties of the material. Without this knowledge, a structure cannot be certified according to the damage tolerance principle.

Thus, each certification approach has its advantages and pitfalls. Before being able to decide which principle is most applicable, SLM structures should be investigated in more detail. Geometrical influences will be similar, nonetheless, the SLM material might behave differently due to the specific production process. Therefore, further investigation in the material is required before deciding on the certifications approach.

2.2. SLM material properties

As described in the introduction, SLM creates a part by adding material instead of removing it. A high power laser is used to melt metallic powders and transform the powder in a solid material. This approach of producing parts results in a very interesting material which is different from wrought Ti-6Al-4V. An overview of the most interesting differences is described in this section.

2.2.1. Microstructure

During the SLM process, a high energy laser beam moves over a metallic powder bed. When the beam passes a certain area, the powder is melted. The large intensity and velocity of the beam results in very high heating and cooling rates. The combination of these process conditions leads to a specific microstructure [13]. The high energy laser beam melts the powder which creates a local temperature above the β transus. Due to the

fast cooling rate afterwards, which is comparable to water quenching, an α' martensitic microstructure is created. Such a microstructure is created when a diffusionless transformation occurs. Parallel to the building direction, columnar prior β grains were observed. These columnar grains are a result of partially remelting the previous layers. An example of a SLM as-built microstructure is shown in Figure 2.1a.

An α' martensitic microstructure is know to be very hard but also very brittle. Besides that, martensitic microstructures are known for their good resistance against crack nucleation due to the very fine needle like structure. However, this also results in a limited resistance against crack propagation.

The presence of the columnar prior β grains results in an anisotropic microstructure. During the experiment of Thijs [13], it was observed that the direction of the elongated columnar grains depends on the heat distribution condition. This heat distribution in turn, is related to the scanning strategy. It was concluded that the columnar prior β grains grow towards the remelted pools. A difference in scanning strategy can be seen in Figure 2.1. Figure 2.1a shows an alternating scanning strategy which creates columnar grains directed upwards. In the other experiment, the author used a unidirectional scanning strategy with a direction from right to left, as is indicated in Figure 2.1b. When looking to the columnar direction, one can see that these columnar grains also tend to move to the left when going up. This shows the direct relation between the scanning strategy and the anisotropy of the material.

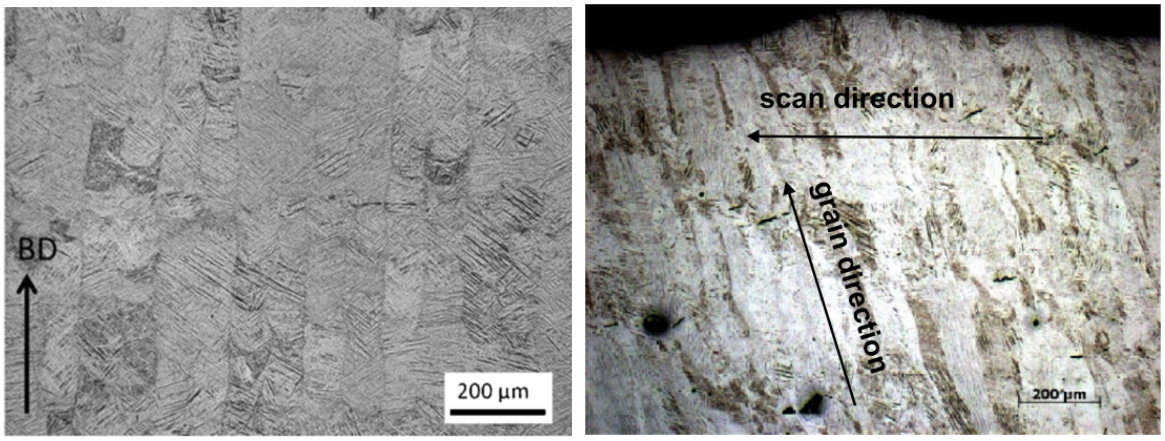

(a) Alternating scanning direction [15]

(b) Unidirectional scanning direction [13]

Figure 2.1: Microstructure of SLM Ti-6Al-4V with different scanning direction - Side view

Next to an anisotropic microstructure, a second anisotropic effect was discovered in as-built SLM parts. The specific production processes caused residual stresses to be created in the material.

2.2.2. Residual stresses

A second anisotropic behaviour in the material was found by previous studies [15][2][6][16]. These studies discovered that the high temperature gradient and local heat distribution creates residual stresses in the material. Understanding the heat distribution during the process is useful in understanding how the residual stresses are created but out of the scope of this research. A thorough explanation can be found in research of Rangaswamy [2].

Studies concluded that large residual tensile stresses, parallel to the building direction, are present at the edges of the specimens, while compressive stresses can be found at the core. The magnitude of these tensile residual stresses at the edge is a large fraction (40% - 50%) of the actual yield strength [2]. Stresses normal to the build direction showed the opposite sign convention, compressive stress at the edge and tension stresses at the core, but the magnitudes were much smaller, which can be seen in Figure 2.2.

Besides the microstructure and residual stresses, a third aspect was found in literature which can be of major interest when deciding on a suitable certification method.

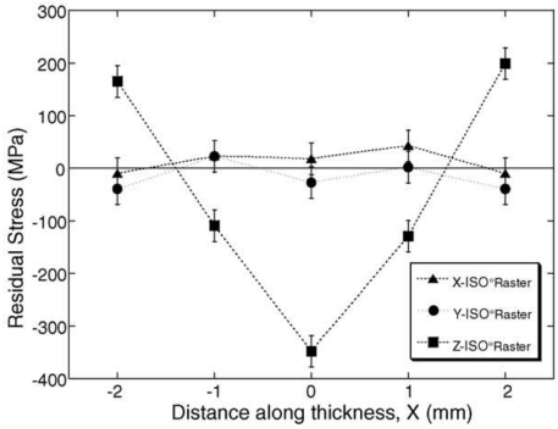

Figure 2.2: Residual stress distribution over the width of 316 stainless steel specimen [2]

2.2.3. Internal defect

Independent studies [17][18][19], found out that initial defects are present in printed titanium. Two different defects, lack-of-fusion and entrapped gas pores, were found in the material. An example of these defects is shown in Figure 2.3. Both defects are different from each other and are created differently. Lack-of-fusion defects are powder particles which were not melted by the laser during production. These defects can be recognized by their elongated shape. Entrapped gas can be recognized by its circular shape. Air is still trapped in the material due to excess energy during production. Both defects will act as stress raisers in the material and therefore act as crack initiators.

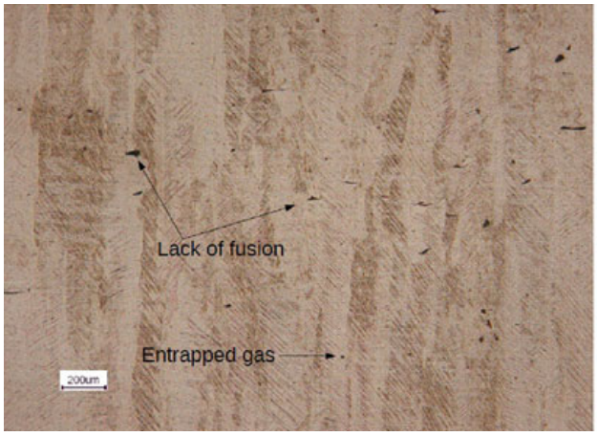

Figure 2.3: Initial defects present in SLM Ti-6Al-4V [3]

Studies have tried to eliminate the defects. Qiu [19] showed that the defects could be shrunk by using a Hot Isostatic Pressing (HIP) treatment. Such a heat treatment combines high temperatures with an isostatic pressure around 1000 bar. Due to this combination, internal defects will collapse and diffusion bond [20]. However, as Qiu showed, the defects could be shrunk but never be eliminated. As they can act as stress raisers, one should take them into account when certifying the part.

When looking back to the three possible certification approaches only the damage tolerance approach takes internal defects into account. The presence of internal defects makes damage tolerance the most preferred approach for SLM certification.

2.3. Certification of SLM structures

In the previous section, the material properties of SLM Ti-6AL-4V were revised. Besides a specific anisotropic microstructure and residual stresses, it was shown that internal defects are present in the material. Even HIP treatments could not fully eliminate these internal pores. Due to the presence of internal defects, damage tolerance is the preferred certification approach, as it considers internal defects. When looking to damage tolerance, three phases during the structures lifetime can be identified. The first is a period where it is assumed that small microcracks are present. In this phase, the size of the crack is too small to be detected by the non-destructive testing (NDT) device. When the crack grows, a minimum detectable crack length will be reached. From this point on, the second phase will start. At this stage, a crack can be detected during inspections of the structure. Finally, the crack will keep growing and the growth rate will increase as its length is increasing. This will eventually lead to a final phase where the crack reaches its critical length. Resulting in the structure to fail.

Certification according to the damage tolerance approach is based on calculating the length of the second phase. Using material and geometrical data of the structure, the time required for the crack to grow from detectable to critical can be determined. When the duration of the second phase is known, a predefined number of inspections can be planned. These inspections are required to find the crack before it will become critical. When a crack is found, the structure can be repaired after which it can be put to service again. A timeline of this damage tolerance approach is given below in Figure 2.4.

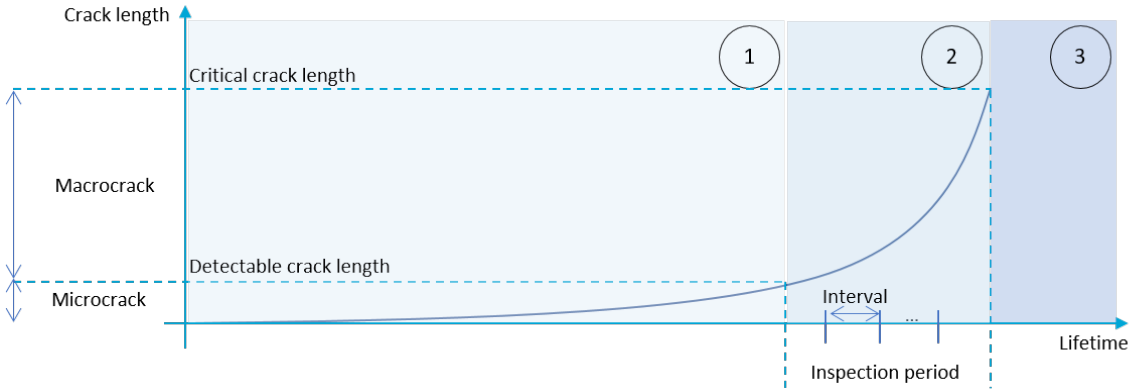

Figure 2.4: Damage tolerance timeline

In general, damage tolerance is all about understanding the resistance of a material (in combination with geometry) against crack growth. This crack growth property is represented by a Paris curve. A Paris curve plots the crack propagation rate against the stress intensity factor (ΔK). The latter is a term which describes the stress state in front of the crack tip. It is a well known term used in the field of damage tolerance. The stress intensity factor considers the applied stress, the crack length and the geometry of the structure. This can be seen in equation 2.1.

$$\Delta K = \Delta\sigma\sqrt{a\pi}\beta \tag{2.1}$$

In this formula, $\Delta\sigma$ represent the applied stress, a is the crack length and β is the geometry term. When the geometry changes from, for example, an edge notch to a centered notch, this β factor will change. Due to this unique combination, crack propagation rates can be compared for different materials even if the part geometry is not the same. This makes it a very powerful tool for the damage tolerance approach. However, one should keep in mind that this term is originally created for linear elastic fracture mechanics and can be used for homogeneous materials. More information about the stress intensity factor can be found in 'Fatigue of Structure and Materials' by Schijve [14].

An example of a Paris curve for raw Ti-6Al-4V is given below in Figure 2.5

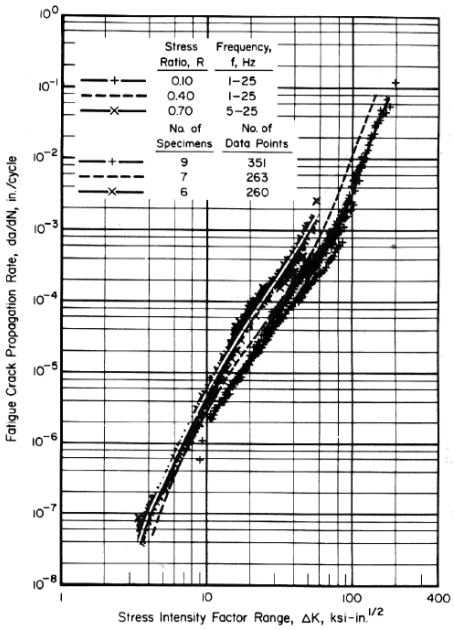

Figure 2.5: Paris curve - Ti-6Al-4V - Thickness = 0.25 inch [4]

The previous chapter showed that Ti-6Al-4V created by an SLM process can not directly be compared to wrought Ti-6Al-4V. Microstructure, residual stresses and defects are significantly different. Therefore, a different Paris curve should be used for SLM Ti-6Al-4V. Nonetheless, this may not be as easy as it sounds.

Literature has shown that small changes in production settings results in large changes in material properties [21]. Besides that, SLM creates Ti-6Al-4V which has an anisotropic microstructure. That may result in orientation dependent mechanical and fatigue properties. In order to cope with these effects, a lot of research has been done in the past years. Many studies have been looking into the effect of the input parameters on the mechanical and fatigue properties of SLM Ti-6Al-4V. However, only a few have been looking into the effect of the anisotropic microstructure and residual stresses on the crack propagation properties. A significant difference in crack propagation properties can have an effect in terms of certification, as certain directions might propagate faster than others.

With that in mind, current Paris curves would not be suitable for new SLM materials since they assume isotropic materials. Understanding the anisotropic effect on crack propagation is crucial for future certification approaches.

2.4. Effect of anisotropy on crack growth

Two main reasons were identified which causes anisotropy in the material namely, the anisotropic microstructure and the residual stresses. The effect of these anisotropies on the crack growth has been studied before by Cain [15] and Leuders [5]. Results from these experiments are shown below in Figure 2.7. These experiments tested compact tension specimens according to the ASTM standard E647 [22]. Those specimens are designed to fail in a plane strain conditions, from which material properties can be obtained. Before looking into the results and conclusions of these experiments, it is important to understand their building direction and heat treatments.

Due to the anisotropic material properties of SLM specimens, orientation of the specimen should be considered when looking to the results. A crack propagating parallel to the build direction is indicated with ZX. Perpendicular means that the crack is propagating perpendicular to the build direction and is indicated with ZX. An illustration is shown in Figure 2.6.

Besides the build direction, it is interesting to see which heat treatments were used in those experiments.

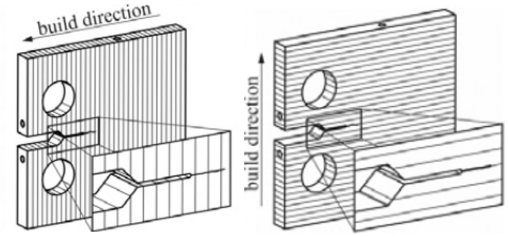

(a) Parallel - XZ (b) Perpendicular - ZX

Figure 2.6: Crack propagation direction with respect to build direction [5]

Residual stresses and internal defects can be diminished by specific heat treatments and might affect the crack growth. Heat treatments used by Cain and Leuders are described in table 2.1.

Table 2.1: Literature results - Heat treatment details

Author	Heat treatment	Label in graph	Details
Cain	As-built	AB	No heat treatment
	Stress Relieved	SR	650° for 4 hours
	Annealing	HT	800° for 2 hours
Leuders	As-built	as-built	No heat treatment
	Stress Relieved	800°	800° for 2 hours
	Hot Isostatic Pressing	HIPed	920° for 2 hours at 1000 bar

The results obtained by both studies are shown below in Figures 2.7.

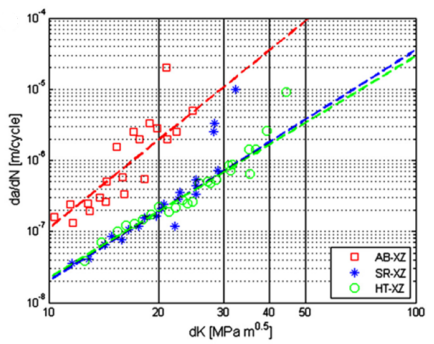

(a) Cain - XZ [15]

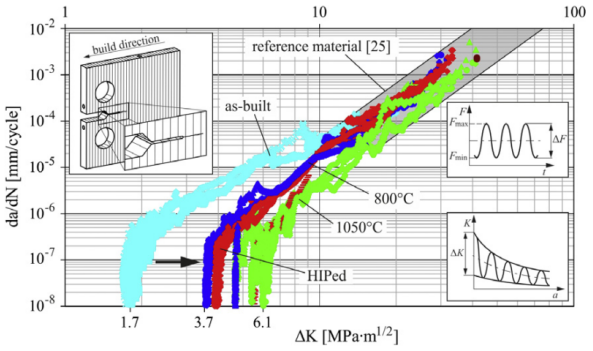

(b) Leuders - XZ [5]

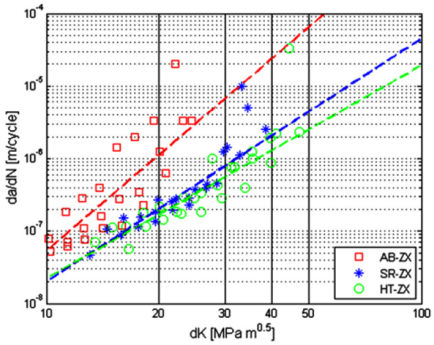

(c) Cain - ZX [15]

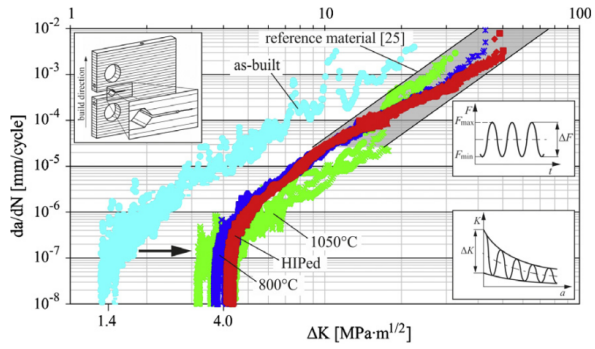

(d) Leuders - ZX [5]

Figure 2.7: Paris curves from literature

When looking at Figure 2.7 some conclusions can be drawn which were found by these studies [15] [5].

- As-built specimens have a lower crack propagation resistance when tested perpendicular to the building direction compared to other directions
- As-built specimens have a lower crack propagation resistance compared to heat treated specimens

Two different effects on crack propagation can be seen. First, an effect of build direction is identified which corresponds to the first conclusion. Next, it is concluded that crack propagation improves with heat treatments. Both phenomena are explained below.

The first observation has been studied by multiple papers [15][23][24]. In all papers, the same explanation for this effect is given. As was described before, residual stresses are present in the specimen. Large tensile stresses at the edges will increase the stress which is experienced by the material at the edge. This effect can clearly be seen in Figure 2.8. When looking to the crack front of XY and XZ it can be seen that the crack fronts are more or less straight lines. These specimens had a crack propagating parallel to the building direction and therefore experience lower residual stresses as can be seen in the figure. On the other hand, when looking to 'c' of Figure 2.8, it can be seen that the crack front in curved. With a crack propagating from the bottom to top, it can be observed that the crack propagated faster at the edges compared to the centre This effect can be attributed to the tensile residual stresses in the material, which are larger at edges compared to the centre The specimen in 'c' is a specimen in which the crack direction is perpendicular to the building direction which is in agreement with the first conclusion which was made before. Due to the large influences of the residual stresses, effect of the anisotropic microstructure is not visible (or not present). As residual stresses are often unwanted in structures, heat treatments were performed.

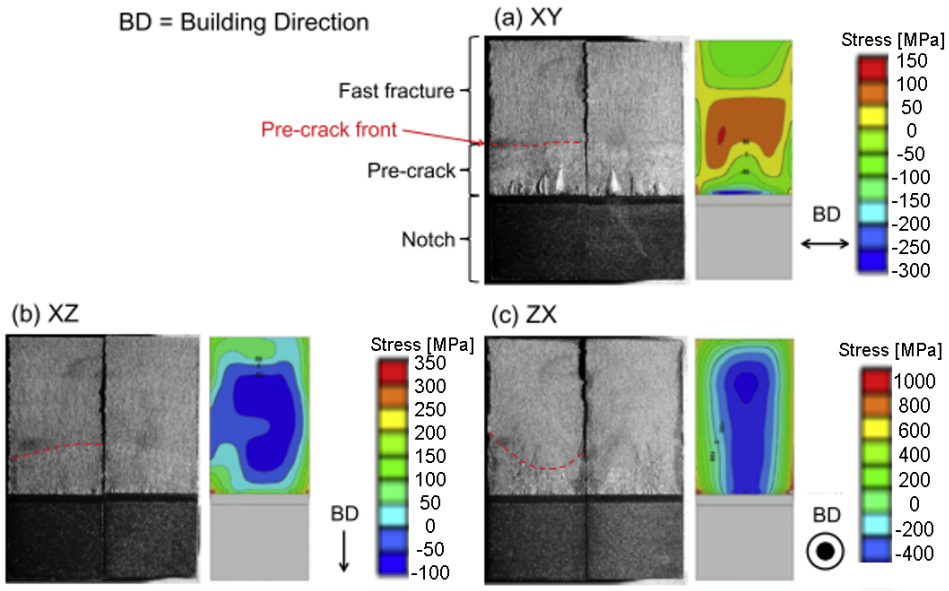

Figure 2.8: Effect of residual stress on crack front [6]

The second conclusion reflects on the effect of the heat treatments. From the results, Figure 2.7, it can be seen that the results of heat treated specimens shifted to the right and are more concentrated. This means that for the same stress intensity factor, there is a lower crack propagation rate. This confirms the second conclusion that heat treatments have a positive effect on crack propagation properties. Multiple studies [15][5][3][25] have drawn the same conclusion based on their experiments. These studies showed that the enhanced crack propagation resistance can be attributed to two aspects. First, the residual stress is relieved. This means that there is no increase of the stress level in the material, which means that the crack experiences a smaller applied stress compared to as-built specimens. The other aspect is the change in microstructure. The dominant microstructure for as-built SLM specimens is α' martensitic, which was discussed before. This microstructure is characterized by its good resistance against crack nucleation but suffers from low crack propagation resistance. By applying a heat treatment, this microstructure can be transformed to a more stable $\alpha + \beta$ lamellar microstructure. This microstructure is known for a better crack propagation resistance.

Due to its coarse lamellar microstructure, the crack constantly has to change direction which results in a lower crack propagation rate [12]. The combination of these two effects results in an improved fracture toughness for heat treated specimens. However when comparing the results, it seems that the difference in crack propagation rate is small for different heat treatments.

Based these literature results, the conclusions can be drawn that heat treated specimens performed better with respect to crack propagation rates. However, little difference can be seen in the effect of build direction in the heat treated results, while a large effect of build direction was identified for as built specimens.

Reviewing the studies that have been done so far, still some knowledge gaps can be found. Experiments have been performed to understand the effect of the anisotropic material behaviour on the crack propagation. However, this has been done by looking to the three orthogonal directions. No one has tested the specimens in an off-axis situation. An angle between the building direction and load direction between 0° and 90° might reveal new phenomena.

Furthermore, in as-built specimens, residual stresses have large influences on crack propagation. As residual stresses are often unwanted in most aerospace structure, heat treatments should be done before the structure can be used. Still, no one investigated the effect of build direction for heat treated specimens in detail. Up to now, there is no foundation to draw clear conclusions in this field.

Next, crack growth is only investigated in a plane strain condition. The material properties can be defined using compact tension specimens. The use of compact tension specimens allows the crack to fracture in a plane strain situation. Although actual crack propagation properties are obtained f with plane strain testing conditions, it is well-known that crack propagation rates improve when tested in plane stress condition. This is caused by the increased fracture toughness of thin specimens. This effect can be seen in Figure 2.9. As aerospace structures are often thin parts, a plane stress condition is highly possible. Therefore, it can be of interest to see how the plane strain and plane stress results relate to each other.

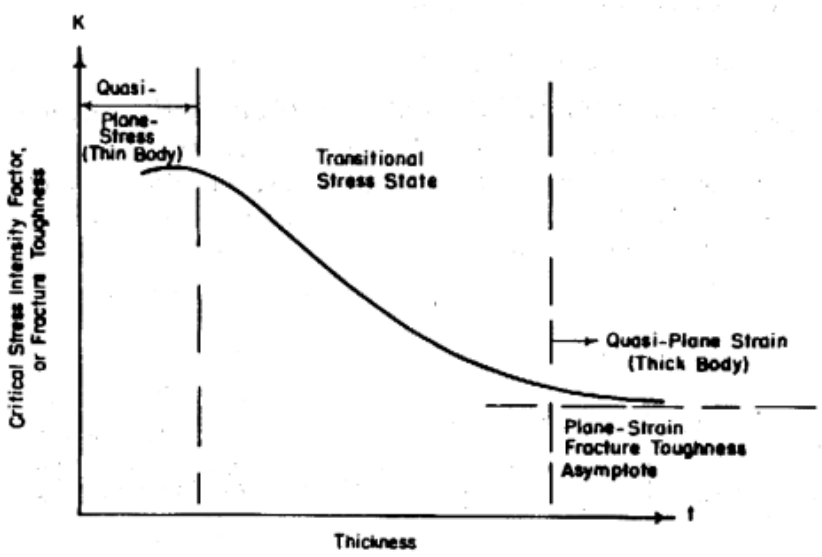

Figure 2.9: Fracture toughness over specimen thickness [4]

Still, a lot of unknown effects on the crack propagation rate are identified. Before certification can be done, these field should be investigated. This leads to the following research scope.

2.5. Research scope

In general, three different knowledge gaps were identified based on literature. First, the effect of build direction on SLM material properties has previously been investigated but only in orthogonal directions. Up

to now, no one has ever looked into the effect of an off-axis build orientation on the crack propagation rate. Secondly, large differences were identified between as-built and heat treated specimens. However, nobody investigated the difference in crack propagation properties of heat treated specimens in more detail. Finally, all SLM crack propagation properties were obtained by compact tension tests. As these test all behave in plane strain conditions, it is unknown how SLM materials will behave in plane stress conditions.

When testing anisotropic specimens off-axis, a fourth interesting field can be identified. When testing off-axis, crack paths might deviate from their original crack path (normal to the applied load). However, there is no information available in literature in this field for SLM materials. Besides the crack propagation rate, it can therefore be interesting to look into the crack propagation direction for all cases.

To limit the research scope, crack propagation rate and direction will be investigated for SLM Ti-6Al-4V with constant specimen dimensions. Ti-6Al-4V will be used as the literature review showed that this material has a lot of potential for the aerospace industry in combination with the SLM technique. Equal specimen dimensions allows the user to eliminate any dimensional effects on the results.

Based on the knowledge gaps, the following research questions were defined:

What is the effect of an off-axis building direction on the crack propagation rate and direction of a Ti-6Al-4V specimen which was created by Selective Laser Melting?

What is the effect of different heat treatments on the crack propagation rate and direction of a Ti-6Al-4V specimen which was created by Selective Laser Melting?

What is the effect of a plane stress condition on the crack propagation rate of a Ti-6Al-4V specimen which was created by Selective Laser Melting?

The aim of this thesis report is to answer all these questions based on experimental data. By answering the questions, clear conclusion can be drawn which can be used in future certification processes.

3

Methodology

By reviewing the literature, knowledge gaps were identified which should be filled before SLM certification can be done. The lack of knowledge in terms of the effect of build orientation led to some research questions. The aim of this thesis is to answer these questions based on experiments. Fatigue tests were performed for single edge notch specimens with varying build orientation and heat treatments. By measuring the crack propagation properties for all specimens, different influences can be revealed. In order to explain any differences, DIC and post-fatigue analyses were performed. Within the remainder of this chapter, the various test, analysis, and data processing methods utilized in this study are detailed in order to provide transparency and confidence in the obtained results.

3.1. Specimen

During this experiment, single edge notch specimens with constant specimen dimensions will be tested. All specimens will be made out of Ti-6Al-4V and created by a Selective Laser Melting (SLM) process. To investigate the effect of the build orientation five different printing angles were chosen as well as two different heat treatments. All specimens which were used in this thesis were provided by the 'Netherlands Aerospace Centre' (NLR).

Below, the specimen configuration, production and heat treatments are explained in more detail.

3.1.1. Configuration

Before testing, the material and dimensions of the specimen were selected. The material and dimensions were fixed for all specimens to make sure that any material or dimensional influences are excluded from the results.

Ti-6Al-4V Grade 5 was selected as the specimen material. Good mechanical properties and the possible applications in the aerospace industry were the base of this decision. The powder size used for the SLM process was 20-63 micron.

For this experiment a 'single edge notch' test specimen was chosen. In such a specimen, the crack will grow from one side to another, initiated by an initial notch. To exclude any influence of the specimen size on the crack propagation properties, all specimens have equal dimensions. When selecting the specimen dimensions, two factors had to be taken into account. First, for the overall dimensions, the printer dimensions had to be considered as well as warping effects when printing the specimens. An increase in specimen dimensions results in larger warping effects. A second factor is the stress state in which a specimen will fail. As discussed before, plane stress conditions should be obtained which can be assured when selecting a thin specimen. Therefore, the thickness was set equal to 2.2 mm. The dimensions can be seen in Figure 3.1.

To investigate the effect of the build direction, five different orientations were selected namely 0, 30, 45, 60 and 90°. Large angle differences were chosen to make the effect easier to detect. By selecting 0 and 90° angles, one would be able to compare the results with same orientations from literature. An angle of 45° was

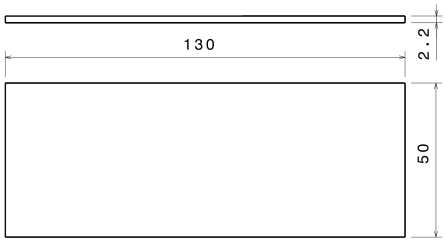

Figure 3.1: Selected specimen dimensions [mm]

chosen to have a specimen which is exactly in between 0 and 90°. Finally, 30 and 60 degrees were selected to have a total of five different orientations.

3.1.2. Production

As was discussed before, five different orientations (0, 30, 45, 60 and 90°) will be used to investigate the influence of build direction on the crack propagation rate. In order to create a certain layer orientation, specimens are printed at an angle and afterwards tested in their longitudinal direction. An illustration of how this works is shown below, in Figure 3.2.

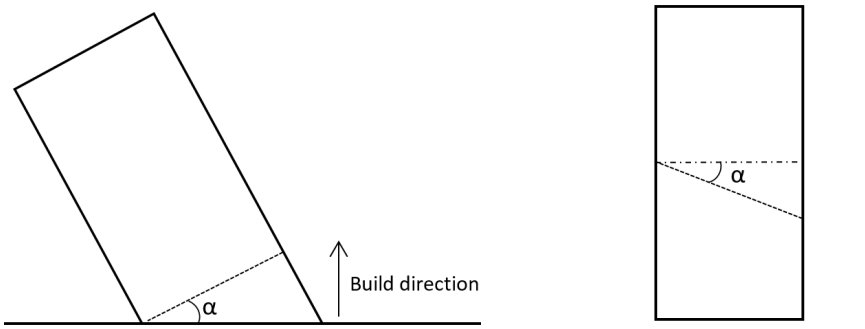

(a) Specimen during producion (b) Specimen during testing

Figure 3.2: Build orientation of SLM specimens

The specimens were produced by the NLR using a SLM 280 HL printer. For the production, a layer thickness of 50 μm was used. Furthermore, a chessboard pattern was selected as the scanning strategy. Every new layer, the position and orientation of the chessboard changes, which is common in SLM processes. The used pattern is shown in Figure 3.3. Further process parameters are shown in table 3.1.

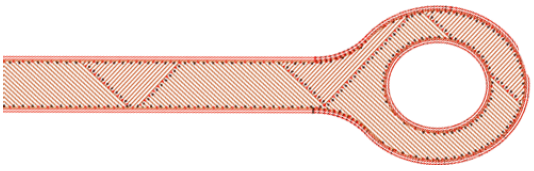

Figure 3.3: Scanning strategy

Table 3.1: Processing parameters

	Contour lines	**Fill Contour**	**Hatch**	**Supports**
Laser Power [W]	100	150	275	150
Scan velocity [mm/s]	400	450	975	750
Laser Intensity [W.mm/s]	0.25	0.33	0.28	0.2

Figure 3.3 shows circular tubes at the end of the specimen plate. These reinforced tubes have to be printed to provide resistance to the specimen from warping and detaching itself from the support base. When a layer cools down it tends to shrink. A summation of multiple shrinking layers results in warping of the material. Printing such reinforced tubes will counteract this movement. After production these internal stresses can be relieved by a heat treatment.

All specimens are printed in batches. For the experiment, multiple specimens of the same type are desired. This gives the opportunity to perform repetitive tests and therefore increase the confidence level of the results. By printing in batches, one can assure that all specimens were created with the same production parameters. This will eliminate influences of production on the crack propagation results. A specimen batch for an off-axis build direction (45 degrees) can be seen in Figure 3.4a.

When the batch is produced, heat treatments are applied. These heat treatments are used to relieve the residual stresses of the material and change the microstructure, to fit the application better. The heat treatments performed in this study are described in the following section.

When stresses are relieved, the specimens can be detached from the support base. To shape the specimens into their final dimensions, they are machined. Machining cuts off the reinforced tubular tubes and removes the excess material. As a positive side effect, machining will create smooth edges which diminishes the change of secondary crack initiation.

As this research focuses on crack propagation, an initial crack is preferred. By manually creating an initial crack, the initiation phase will skipped. This means that only the crack propagation phase will be measured. An edge notch of 5 mm was created using Electrical Discharge Machining (EDM).

The final specimen dimensions can be seen below, in Figure 3.4. Where only α is variable and equal to 0, 30, 45, 60 or 90°.

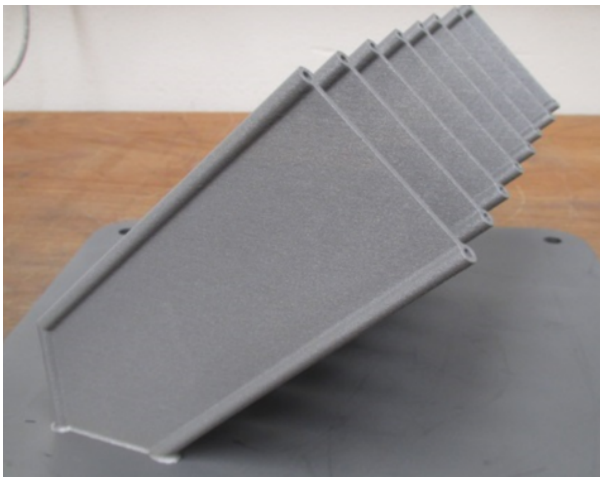

(a) Specimen batch

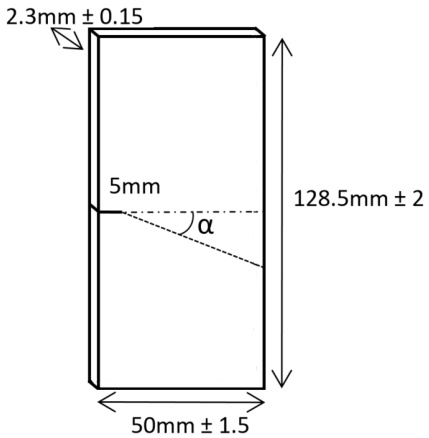

(b) Specimen during testing

Figure 3.4: Specimen dimensions

3.1.3. Heat treatments

Literature showed a large difference in crack propagation rate for as-built and heat treated specimens. This was attributed to the presence of the residual stresses in the build direction. Keeping in mind that residual stresses are often unwanted, it is unlikely that as-built parts would be used in aerospace structures. Therefore, it is interesting to see if differences in crack propagation properties can be found between two heat treatments.

Besides residual stresses, internal defects were also found to be present in SLM material. Due to these internal defects, the damage tolerance approach was selected as a preferred certification method. Thus, it is

interesting to see if these internal defects influence the crack propagation properties.

In the end, two different heat treatments were selected to investigate this. First, a stress relieving treatment was chosen which will only relieve the residual stresses. As a second heat treatment, a stress relieving treatment is followed by a Hot Isostatic Pressing (HIP) treatment is selected. This treatment should relief the stress but also shrink the pores inside the material. The exact details of the heat treatments are listed below and shown in Figure 3.5.

Stress relief treatment (SR)

1. Anneal at 735°C ± 13 during 60 minutes
2. Fast cool under protective atmospere (Argon) to room temperature

Stress relief treatment + Hot Isostatic Pressing treatment (HIP)

1. Anneal at 735°C ± 13 during 60 minutes
2. Fast cool under protective atmospere (Argon) to room temperature
3. HIP: Increase temperature to 920°C ± with a pressure of 1000 bar -0/+50 for 120 minutes
4. Air cooling to room temperature

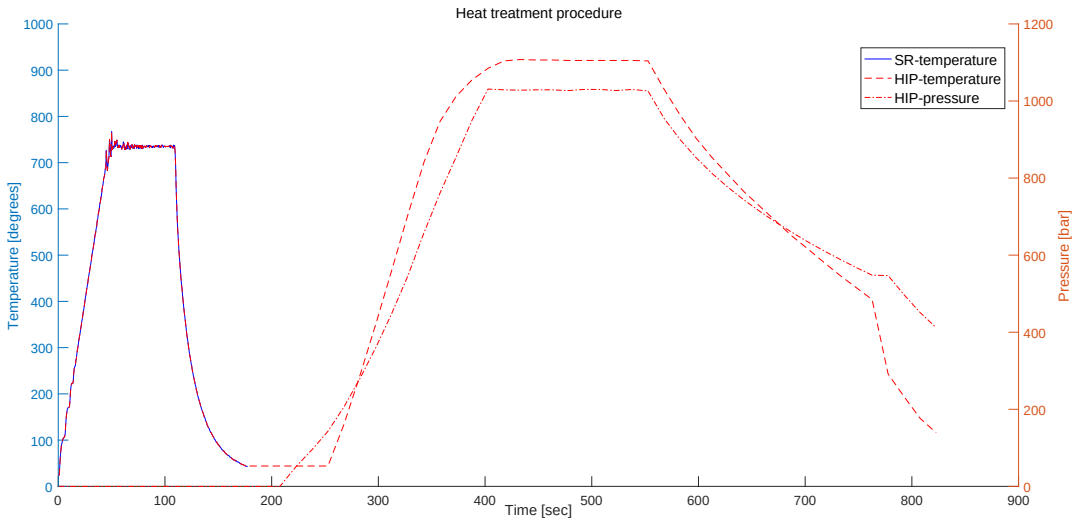

Figure 3.5: Temperature and pressure log for both heat treatments

Finally, a combination of five different orientations and two heat treatments results in ten unique specimen types. For each type, four specimens were made in order to create repetitive tests. Every specimen has a unique specimen code to keep them separated from each other. An example for the 0 degrees specimens is shown below in the table 3.2.

Table 3.2: Coding for 0 degrees specimens

Orientation	0 °							
Heat treatment	SR				HIP			
Specimen code	00-01	00-02	00-03	00-04	00-05	00-06	00-07	00-08

3.2. Test setup

Based on the research scope, (Section 2.5), both the crack propagation rate and direction should be measured. Fatigue tests are a well-known concept where the specimen is subjected to a cyclic load cycle. This

cyclic load cycle will grow a crack, from which the crack propagation rate and direction can be measured.

For this thesis, fatigue tests are performed at the faculty of Aerospace Engineering, where the 100kN MTS machine was used. This machine has a class-1 load cell which means that an accuracy of 1% is achieved. However, in reality, the machine has an accuracy of 0.2%.

In order to create a correct Paris curve, crack propagation rates should be measured over a certain range of the stress intensity factor (ΔK). As described before, the stress intensity factor depends on three aspects, the applied stress, crack length and specimen geometry. Increasing one of these aspects during the experiment will change the stress intensity factor. By keeping the applied load constant, the crack length will increase which will result in different stress intensity factors. Other approaches are also possible which will give the user more control on the situation. However, for this experiment, a constant load and increasing crack length was sufficient to gather the correct data. Other parameters as the R-ratio and frequency are equal to respectively 0.1 and 10Hz. These values are widely used in crack propagation experiments [5][26][27] and therefore will also be used in this test.

The selection of the maximum applied load is based on preliminary tests performed with one set of specimens. Experiments in literature were performed with Compact Tension specimens and therefore tested in plane strain conditions. Due to the uncertainty of how the material will behave for certain loads, a preliminary test was set up to determine the correct load. Based on this test, a maximum applied load of 10kN was determined. All details about this test phase can be found in Appendix A.

Table 3.3, summarises all the test parameters used in this experiment.

Table 3.3: Fatigue test parameters

Load cycle	Constant
R-ratio [-]	0.1
Frequency [Hz]	10
Maximum Load [kN]	10

With these test parameters, fatigue tests can be performed. During the experimental phase, not all test requirements were met. According to the ASTM standards [22], a height over width (h/w) ratio of 1 should be used, where the height is the distance between the crack and the clamp. However, due to the specimen dimensions and clamp area required, a maximum h/w of 0.8 could be obtained. In the end, all specimens were tested using this h/w ratio. The effect of this lower ratio on the results is discussed in Chapter 5.

In this experiments, the crack propagation rate and direction should be measured. Therefore, different measurement techniques are used. Three different approaches are used to measure the crack propagation rate. By using different methods, the results can be validated or used as a backup when a technique fails. First, an extensometer will be used which will measure the crack mouth opening displacement (CMOD). By using a theoretical relation between the CMOD and the crack length, the crack length for every cycle can be calculated. This will eventually result in a crack propagation rate for every cycles. Next, a camera will be used as a visual inspection approach. Pictures of the crack length will be made every 1000 cycles. By manually measuring the crack length and corresponding number of cycles, a crack propagation rate can be calculated. Finally, crack propagation rates can be directly measured at the fracture surfaces. Every cycle, a striation is created at the fracture surface, by measuring the striation spacing crack propagation rates can be calculated.

As a second research objective, the crack propagation direction should be measured. This will be done by measuring the crack path from the pictures captured by the camera.

Finally, a measurement approach is present which gives additional information to explain the crack propagation phenomena observed. By analysing the strain field in front of the crack tip, some valuable information may be obtained. This strain field is measured using Digital Image Correlation (DIC). All measurement techniques are described in more detail in Section 3.3.

An illustration of the test setup is shown in Figure 3.6. Figure 3.6a shows a front view corresponding to the view when looking from the camera for visual inspection. One should keep in mind that the other side of the specimen is speckled as the DIC cameras are placed on the other side. Figure 3.6b shows the position of all the cameras. In Figure 3.7, the real life test setup is shown.

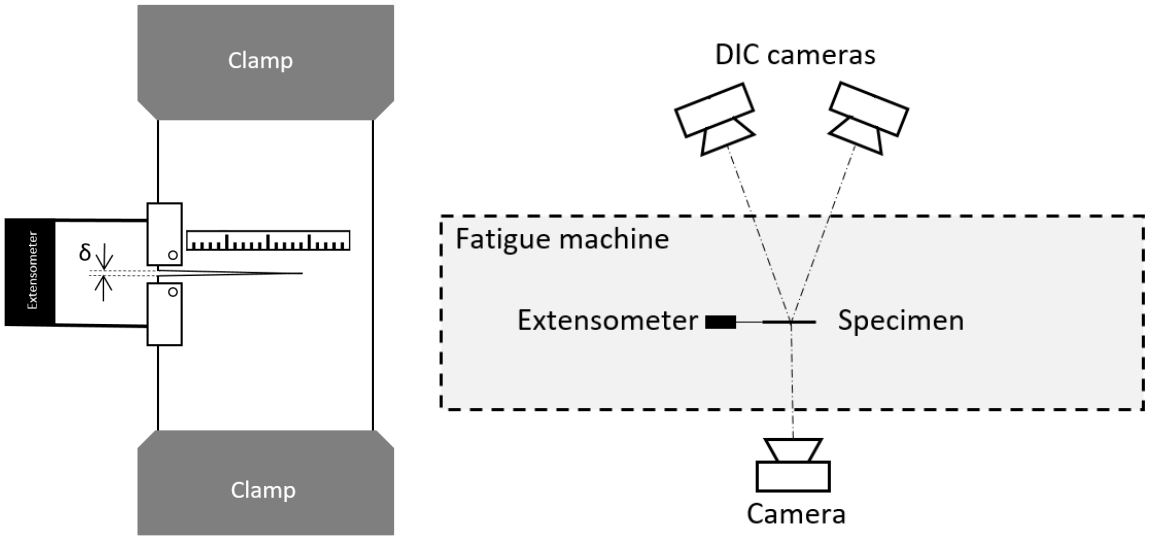

(a) Front view (b) Top view

Figure 3.6: Final test setup - Illustration

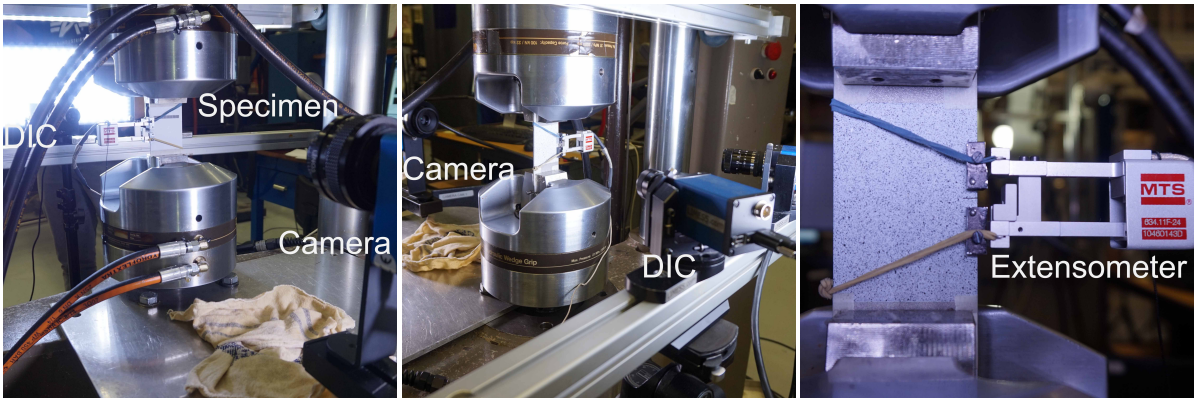

(a) Camera side (b) DIC side (c) Extensometer - DIC side

Figure 3.7: Final test setup - Lab

Finally, a test matrix was set up, which consists of all experiments. By looking at the matrix, one can see which specimen is and what measurement techniques were used during this test. Fractography and microstructural analysis were are performed after the actual fatigue test.

The test matrix is shown below in table 3.4.

Table 3.4: Test matrix

Build Orientation	Heat treatment	Specimen code	Paris curve	Striation count	Crack path	DIC	Fractography	Microstructure
0°	SR	00-01	X		X		X	
		00-02	X		X		X	X
		00-03	X		X		X	
		00-04	X		X	X	X	
	SR + HIP	00-05	X		X		X	
		00-06	X		X		X	X
		00-07	X		X		X	
		00-08	X	X	X	X	X	
30°	SR	30-01	X		X		X	
		30-02	X		X		X	X
		30-03	X	X	X		X	
		30-04	X		X	X	X	
	SR + HIP	30-05	X		X		X	
		30-06	X		X		X	X
		30-07	X		X		X	
		30-08	X		X	X	X	
45°	SR	45-01	X		X		X	
		45-02	X		X		X	X
		45-03	X		X		X	
		45-04	X		X	X	X	
	SR + HIP	45-05	X	X	X		X	
		45-06	X		X	X	X	
		45-07	X		X		X	
		45-08	X		X		X	X
60°	SR	60-01	X		X		X	
		60-02	X		X	X	X	
		60-03	X		X		X	X
		60-04	X		X		X	
	SR + HIP	60-05	X		X		X	
		60-06	X	X	X		X	
		60-07	X		X		X	X
		60-08	X		X	X	X	
90°	SR	90-01	X		X		X	
		90-02	X		X		X	X
		90-03	X		X		X	
		90-04	X	X	X	X	X	X
	SR + HIP	90-05	X		X		X	X
		90-06	X		X	X	X	
		90-07	X		X		X	
		90-08	X		X		X	

3.3. Measurement techniques

As described before, different measurement techniques were used during this experiments. Crack propagation rate will be measured at three different levels during the experiments. Besides the crack propagation rate, also the crack propagation direction should be measured. This can easily be done by visually looking at the specimen surface.

The measured crack propagation data may reveal new interesting phenomena. To be able to explain these phenomena, more information might be needed. Due to the heat treatments, residual stresses are probably relieved in this experiment. However, it can still be interesting to see how the stress/strain field behaves in front of the crack tip. Furthermore, understanding the fracture mechanisms can help in explaining the crack propagation rate or direction. Therefore, a fractography analysis will be performed using the Scanning Electron Microscope (SEM). As a last source of information, microstructural analyses will be performed. The anisotropic material behaviour and applied heat treatments will result in different microstructures for all specimens. Having a look at these microstructures and being able to identify the differences and equalities can help in explaining the overall results.

Below all details about the measurement methods are explained as well as the required specimen preparation.

3.3.1. Crack propagation

Three different crack propagation measurements will be used. All approaches differ from each other, in the way they are used as well as the amount of data points received and the accuracy of the results.

As a primary measurement approach, an extensometer will be used. This extensometer will measure the crack mouth opening displacement (CMOD). Using a theoretical relation, the crack length can be calculated with this CMOD, from which the crack propagation rate can be calculated. The extensometer measures the CMOD for every cycle, which was the reason why this technique is set as a primary measurement technique. When having a data point for every cycle, an accurate crack propagation rate is calculated over its whole lifetime. However, two post processing steps are needed which increases the possibility of errors.

Visual inspection was selected as a second measurement approach. By taking pictures at certain moments in time, the crack length can be measured manually. When knowing the crack length and corresponding cycle, the crack propagation rate can be calculated. This gives the opportunity to use this technique as a back up technique and to verify the data obtained by the extensometer. Defining the crack length versus number of cycles may require more time but will always give a correct approximation of the crack propagation rate. However, human errors may still be present when manually measuring the crack length.

Finally, as a third measurement approach, the crack propagation rate can be measured directly by measuring the striation spacing. This technique is very accurate as the crack propagation rate is directly measured at the fracture surface. No post processing is needed which means that it is less prone to errors. However, striation counting is very time inefficient which results in only a few data points. Therefore, this technique can be used to validate the other crack propagation methods.

The three measuring approaches are illustrated below in Figure 3.8. Figure 3.8a shows all the processing steps which have to be taken before the crack propagation rate is calculated. As can be seen only striation counting measures the crack propagation rate directly. For the other two approaches, data processing steps are required. These post processing steps are explained in the following section, Section 3.4. Figure 3.8b shows a small assessment of the methods, which were described before.

Extensometer

As a primary measurement technique, the crack mouth opening displacement should be measured correctly. This can be done by placing an extensometer at both sides of the fracture surface. The extensometer used for this experiment is the MTS (Model number:634.11F.24), which can be seen in Figure 3.7c. This extensometer has a travel range from +5 to -2.5mm, which is sufficient for this experiment.

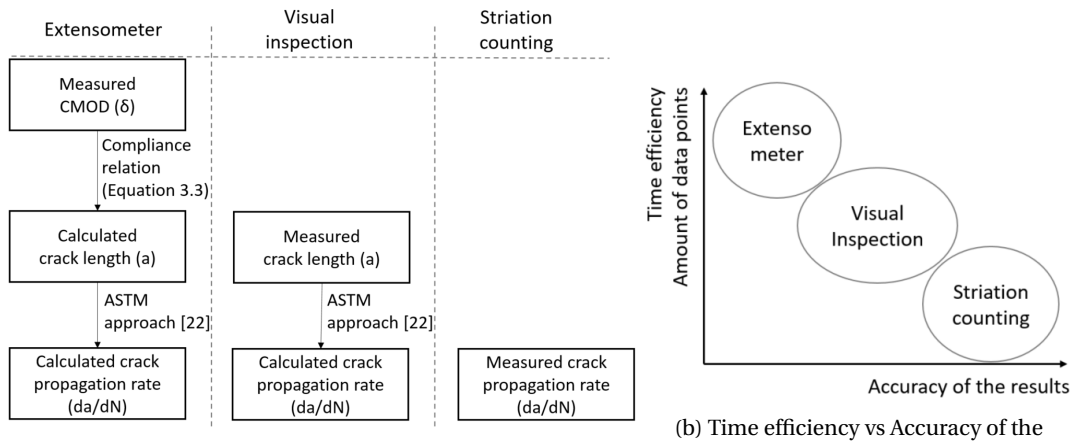

(a) Steps required

(b) Time efficiency vs Accuracy of the results

Figure 3.8: Crack propagation measurement approaches

However, due to the geometry of the specimens, little space is available for this extensometer. Therefore, the design of an extensometer extension was required, as well as some adjustments to the specimen. This extension allows the user to attach the extensometer to the specimen and measure the crack tip opening at a different location. A pictures of these extensometer extensions is shown in Figure 3.9a.

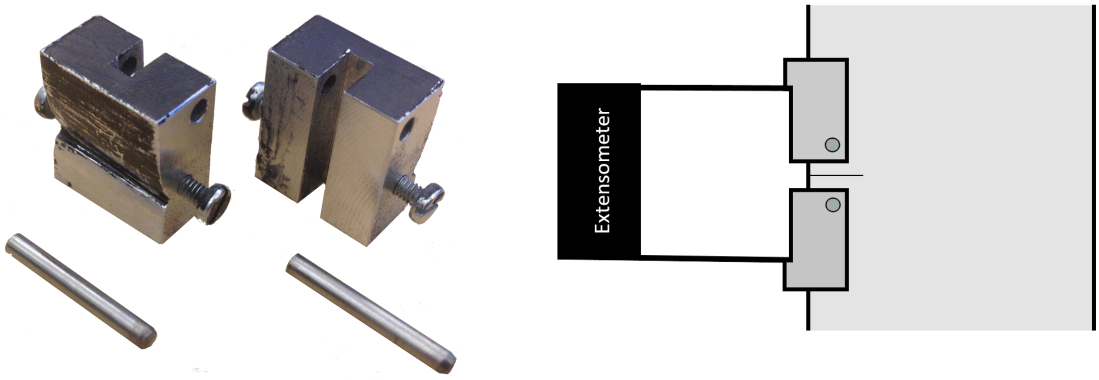

(a) Extensometer extension

(b) Extensometer extension setup

Figure 3.9: Extensometer setup

By drilling little holes at both sides of the crack, the extension can be attached to the specimen. An extensometer measures the strain during the fatigue test. Thus, when the extensometer is calibrated at the start of the test, the actual crack opening displacement will be measured.

By drilling holes in the specimen, the stress field might be changed and shield the initial crack length. In order to limit this shielding, the initial crack length was made long enough to be away from the holes and potential stress shielding.

It is of major importance that the extensometer does not change position during testing, as this gives wrong data. Ideally, one would like to fix the extensometer to the extensions/specimen. However, when failure occurs a very large displacement is created which would break the strain gauges and therefore the extensometer. Thus, it was decided to use rubber bands to keep the extensometer in place. The stiffness of the rubber bands should be high enough so it does not allow movement when the test is running but it should allow the extensometer to detach from the specimen when it breaks.

By placing the extensometer at the specimen, as is shown in Figure 3.7c, and calibrating the extensometer, correct data should be gathered.

Visual inspection

Visual inspection is based on manually measuring the crack length from pictures taken by a camera. To simplify and increase the accuracy of this measuring process, millimetre tape was attached to the specimen. This allows the user to directly measure the crack length from the picture. Figure 3.10 shows how this looks in real life.

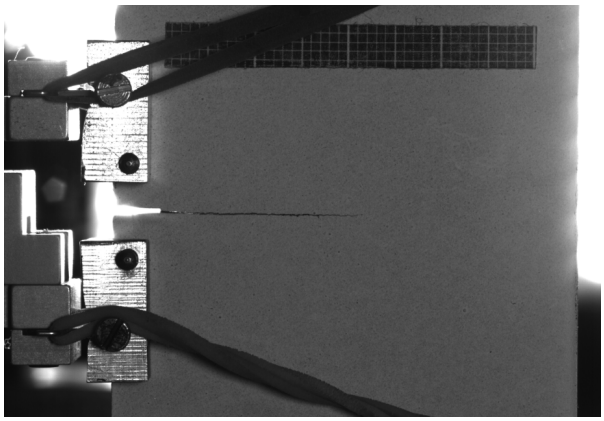

Figure 3.10: Accuracy of the visual inspection data

To calculate the crack propagation rate, pictures should be taken at predefined moments in time. Based on preliminary tests, it was decided that a picture would be made every 1000 cycles, as the lifetime was predicted around 150000 cycles. During the first 50000 cycles, this interval would probably be to small to see changes in crack growth between each picture. However, at large crack lengths, a small interval is desired to create enough data points. Every 1000th cycle, the machine will keep the maximum load for one second. During this second, the camera is triggered to take a picture when the crack is clearly visible. To further improve the visibility of the crack length and the accuracy of the results, specimens were painted white to increase the contrast of the pictures. An example is shown in Figure 3.10.

Striation counting

Striation counting is the only technique where the crack propagation rate can be measured directly. The striation spacing, which manually can be measured using the SEM, is equal to the crack propagation rate as a striation is created every cycle.

However, before measurements in the SEM can be done, the specimen should be prepared. Preparation of the specimen is explained in Section 3.3.4, 'Fractography'.

3.3.2. Crack path

To measure the crack path, camera images will be used. By analysing the pictures made by the 'Visual Inspection' camera, the change in crack propagation direction can be seen.

To visualise the overall crack path, a picture of the broken specimen will be made with a millimetre paper background. This will give a more precise idea of changes in the crack propagation direction. Processing of this data will be discussed in Section 3.4.

3.3.3. Strain field

Visualisation of the strain field can be of interest when analysing the crack propagation properties. A well-known technique to map the strain field is Digital Image Correlation (DIC). DIC is a non-contact measurement technique which uses two cameras to track displacement on the surface.

DIC is based on comparing images to track differences. By having a speckle pattern on the surface of the specimen, DIC can track unique patterns and therefore calculate deformations. These deformations can afterwards be translated in strains, shear, translations and rotations.

In order to perform a DIC analysis, the surface should have a speckled pattern. The smaller these unique patterns are, the more accurate a DIC analysis can be done. As a rule of thumb, a speckle size around 3 pixels is needed for an optimal DIC analysis. Speckles smaller than 1 pixel would be too hard to distinguish. However, a larger size would result in larger subsets needed which lowers the accuracy of the results. The actual size (in pixels) of the speckles is shown in Figure 3.11. The average speckle area is around 3x3 pixel, which is in agreement with the rule of thumb.

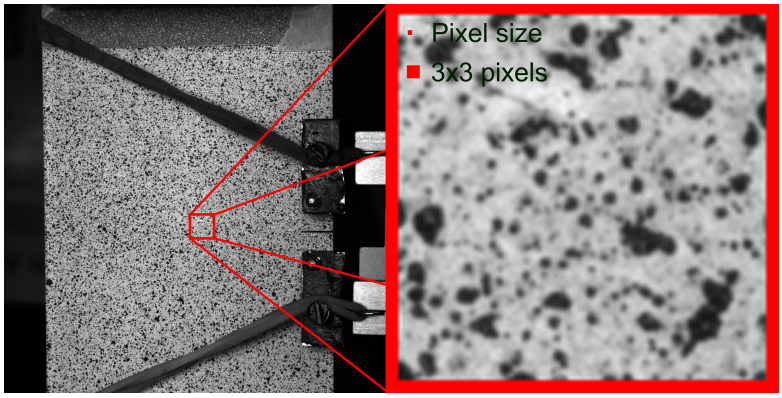

Figure 3.11: Speckle size - Specimen_60_8

Besides the speckle pattern, calibration of the DIC camera is of major importance. Without performing the calibration in a correct manner, wrong strain data will be obtained. To ensure good calibration and increasing the confidence level of the data, 25 calibration pictures were used. A calibration was only accepted if the overall calibration error was around 0.02.

For the analysis of the DIC images, a program called 'Vic3D' was used. Based on the images, Vic3D is able to calculate the deformation and strains on the surface of the specimen. As discussed before, the program will calculate deformations and strains by comparing two pictures and tracking the unique patterns.

3.3.4. Fractography

Measuring crack propagation properties does not tell anything about the fracture mechanisms. Fractography can help explaining what fracture mechanisms are present during failure. By looking to the fracture surface, one can identify where the crack started, how the crack front formed over the surface and where the final failure started.

During this thesis, fractography was performed using the Scanning Electron Microscope (SEM), which is located at the faculty of Aerospace Engineering. Before the specimen can be used in the SEM, some preparation is needed. The only step which should be taken before the analysis can be performed is cutting the specimen so it fits the SEM. When the specimen has the right dimensions, it can be placed in a support. This support can be pushed in the SEM. An example is shown in Figure 3.12a.

3.3.5. Microstructural analysis

Processing parameters, as well as heat treatments, change the microstructure of the specimens. Literature showed that the microstructures have an anisotropic behaviour. Having a look at the microstructure is required to examine the influence of this microstructure on the crack propagation properties.

A microstructural analysis can be done using an optical microscope. However, before the microstructure can be seen, some preparation of the specimen is needed. The interesting areas should be embedded in a

small cylinder which afterwards should be grinded, polished and etched. Below, all the steps which were taken to perform a microstructural analysis are listed. An example of a prepared specimen is shown in Figure 3.12b

1. Cut the specimen in small parts to fit in the cylinder
2. Embed the parts in a cylinder and fill the cylinder with the embedding material (Techovit 4071)
3. Grind the surface until the location of interest is reached. Grinding is done in three steps, gradually decreasing the grain size. First 180, followed by 320 and finally 1000.
4. Polish the specimens in three phases. First with 6μm, followed by 3 μm and finally 1μm.
5. Etch the cylinders for 10 seconds with 200ml H_20, 100 ml HNO_3 and 20 ml HF.

After carefully performing these steps the microstructure should be visible using an optical microscope or the SEM.

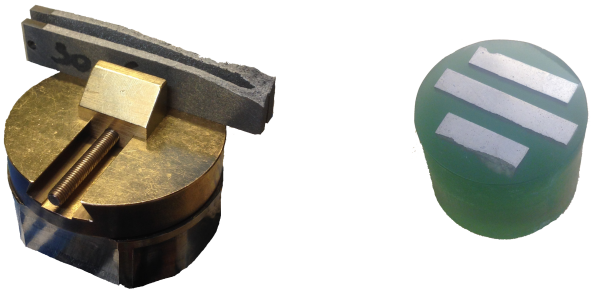

(a) Fractography (b) Microstructural analysis

Figure 3.12: Prepared specimens

3.4. Data Processing

Different measurement approaches are used to measure the crack propagation rate, crack path, strain field, fracture surface and microstructure. However, before the some data sets can be analysed, post processing is needed.

Three different approaches were used to measure the crack propagation rate. Figure 3.8, illustrated what was measured by these techniques. From the three methods, only striation counting measures the crack propagation rate directly. The extensometer measures the crack opening mouth displacement, which means that two processing steps are required before the crack propagation rate is obtained. First, the crack length should be calculated from which the crack propagation rate can be calculated. Visual inspection skips one step but still some processing should be done. By measuring the crack length instead of the crack propagation rate, this calculation step is still required. When all crack propagation rates are known, the stress intensity factor should still be calculated for all methods to create the Paris curves.

For the crack path and strain field, post processing steps are needed to compare the results in a more quantitative way. Both measurement techniques, provide visual data which can be hard to compare. Therefore, post processing is needed in order to compare the results in an easier way using plots.

Below, all required post processing steps are explained in more detail.

3.4.1. Crack propagation data

The processing steps required to calculate the crack propagation rate for extensometer and visual inspection data are described below. Before explaining these, the calculations required to obtain the stress intensity fac-

tor are shown first, as they are necessary to create the Paris curves for all approaches.

With a calculated crack propagation rate for the three measurement approaches, only the stress intensity factor (ΔK) should be determined to create the final Paris curve. An equation for the stress intensity factor was given before, in Equation 2.1, and is shown again below in Equation 3.1. As discussed before, the β factor depends on the geometry and changes for different specimens. Tada [28] provides β factors for all kind of specimens. The β factor for a single edge notch specimen is shown in equation 3.2. Where a is the crack length and w is the width of the specimen.

$$\Delta K = \Delta\sigma\sqrt{\pi a}\beta \tag{3.1}$$

$$\beta = 1.12 - 0.231\left(\frac{a}{w}\right) + 10.55\left(\frac{a}{w}\right)^2 - 21.72\left(\frac{a}{w}\right)^3 + 30.39\left(\frac{a}{w}\right)^4 \tag{3.2}$$

Finally, the stress intensity factor can be calculated for all crack lengths. In the end, a Paris curve is created by plotting the crack propagation rate ($\frac{da}{dN}$) versus the stress intensity factor(ΔK).

Below, the post processing steps for the extensometer and visual inspection data are shown.

Extensometer

As discussed before, the extensometer measures the Crack Mouth Opening Displacement (CMOD). From this displacement, the crack propagation rate can be calculated, however two processing steps are needed. First, the CMOD should be transformed to a crack length, after which, the crack propagation rate can be calculated from all crack lengths and corresponding cycles. The processing steps are illustrated in Figure 3.13.

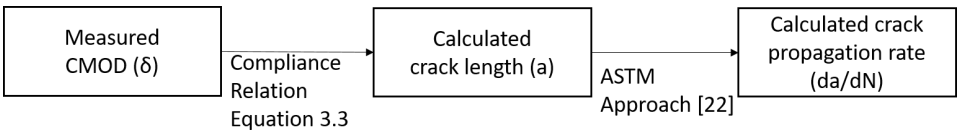

Figure 3.13: Data processing steps required - Extensometer data

The extensometer gives the crack mouth opening displacement for every cycle throughout the test. However, this CMOD should first be related to the crack length for every cycle. Consequently, a relation between the CMOD and the crack length is needed. 'The stress analysis of cracks handbook' of TADA [28] provides those kind of theoretical relations for different situations. For the single edge notch specimen, an equation is provided, which is shown below in equation 3.3.

$$\delta = \frac{4\sigma a}{E'}\frac{1.46 + 3.42(1 - cos\frac{\pi a}{2b})^2}{(cos\frac{\pi a}{2b})} \tag{3.3}$$

In this equation, the crack mouth opening displacement is denoted by δ, σ is the applied stress and E' is the stiffness term. This stiffness term, E',changes for specimens loaded in plane strain or plane stress conditions. Since the test is performed in plane stress conditions, E' equals E, which is the material stiffness. Furthermore, the crack length is denoted by a in the equation while b is the specimen width. Using this theoretical equation, the crack length for every cycles can be calculated, in matlab.

With all crack lengths and their corresponding number of cycles known, a representable crack propagation rate can be calculated. The crack propagation rate is calculated using the Incremental Polynomial Method which is provided by the ASTM Standard E647 [22]. This method calculates the crack propagation rate by fitting a second-order polynomial to sets of 2n+1 successive data points. In this experiment, n was set equal to 3. By fitting the curve, the crack propagation rate is calculated for different moments in time.

In the end, a crack propagation rate is calculated based on the CMOD measured by the extensometer.

Visual Inspection

Every 1000 cycles, the specimen is photographed. By manually measuring the crack length at different moments in time, the crack propagation rate can be calculated. Since the crack length is directly measured, only one processing step is required to calculate the crack propagation rate. This is illustrated by Figure 3.14.

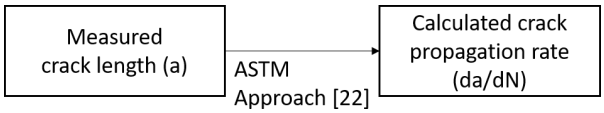

Figure 3.14: Data processing steps required - Visual inspection data

When the crack length is measured from the pictures and the corresponding cycles is known, the crack propagation rate can be calculated. In order to do this, the Incremental Polynomial Method will be used which was explained in the previous section.

3.4.2. Crack path data

Using camera images, the crack path can be identified. Comparing the crack paths against each other can be rather difficult. Plotting them together in a graph will make it easier to identify differences. Therefore, the pictures are post processed first.

An online program called 'WebPlotDigitizer' was used to subtract the crack path coordinates. The program gives the x and y-values of a selected point. When putting points on the crack path every millimetre, an accurate set of x and y locations is obtained. Afterwards, these can coordinates be plotted using matlab which will give the crack path in a digital form.

3.4.3. Strain field data

DIC data is used to visualise the strain field during the experiment. However, the results created by Vic3D are videos. Comparing videos in a quantitative manner is rather difficult. Therefore, the results are post-processed using matlab.

Using Vic3D, the surface has to be meshed to let the technique work. However, when meshing this area the crack opening will be considered in the analysis. As the crack grows, the distance between the two fractured sides will increase. This distance may be interpreted by the program as large strains. To avoid this misinterpretation, the cracks are cut out of the meshed subset area.

Comparing the DIC results will be done by analysing the magnitude and the orientation of the strain fields. When a crack grows, the strain field changes. In order to compare the results in a correct way, the strain field should be compared for equal crack lengths. Four different crack lengths were selected namely, 10, 20, 25 and 30 mm.

The analysis of the strain field will be done based on contour plots showing the Von Mises strain. The Von Mises strain was chosen as plastic zones are a combination of the strain and shear strain in all directions. Every specimen will have a contour plot for each crack length. To keep the contour plot easy to compare, three different strain ranges are used. These ranges are listed below.

- Low strain values. Von Mises strain is smaller than 0.0025.
- Medium strain values. Von Mises strain is between 0.0025 and 0.0075.
- High strain values (Plastic zone). Von Mises strain is larger than 0.0075.

Using certain ranges makes it easier to compare the magnitude and direction of the strain field. In the medium range, the material still behaves elastic but it gives an indication how the orientation of the strain field looks like. The higher strain range gives an indication if large plastic zones are present. The yield strain value was calculated using the yield stress of the material and the stiffness of the material. A yield stress of

825 MPa was used for all specimens, which is a value received from the NLR. With a stiffness of 110 GPa [12], a yield strain equal to 0.0075 was calculated.

4

Results

In order to come up with results, fatigue tests were performed at the faculty of Aerospace Engineering. By using a constant load cycle, a propagating crack was created. Crack propagation rates were measured using an extensometer, visual inspection and striation counting. As a second research objective, the crack path was measured using a camera. Further information during the test was obtained by a DIC cameras, which could be used to analyse the strain field during the test. After the tests, fractography and a microstructural analysis were also performed to gain more information about the fracture surface and microstructure.

All this gathered information is shown in this chapter. As some post processing was needed for a few measurement approaches, the raw results will be shown as well as the processed results. Analysis of the results revealed that the crack propagation rate is not affected by a change in build orientation or heat treatment, even if the specimen was printed off-axis. Nevertheless, the off-axis printing direction, as well as the choice of heat treatment, did seem to influence the crack path. For three specific off-axis specimens, repetitive crack deflections were found in all their tests. DIC results showed similar results for all cases and only small increases in strain were found parallel to the applied stress for HIPed specimens. As was expected, a lamellar microstructure was observed during the microstructural analysis. Both the build orientation and heat treatment influenced the microstructure as they respectively changed the anisotropic direction or increased the grain size.

4.1. Crack propagation rate

Measuring the crack propagation rate was done using three different measurement approaches. By measuring the crack mouth opening displacement with an extensometer, manually measuring the crack length from pictures and measuring the striation spacing, the crack propagation rate was measured in three independent ways. Except for the striation counting, the data had to be post processed to obtain the crack propagation rate. The processing steps required were described before in Section 3.4.

Figure 4.1 shows both the raw and processed results for the extensometer measurements. On the left, the crack mouth opening displacement is plotted versus the number of cycles. This CMOD can be changed into the crack length using Equation 3.3. This results in the crack length versus number of cycles, which is shown on the right in Figure 4.1b.

The results from visual inspection are shown in Figure 4.2. This figure shows how the results are manually measured from the pictures and transformed in a crack length versus number of cycles plot.

Finally, Figure 4.3 gives an example of measuring the crack propagation rate directly. The distance of a number of striations is measured which is eventually divided by the number of measured striations.

When processing the extensometer and visual inspection data as described in Section 3.4 and dividing the striation distance by the number of striations measured, the actual crack propagation rate can be calculated.

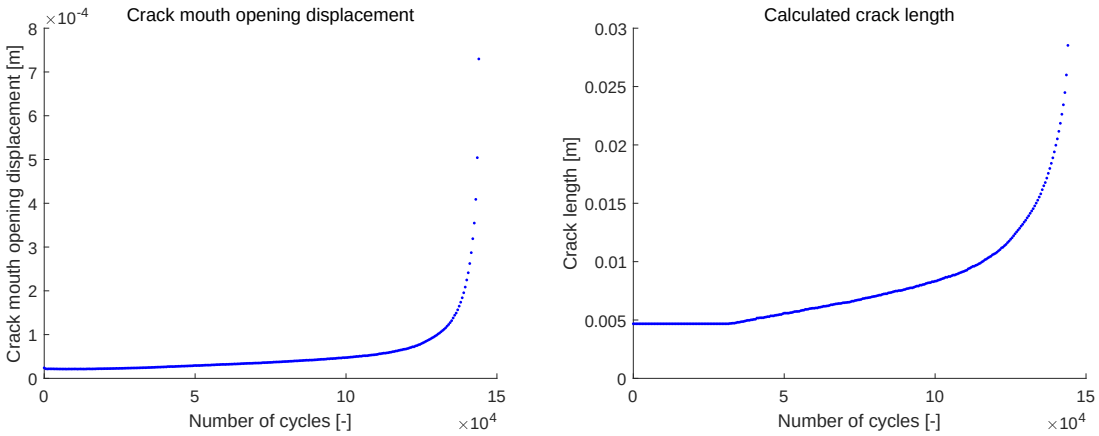

(a) Measured crack mouth opening displacement (b) Calculated crack length

Figure 4.1: Raw and processed extensometer data - Specimen_60_6

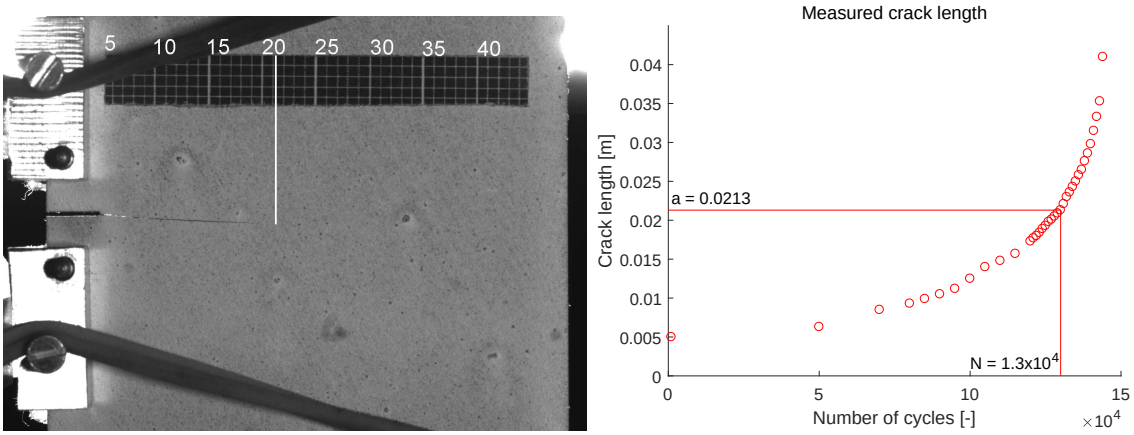

(a) Single crack length measurement at cycle 130000 (b) Measured crack length

Figure 4.2: Raw visual inspection data - Specimen_60_6

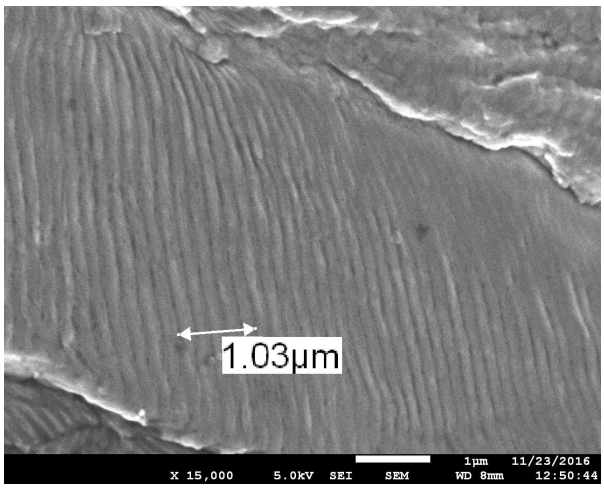

Figure 4.3: Striations measurement for specimen_60_6 - Distance of 5 striations measured

By plotting the crack propagation rates with the calculated stress intensity factors, Paris curves are obtained. When plotting all Paris curves together in one plot, similar results should be obtained as they all measured

the same crack growth. This is done in Figure 4.4, where the Paris curves for specimen_60_6 are plotted.

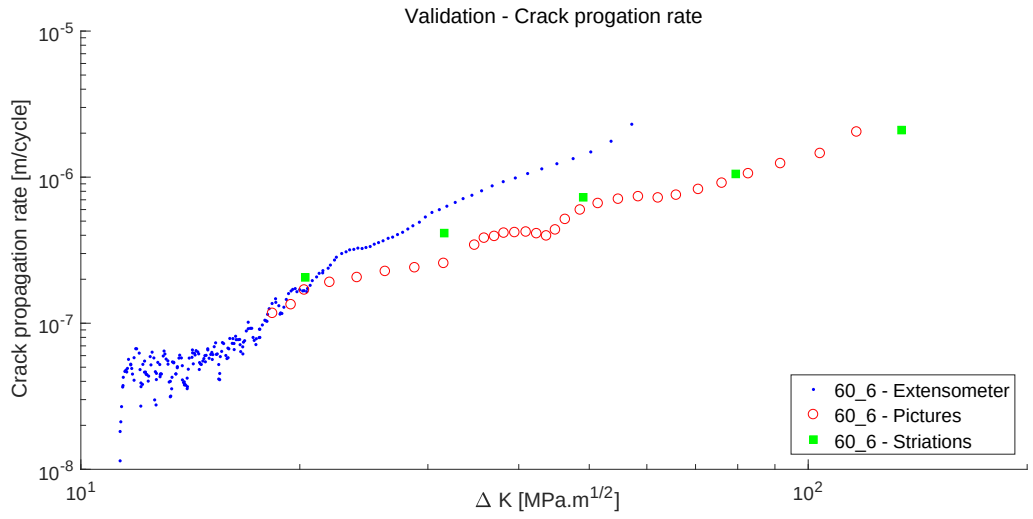

Figure 4.4: Crack propagation rate data - Three different measurement approaches

In Figure 4.4, differences in the results can be seen. As the striation counting method measures the crack propagation rate directly, it can be concluded that these results represent the crack propagation rate correctly. As can be seen in the results, the Paris curve based on the Visual inspection data corresponds to the Paris curve obtained by measuring the striation spacing. As these results are obtained independent from each other, it can be concluded that also the visual inspection results represent the crack propagation rate well. However, the Paris curve calculated from the extensometer data does not comply with the other two results. In order to find out what caused this misfit, the crack length over the lifetime is plotted for both the extensometer data and the Visual inspection data. This can be seen below in Figure 4.5.

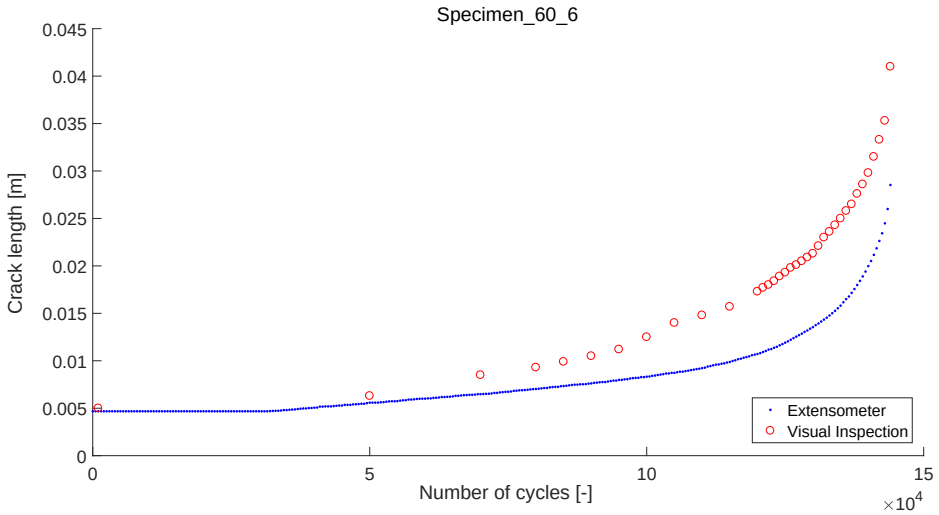

Figure 4.5: Crack length vs number of cycles - Extensometer and Visual inspection

The calculated crack length does not match the crack length measured from the pictures. For small crack lengths the data looks similar. However, with increasing crack length, the error also increases. Based on these crack lengths, it can be said that the TADA equation, Equation 3.3, underpredicts the actual crack length. Calculating a crack propagation rate from this data would result in a lower crack propagation rate. As these crack lengths will also be used to calculate the stress intensity factors, lower ΔK values will be calculated, which will

result in a steeper Paris curve, as can be seen in Figure 4.5. Thus, it can be concluded that a direct implementation of the equation cannot done. The reason for this mismatch can be explained by one of the test setup limitations, the height over width ratio which was lower than preferred. A full explanation is provided in the discussion of this thesis, Chapter 5. Besides this, one should also consider that the CMOD measured, it not the real CMOD. As the CMOD is measured at another locations, small strains in the material might also be measured.

As the extensometer results do not represent the correct crack propagation properties and little data points from the striation counting are available, only the Paris curves based on the Visual inspection data will be used. The Paris curve for all specimens are shown below. To clearly show the effect of the individual variables, the results are plotted twice. First, the heat treatments will be used as a fixed parameter. This will allow the reader to see the effect of the build direction. Then, the build direction is kept constant allowing the reader to see the effect of a different heat treatment on the Paris curve.

Effect of build direction

The effect of the build direction can be seen when plotting the results in two separate graphs. Both graphs can be seen below in Figure 4.6.

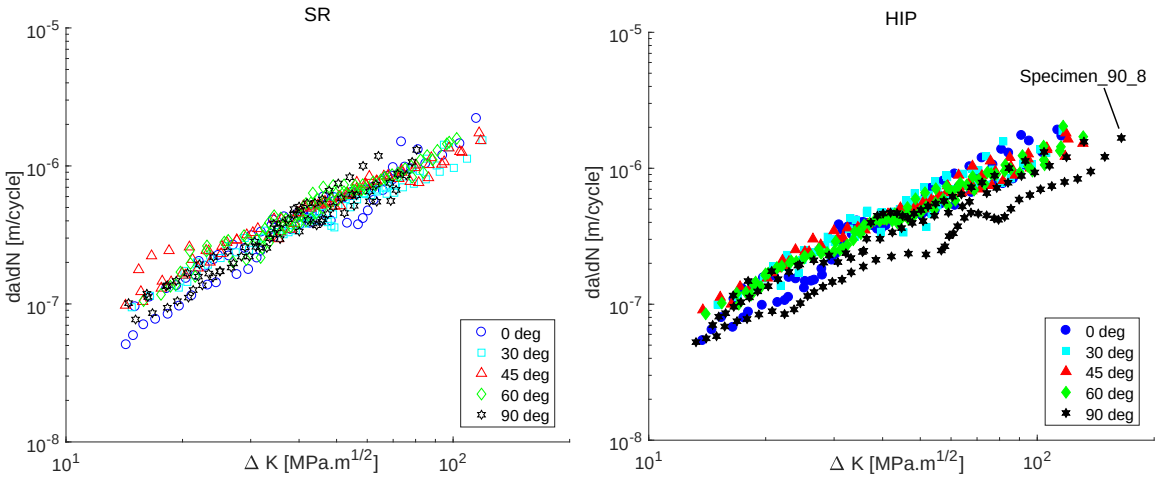

Figure 4.6: Paris curve - Effect of orientation for both heat treatments

By looking to the results, no large differences in the results can be seen. All results are very similar, similar crack propagation rates over the whole stress intensity range and similar slopes.

Although the results look similar, one outlier can be identified for the HIP specimens. The results of specimen_90_8 seems to be shifted to the right. Which means that the crack propagation rate is better for this specimen. Based on these results only, no explanation can be given for this outlier. Further investigation is needed to explain this results, this is done in Chapter 5.

Looking to the results in more detail, one may argue that the crack propagation rates are smaller for 0 degree specimens at low values of ΔK. This effect is noticeable for both the SR and HIP specimens.

Overall, it can be said that the results looks similar in all cases, which means that there is no or little effect of an (off-axis) build direction on the crack propagation rate.

Effect of heat treatment

A similar analysis is performed to investigate the effect of the two different heat treatments. For this case, the results are shown in five different plots, all having a different build direction. This can be seen below in Figure 4.7.

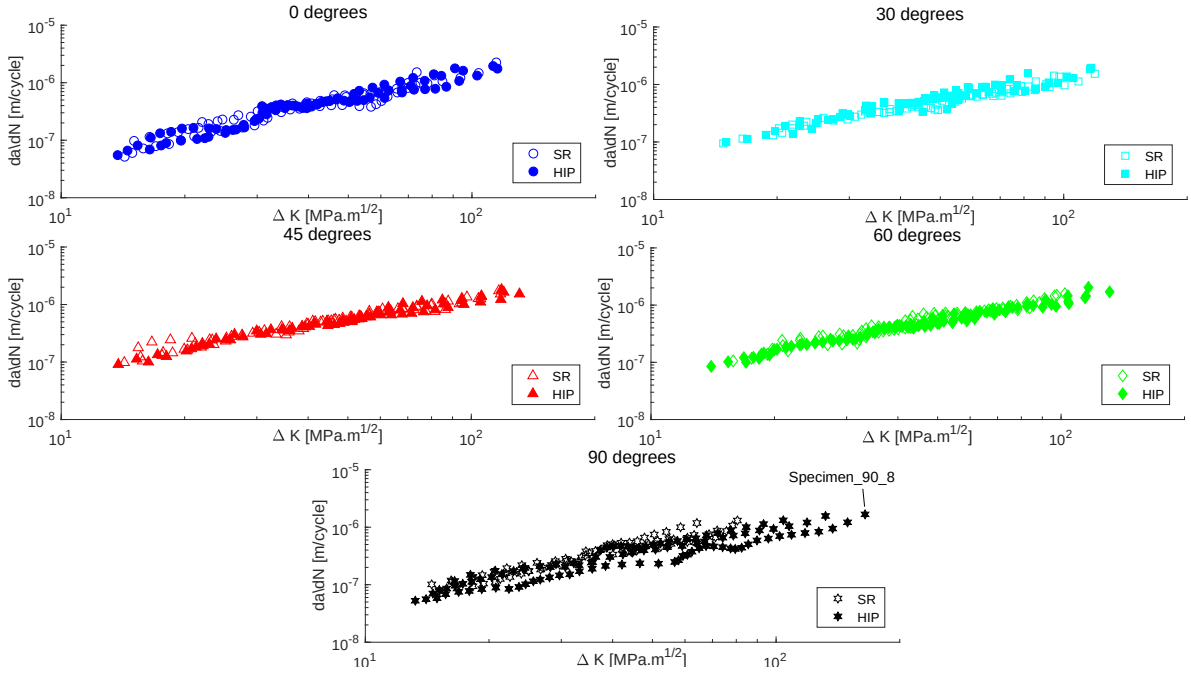

Figure 4.7: Paris curve - Effect of heat treatment for all orientations

Again, the results look similar for all different build orientations. No large differences can be seen which leads to the hypothesis that heat treating the material with a SR or a HIP treatment would result in similar crack propagation rates.

In general, the hypothesis can be made that a different build orientation or heat treatment does not affect the crack propagation rate of SLM Ti-6Al-4V.

4.2. Crack path

Information about the crack path direction is obtained by making pictures of the specimen. Chapter 3, described how these pictures were made and post processed. Post processing was done to digitalize the crack path which makes the analysis of the results easier. A raw result and the digitalized crack path can be seen in Figures 4.8a & 4.8b. Figure 4.8c shows a superposition state where it is shown that the digitalized crack path is equal to the real crack path.

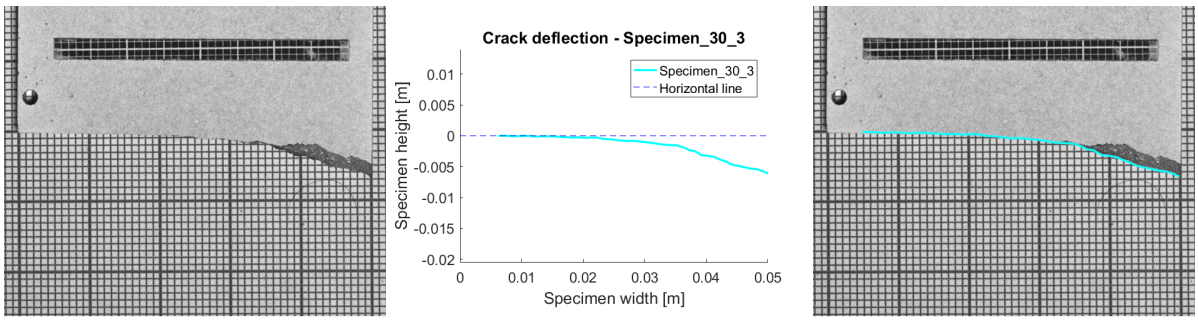

(a) Real crack path (b) Crack path in matlab (c) Crack path superposition

Figure 4.8: Crack path superposition - Specimen_30_3

Figure 4.9 shows the results for all post processed crack paths. Both heat treatments are plotted separately which makes it easier to compare the results. Crack path results plotted according to their build orientation are shown in Appendix B.2, as well as a plot with all crack paths together.

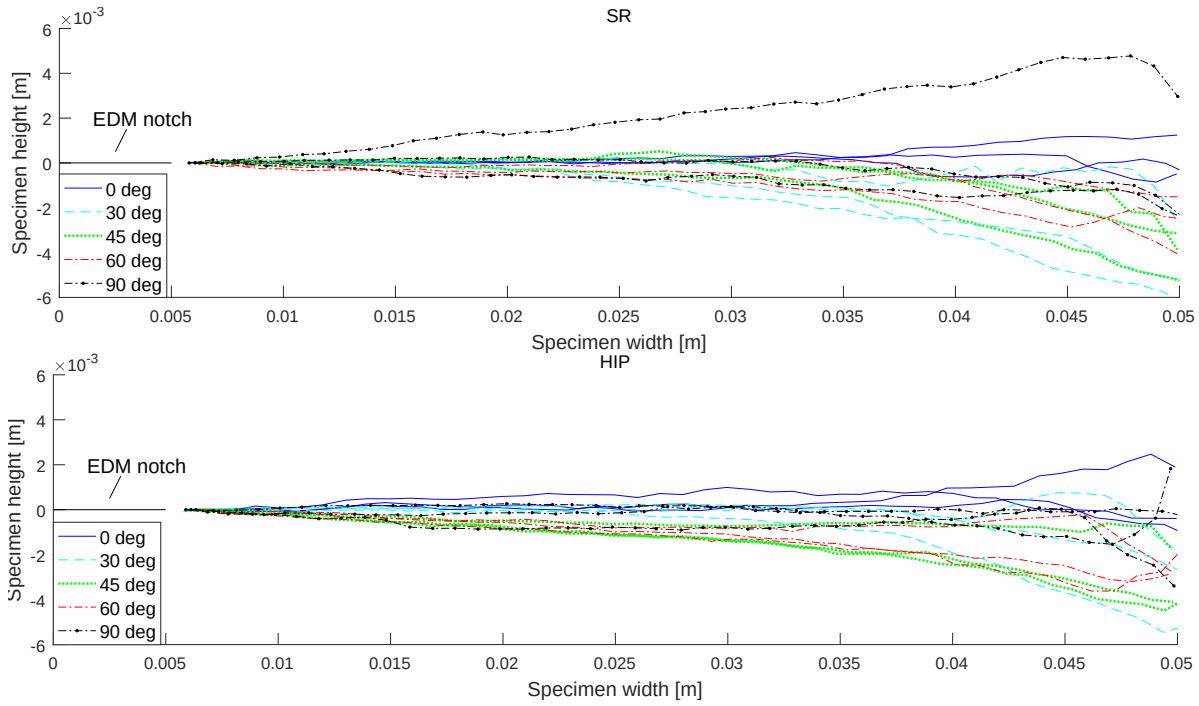

Figure 4.9: Crack path - Effect of build direction

By looking to the results, some interesting observations can be made.

First, it is clear that some crack paths do not follow the expected crack propagation direction, which is perpendicular to the applied load (horizontal in the plots). Instead, some cracks move away from the horizontal line when the crack length increases.

If a crack tends to deviate, it can be seen that in all cases (except one outlier) the crack deflects downwards. However, this crack path deviations are rather small with a maximum crack path slope of -4° (Specimen_60_6).

Largest crack path deviations can be seen for 30° with a stress relieving heat treatment and 45° & 60° which had a HIP treatment. For these specimens, crack deviations occurred for all tests. Therefore, it seems that a combination of the build orientation and applied heat treatment affects the crack propagation direction.

A final interesting observation can be made when looking to the crack length where crack deflection occurs. For 30° - SR, the crack turns at a crack length around 0.02m and has a steeper slope and more scatter in the results. Whereas the crack deflection for 45° & 60° - HIP starts at the initial crack length and has a constant slope with little scatter in the results.

4.3. DIC

In order to explain possible effects of build orientation and/or heat treatment on the stress/strain field, a DIC analysis was performed. Using two cameras, pictures were made of the speckled specimen surface, which were processed by 'Vic3D'. The quality of a DIC analysis depends on the level at which unique pattern can be tracked on the surface. Vic3D meshes the surface of the specimens, to create these unique meshes. Due to the speckle size on the surface, a subset size was of 29 was used for all specimens. This subset size was selected based on the mean uncertainty error provided by Vic3D which was kept around 0.01.

Raw results from the DIC analysis can be seen in Figure 4.10, where the Von Mises strain can be seen for

specimen_60_6.

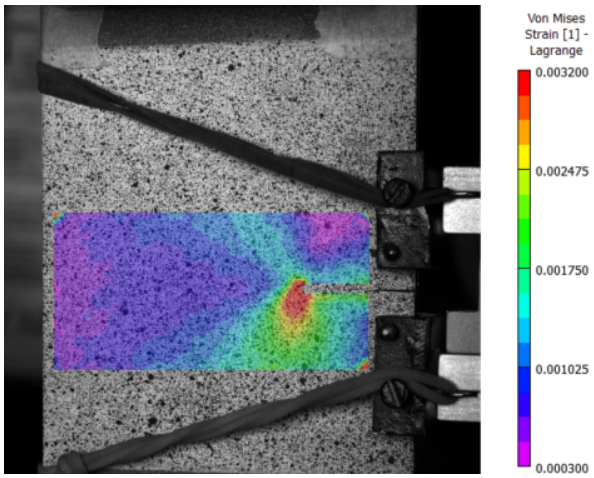

Figure 4.10: Raw DIC results - Specimen_0_4 - Crack length = 0.02 m

However, as was described before in Section 3.4, analysing such pictures can be rather difficult. Therefore, the results were post processed by plotting contour plots for four different crack lengths namely, 10, 20, 25 and 30 mm. To keep the contour plot easy to compare three different strain ranges are used. These ranges are listed below.

- Low strain values. Von Mises strain is smaller than 0.0025.
- Medium strain values. Von Mises strain is between 0.0025 and 0.0075.
- High strain values (Plastic zone). Von Mises strain is larger than 0.0075.

Below, the strain fields are plotted. Only a selection is shown below, all other results are shown in Appendix B.3. However, this selection gives a good representation of how the results look like. When looking at the results below (Figures 4.11 & 4.12), one should keep in mind that the crack is running from right to left, as the cameras were positioned at the other side of the specimen. Besides that, the DIC specimens were flipped (up side down) in the fatigue machine to eliminate any influences of the fatigue machine. For the analysis of the results, the strain fields are flipped again to their original position. This is why the processed results, in Figures4.11 & 4.12, might look upside down compared to the raw Vic3D results in Figure 4.10.

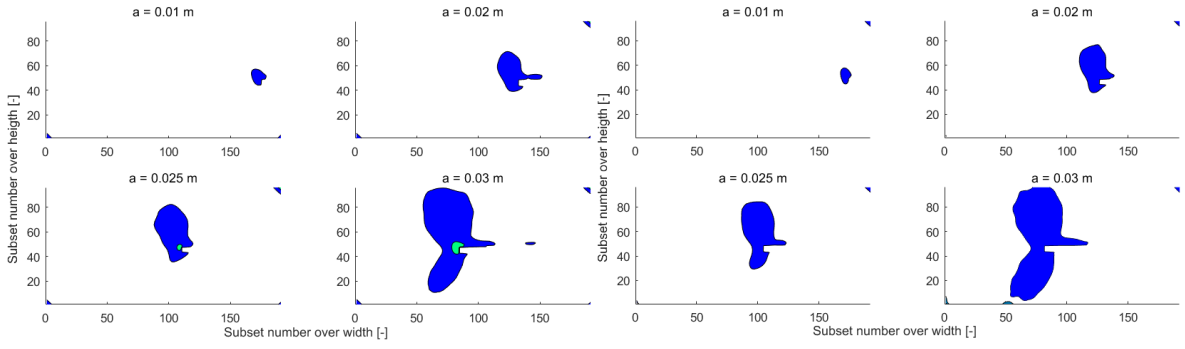

(a) Specimen_0_4 (b) Specimen_45_6

Figure 4.11: Strain field - White: VM < 0.0025; Blue: 0.0025 < VM > 0.0075; Green: VM > 0.0075

Besides contour plots, the strain values in X and Y direction over the height of the specimen are also shown. These results can be used to explain differences in the Von Mises strain fields. Strains in X and Y

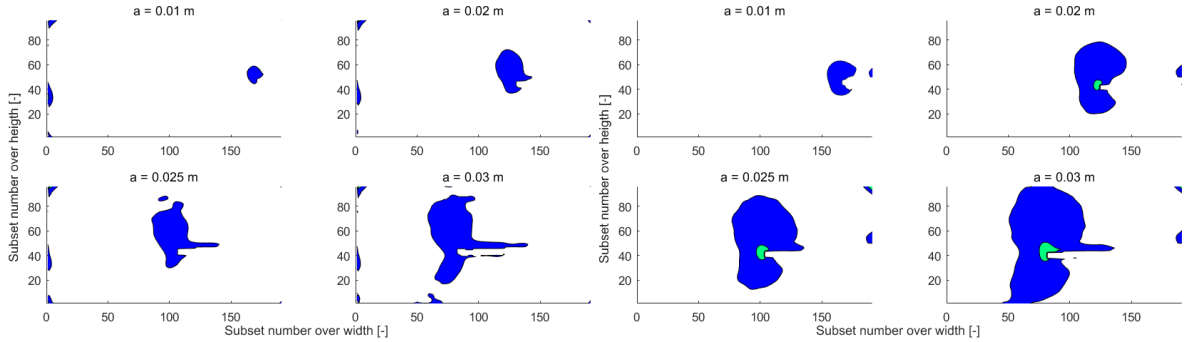

(a) Specimen_60_2 (b) Specimen_90_6

Figure 4.12: Strain field - White: VM < 0.0025; Blue: 0.0025 < VM > 0.0075; Green: VM > 0.0075

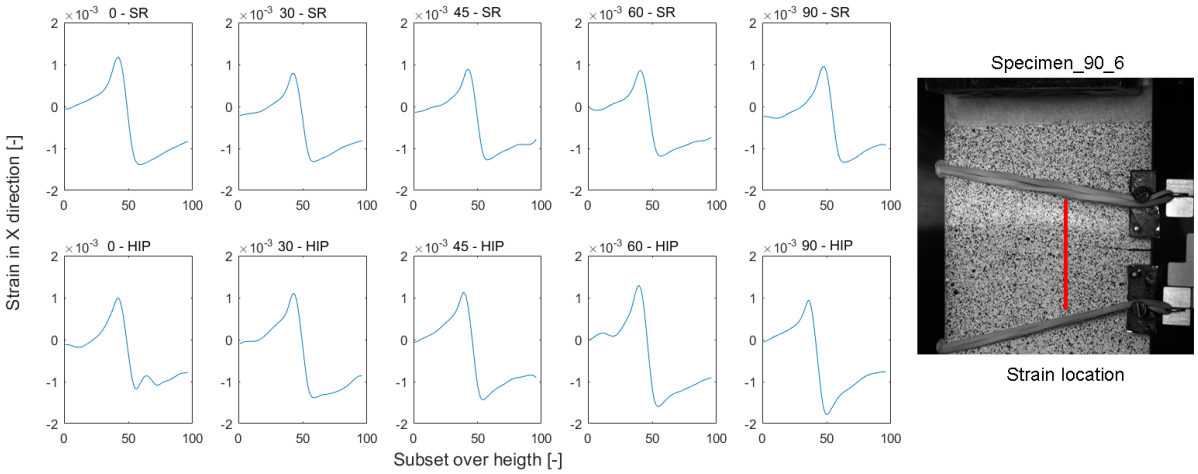

Figure 4.13: Strain in X direction over the height of the specimen

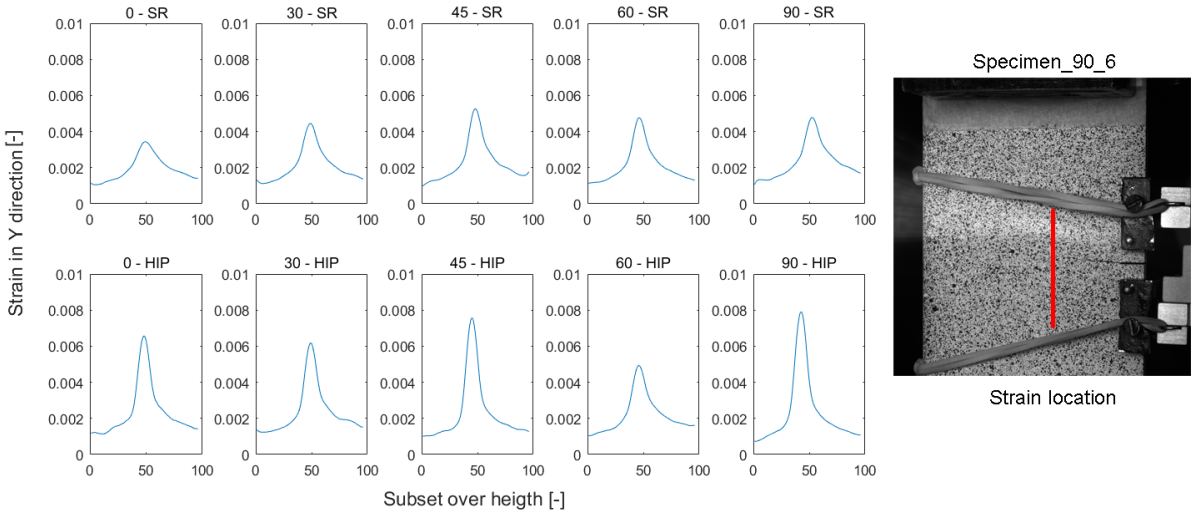

Figure 4.14: Strain in Y direction over the height of the specimen

direction are measured for a crack length of 20mm.

Looking to the strain fields no large differences can be identified. However, some observations can be

made.

Overall shape and size of the Von Mises strain fields look similar for all specimens. However, one outlier can be identified which is specimen_90_6.

The shape of the strain field for specimen_90_6 looks different compared to other. The size of the strain field larger than 0.0025 and larger than 0.0075, is bigger compared to other specimens. Figure 4.14 shows that the strain in Y direction is larger for specimen_90_6, while the strain in X direction is similar to all other specimens (Figure 4.13). This increased strain in Y can be the reason for a larger Von Mises strain. Nevertheless, more information about the specimen is needed to find out the cause of the increased strain in Y direction.

When looking at the X and Y strains at a crack length of 20mm, it can be seen that all strains in X direction looks similar for all directions and orientations. When comparing the strains in Y direction, one can argue that larger strains are measured for the HIPed specimens. Larger strains near the crack tip are measured with equal applied stresses. However, in the far field the strain are relative the same for SR and HIP. Therefore, the hypothesis can be made that the yield stress is a bit lower for HIPed specimens. This effect was also found by Vrancken [25], who accounted this effect to the higher temperatures used during the HIP treatment which results in coarser α and β. Therefore, one can hypothesize that the yield stress is lower for HIPed specimens, however no mechanical tests were performed to confirm this hypothesis. Analysis of the microstructure on the other hand may confirm that coarser α and β grains are present for HIPed specimens.

Finally, one may also argue that the difference in strain between SR and HIP is larger for smaller build orientations. However, nothing is mentioned about this effect in literature and microstructural analysis is needed to explain this effect.

4.4. Fractography

For the analysis of the fracture surface, the Scanning Electron Microscope (SEM) was used. For every specimen, overview pictures were made at four different locations at the fracture surface. A picture was made at the start of the crack (1), in the middle of the crack propagation phase (2), the transition phase (3) and final failure region (4). Figure 4.15 gives an impression where these location are situated.

Pictures shown below were made at location '2', which is a crack length in between the initiation and final failure phase.

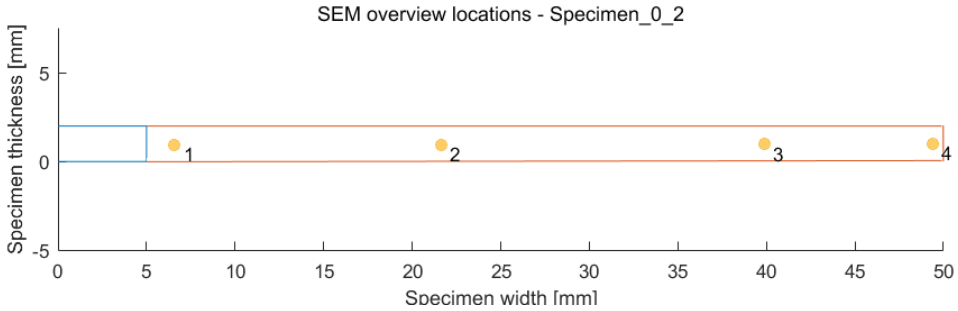

Figure 4.15: SEM overview locations

Overview pictures are shown for four different specimens in Figures 4.16 & 4.17. Two different orientations are shown, one orthogonal (0 degrees) and one with an off-axis (30 degrees) build direction. For both orientations, a SR and a HIP specimen are given. Again, these specimens give a good representation for all other specimens which were tested.

When analysing the pictures, it is clear that the fracture surface is rather rough for all specimens. Due to this roughness, crack fronts could not be identified.

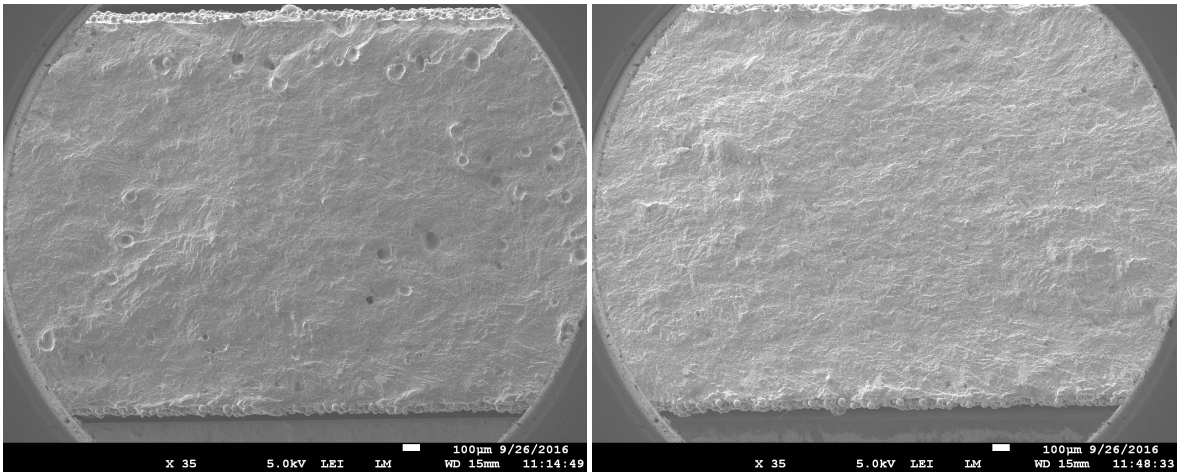

(a) Specimen_0_2 (b) Specimen_0_6

Figure 4.16: Fracture surface - 0 degrees build direction

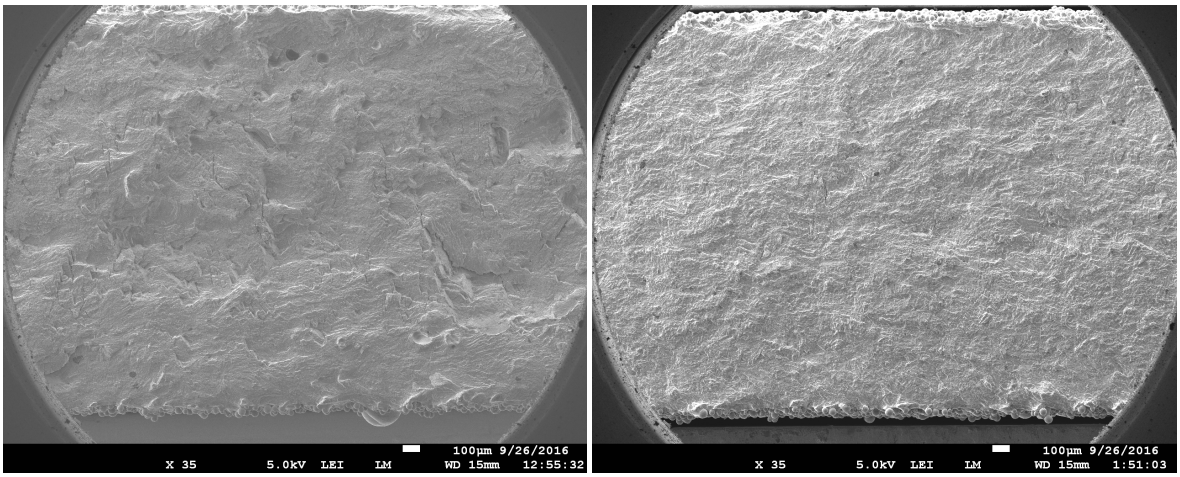

(a) Specimen_30_2 (b) Specimen_30_6

Figure 4.17: Fracture surface - 30 degrees build direction

Comparing the two heat treatments, a difference in void content can be seen. Specimens which had a HIP treatment show less voids. This result can be accounted to the heat treatment combination of the elevated temperature with a applied pressure. This combination drastically diminished voids in the material, which is one of the advantages of using such a heat treatment.

For all specimens, striations could be found at the fracture surface. These striations were used before to measure the crack propagation rate. However, striations were more difficult to find for SR specimens compared to HIPed specimens. This increased visibility for HIPed specimens, can be due to the lower yield stress which is a result of the increased grain size. Microstructural analysis should confirm this increase in grain size for HIPed specimens.

When looking to specimen_30_2, in more detail, cracks over the thickness of the material could be found. These sort of cracks were found at multiple fracture surfaces but only when the specimen was printed off-axis and has a SR heat treatment. A more detailed picture is shown in Figure 4.18.

In general, all fracture surface looked similar to the ones showed before. However, one exception was identified which showed areas of flattened peaks. In Figure 4.19, such a peak can be seen at the fracture surface of specimen_90_8.

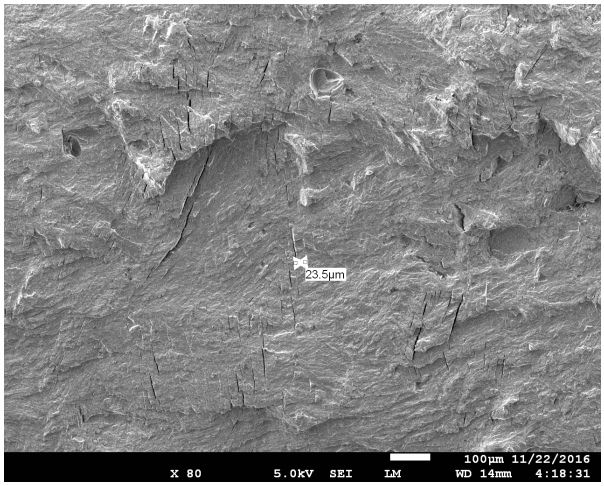

Figure 4.18: Cracks running over the fracture surface in the thickness direction

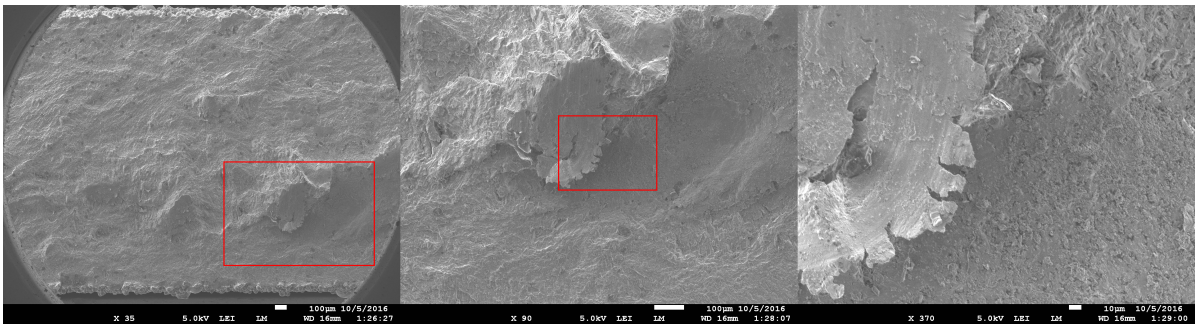

Figure 4.19: Flattened peaks at fracture surface - Specimen_90_8

Based on the picture, one can argue that the peak might have come in contact with something. This hard contact resulted in a flat peak and signs of rough fracture at the sides of this peak. This kind of contact can be created when the fracture surfaces hit each other during the test (crack closure) or by mishandling of the fracture surfaces after testing. In order to come up with a correct explanation, more information is needed. In Chapter 5, all results will be combined and discussed in more detail.

4.5. Microstructural analysis

Results of the microstructural analysis can be used to understand the potential influences of the microstructure on the crack propagation rate and direction. As the microstructure is highly correlated to the manufacturing process, differences in the microstructure are expected. For both heat treatments, a $\alpha + \beta$ lamellar microstructure with columnar prior β grains was observed. The microstructure is influenced by both the build orientation and heat treatments. A different build orientation changes the direction of the prior β grains where a different heat treatment changes the width α and β. In the following section, the effects are explained in more detail.

Effect of build direction

The microstructure and corresponding grain orientation of two specimens are shown below in Figure 4.20. These specimen were chosen due to their difference in build direction and heat treatment. The angle shown in the picture is the angle between the horizontal line and the grain orientation which is called θ, as shown in Figure 4.21. The θ values for all other specimens are given in table 4.1.

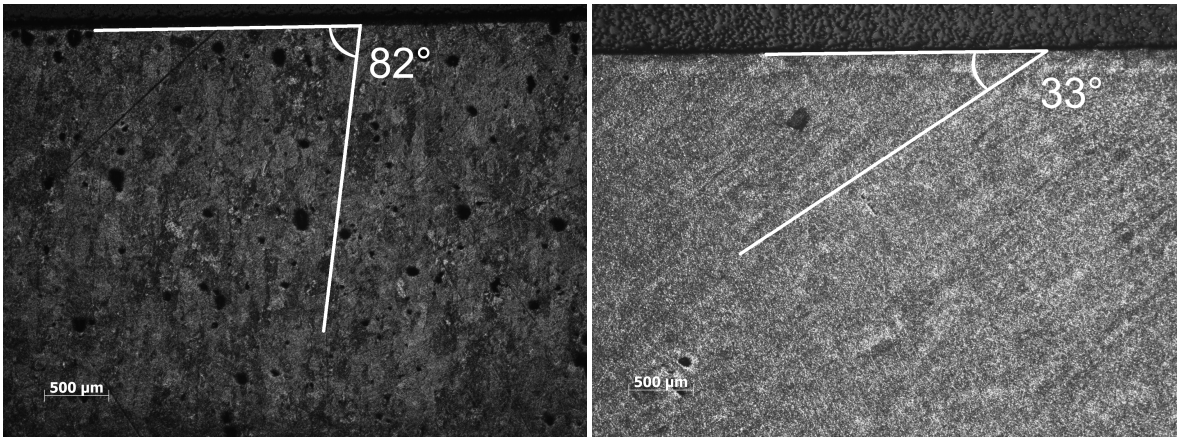

(a) Specimen_0_2 (b) Specimen_45_8

Figure 4.20: Grain orientation

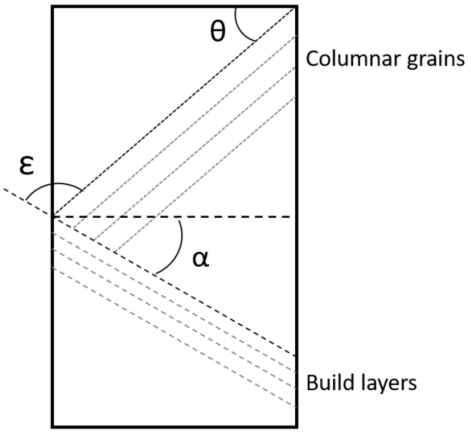

Figure 4.21: Angle description

Table 4.1: Angles for all specimens

Layer Orientation	Specimen	θ	ϵ
0	SR	82	98
0	HIP	79	101
30	SR	56	94
30	HIP	59	91
45	SR	31	104
45	HIP	33	102
60	SR	23	97
60	HIP	20	100
90	SR	-16	106
90	HIP	-14	104

The pictures confirm the presence of columnar grains. For both heat treatments, anisotropic behaviours can be seen. When looking to the measured angles, it can be seen that the direction of the columnar grains changes with a change in build direction, as was expected.

The angle between the layer orientation and the grain direction (α) is larger than 90° for all specimens. Although, they are all larger than 90°, the angle is not constant. For the same the build direction, the angle for SR and HIP specimens is similar. However, there is a large variation in angle when comparing the layer orientations. The angle variation can be different due to the difference in heat distribution when printing the specimens off-axis. However, this is not investigated in more detail as this is out of the scope of this research.

In general, it can be concluded that the build direction influences the orientation of the columnar grains. Where as a difference in heat treatment does not affect the direction or anisotropy of the material.

Effect of heat treatment

For this experiment, a stress relieving heat treatment was used as well as an HIP process. For both treatments, the microstructure is shown below in figures 4.22, 4.23 & 4.24.

Both heat treatments result in a $\alpha + \beta$ lamellar microstructure with predominantly α lamellae and columnar prior β grains. A few differences can be identified between both heat treatments.

Comparing the void content for both heat treatments, it can be said that less voids are present in the HIPed specimen. The same conclusions was found earlier when looking at the fracture surface.

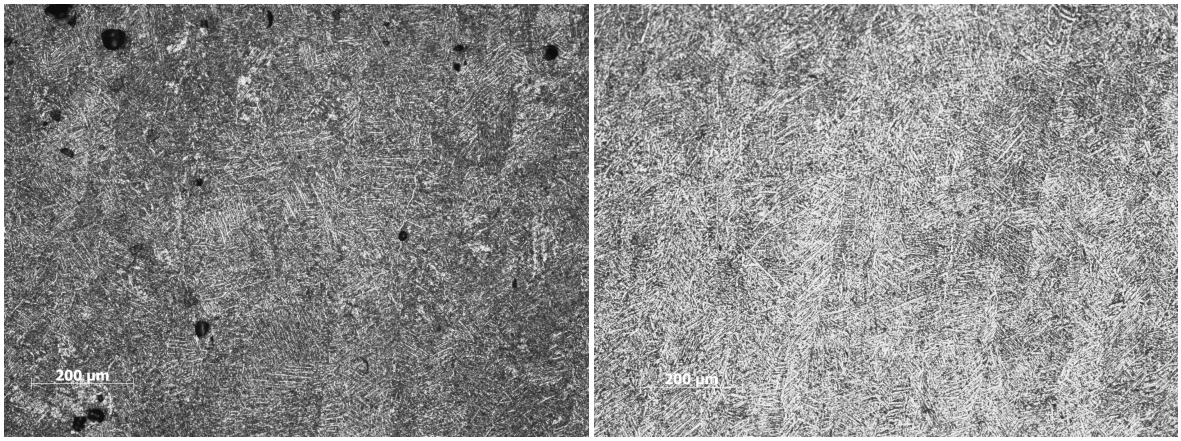

(a) SR (b) HIP

Figure 4.22: Microstructure for two different heat treatments - Magnification: 10x

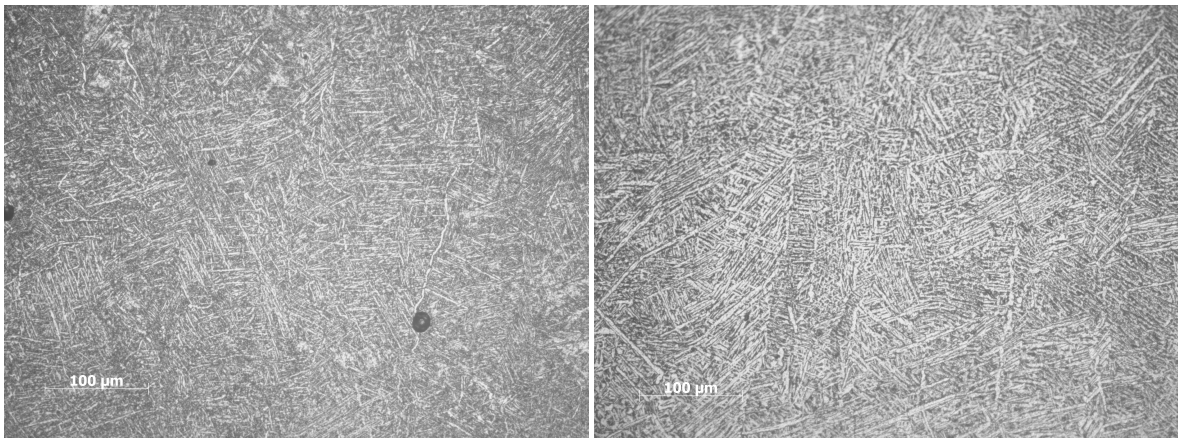

(a) SR (b) HIP

Figure 4.23: Microstructure for two different heat treatments - Magnification: 20x

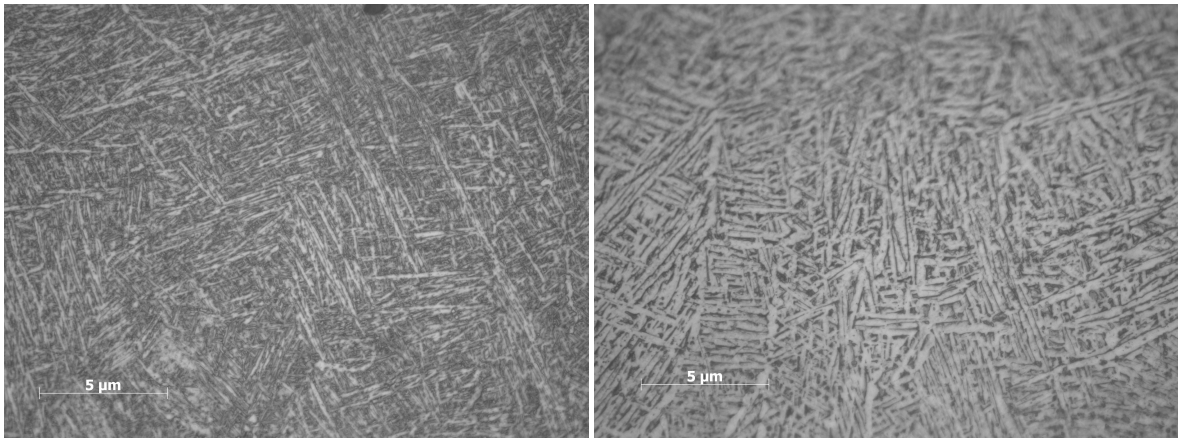

(a) SR (b) HIP

Figure 4.24: Grain size for two different heat treatments - Magnification: 50x

For both heat treatments, α lamellae are dominant in the microstructure. However, it seems that the α lamellae are coarser when the material had the HIP treatment. This can be accounted to the higher temper-

ature used during the extra HIP treatment. A temperature close to the β transus allows the grains to grow.

Fracture mechanism

Little is known about the fracture mechanism happening in SLM Ti-6Al-4V. Simonelli [24], stated that intergranular fracture along prior β grain boundary happened. These was observed when tested heat treated (730°) SLM specimen in a high cycle fatigue test. On the other hand, transgranular fracture was found to be the dominant fracture by Rafi [29]. In the heat treated (650°) SLM specimens, transgranular fracture happened due to separation at the α' martensitic plate interface.

Pictures of the microstructure are made near the crack path. Observation of the crack paths showed only a little amount of intergranular fracture for all specimens. Two reasons can be accounted for this. First, the predominant presence of the α lamellae. Intergranular fracture happens at the prior β grain boundaries, which is hard when only few are present in the microstructure. A second reason is the direction of the columnar prior beta grains. Due to the anisotropy property, there is an angle between the crack path and the prior beta grains.

The primary fracture mechanism found is transcolony fracture. The crack propagates through the α colonies. This happens parallel to lamellae direction or perpendicular to this direction. Both situations are shown in Figure 4.25. However, the fast cooling during the production process resulted in small α colonies. Which means that many small colonies have to be crossed and the crack has to change direction often.

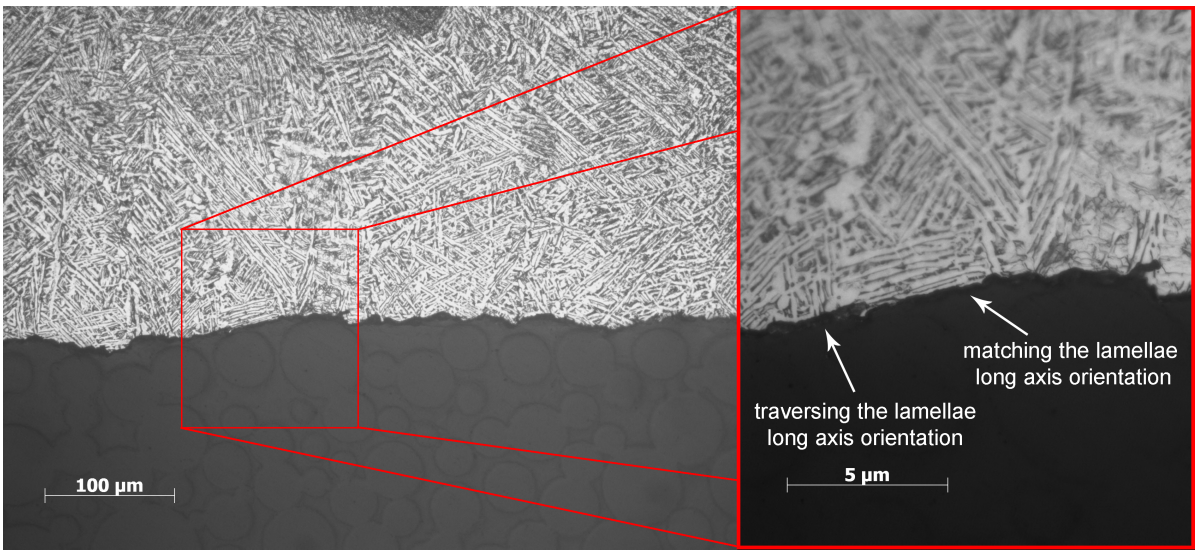

Figure 4.25: Fracture mechanism

5

Analysis and Discussion

In the previous chapter, raw and processed results were shown. The current chapter will discuss the results and draw conclusions based on them.

First, the effect of the smaller height over width ratio on the results will be discussed. A smaller h/w ratio influences the stress intensity factor as well as the crack mouth opening displacement. Therefore, when discussing the results the effects should be taken into account.

In the Paris curves, an outlier was observed which performed better than the other specimens. These improved crack propagation properties were caused by crack closure which were created by initial deformations of the specimen. The analysis and evidence for this cause are shown in this discussion.

Afterwards, the effect of build orientation and heat treatment on the crack propagation rate and direction are discussed. For both the rate and direction, the data obtained by all different measurement approaches are combined to come up with suitable hypotheses to explain the measured results.

In the end, the Paris curves obtained during the thesis will be compared to results from literature. Especially, the difference in plane stress and plane strain results will be described.

5.1. Effect of height over width ratio on crack propagation results

During the fatigue experiments, a height over width ratio of 0.8 was used while the ASTM standard [22] and TADA [28] require a ratio equal to 1. According the John [7], a difference in the height over width ratio affects both the stress intensity factor (Δ K) and the crack mouth opening displacement (CMOD). Before discussing the results, the effects on the results should be clear. As an h/w ratio of 0.8 was used in all fatigue tests, the relative performance of the results can be discussed. However, when comparing to the literature, a correction factor should be taken into account.

Effect on the stress intensity factor

A decrease in h/w, results in a decrease of the stress intensity factor, where the error increases with an increasing crack length [7]. Following this reasoning, the stress intensity factors in this thesis are overpredicted. This means that the Paris curves show better crack propagation performances compared to a real life situation.

This study focusses on the effect of build orientation and heat treatment on the crack propagation rate. As an equal h/w was used in all cases, conclusions can still be made on relative performance. However, when comparing to the literature, a correction factor should be considered to cope with this error.

A Finite Element Method (FEM) model was created to calculate the effect of a decrease in h/w and a correction factor was calculated. The FEM model and calculations can be seen in Appendix C. This correction factor is only used when comparing the results with respect to literature, which is done in Section 5.5.

Effect on the crack mouth opening displacement

Due to decrease in height over width ratio, a smaller crack mouth opening displacement is measured for equal crack lengths. Again this effect increases with increasing crack length, as John observed in his study [7].

In this thesis, the crack mouth opening displacement was calculated however did not match the expected results. For small crack lengths, the calculated crack length was similar to the measured crack length, however with increasing crack length the error increases and the crack length was underpredicted. The error in the results can be accounted to the smaller CMOD measured while still using the equation from TADA which assumes a h/w ratio equal to 1 [28].

Again, a correction factor can be calculated, however due to some other problems and an insufficient amount of valuable extensometer data, the decision was made to drop this data and use the visual inspection data to create the Paris curves.

5.2. Crack closure in specimen_90_8

The Paris curve results, Figure 4.7, showed one outlier which had improved crack propagation performance compared to the other specimens. Based on the fracture surface pictures, Figure 4.19, it is believed that crack closure caused these improved crack propagation properties.

During the fractographic analysis, flattened peaks were found at both sides of the fracture surface, as shown in Figure 5.1. When comparing both sides of the fracture surface, the flattened peaks were found at the same locations. Which leads to the hypothesis that the surfaces were in contact during the fatigue test and crack closure happened. The log-file of the fatigue machine did not show a change in the load cycle, meaning that the minimum load applied at the specimen was equal to 1kN. As the specimen was in tension throughout the whole fatigue test and still the crack closed, large plastic deformations in the wake of the crack should have been present. Nevertheless, during this experiment, the strain field was not measured so the hypothesis cannot be fully confirmed.

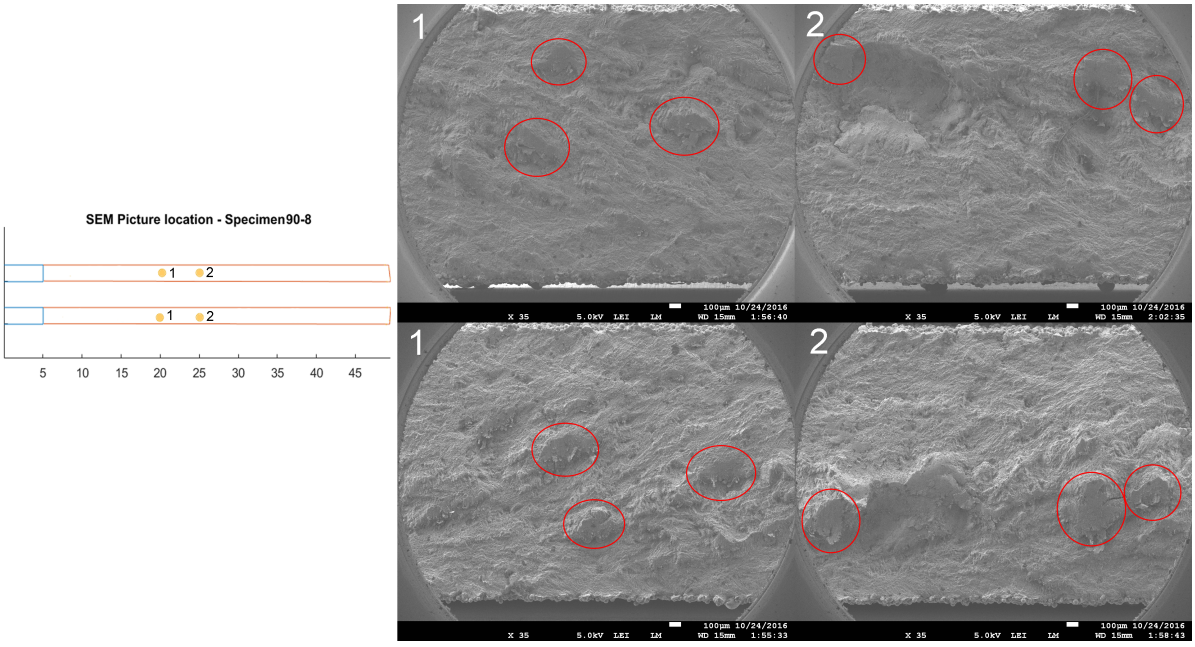

Figure 5.1: Crack closure at both fracture surfaces - Specimen_90_8

Still, it is interesting to know, what could have created this increased large plastic zone. Looking back to the fracture surface, it can be seen that the flattened peaks only occur at one side of the specimen. Over the whole crack length, flattened peaks were only found at one side of the specimen thickness. Therefore, if

internal stresses were present and created the large plastic zone, they were only present at one edge of the specimen.

The specific distribution of internal stresses can be explained when looking to the shape of the specimen_90_8 before testing. After production some specimens had some initial curvature over the height of the specimen. Figure 5.2 shows the picture after failure, still the initial curvature can be seen.

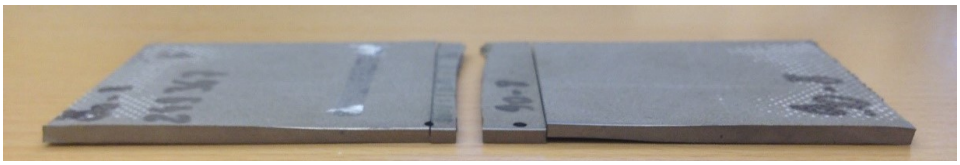

Figure 5.2: Initial deformation Specimen_90_8

When clamping specimens with initial deformations in the fatigue machine, small internal stresses will be created. The side where all the flattened peaks occurred corresponds to the concave side of specimen_90_8. This shows that internal tensile stresses together with the applied stress can have resulted in larger plastic zones. As said before, the strain field was not measured in this phase of the experiment which means that this hypothesis cannot be fully confirmed. However, specimen_45_6 and specimen_90_6 had similar (but smaller) initial deformations. When looking to the DIC results for both specimens, Figure 4.14, larger strains in Y direction are observed which were can be accounted to the initial deformations.

As the hypothesis states that the improved crack propagation properties were caused by crack closure due to initial deformations, the results for specimen_90_8 will be excluded for the conclusions.

5.3. Effect of build orientation and heat treatment on crack propagation rate

Based on the results, the hypothesis can be made that the crack propagation rate is independent of build direction and heat treatment. A change in the build direction or the use of a stress relieved treatment or a HIPing treatment, does not change the crack propagation properties of the material. This hypothesis is confirmed by Figure 5.3 where the mean and standard deviations for each type of specimen are plotted. A lot of overlap can be seen in the results for both the average average crack propagation rates as well as the standard deviations.

This result is rather remarkable and was not expected at the start of this thesis. Beforehand, different Paris curves were expected for different combinations of build orientation and heat treatment.

Literature showed that large tensile residual stresses parallel the building direction were the main reason for different crack propagation rates. Changing the building direction would thus result in different crack propagation rates. However, no or little variations in crack propagation rates are measured. Therefore, it looks like the heat treatments were successful in relieving the main residual stresses in the SLM Ti-6Al-4V specimens.

Secondly, it was expected that for small cracks, an increase in build direction angle would result in faster in crack growth. This hypothesis was based on the idea that for small cracks the influence of the microstructure is rather large and more energy at the crack tip is needed to propagate through grain boundaries. When a crack propagates from one grain to another, it has to change direction as the lattice orientation within the grains is different. In order to grow, the slip plane has to change direction, which requires more energy. Crack propagation within the α colonies would therefore be easier as the lattice direction would be equal. Relating this theory to this experiment, it would mean that for 0 degrees, more energy is required as the crack has to pass more prior β grain boundaries. While in an ideal situation, a crack would not need to pass any prior β grains for 90 degrees, when the crack runs parallel to the columnar grains. To summarise this means that the energy needed for crack propagation would be deceasing for increasing angles, which means that fast crack propagation rates would be measured. However, this effect is not observed. Figure 4.7 shows that both

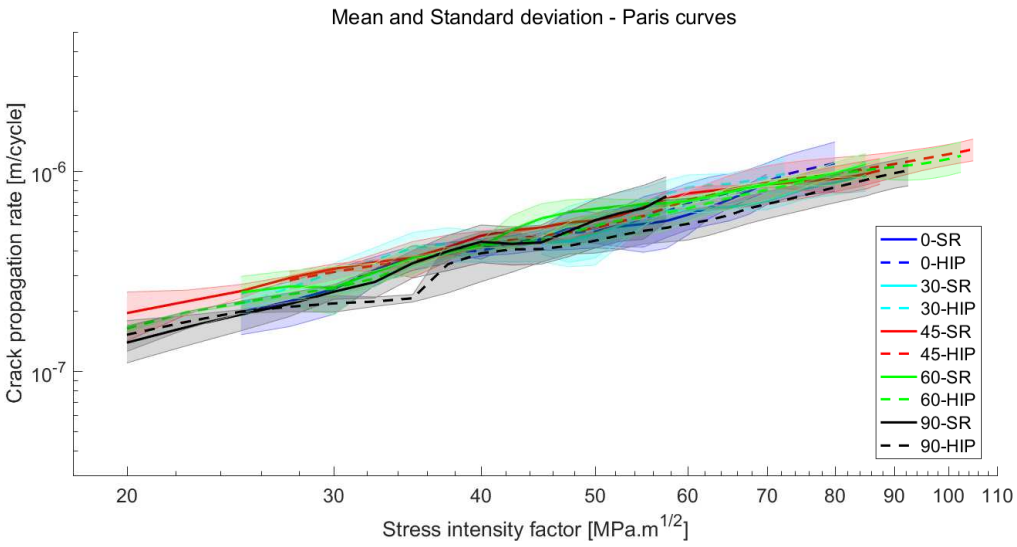

Figure 5.3: Mean and standard deviation - Paris curves

0 degrees and 90 degrees have similar crack propagation rates for small cracks. This observation would thus disprove the hypothesis. Nevertheless, it is possible that when an experiment is performed near the stress intensity threshold (stage I fracture), a difference due to build direction may be visible.

Furthermore, it can be seen that crack propagation rates for 90 degrees specimens are similar to the other directions. The crack propagation direction for 90 degrees specimens is more or less parallel to the columnar prior β grains. Therefore, it was expected that higher crack propagation rates would be measured, as the crack can follow the columnar grain boundaries and fail in an intergranular way. As the crack would be able to follow the columnar grain boundaries, less obstructions in the microstructure are expected, which would result in less energy required. However, crack propagation rates were similar for all build orientations, which means that a similar amount of energy was needed to grow the cracks. A possible explanation was found during the microstructural analysis.This analysis showed that the direction of the columnar prior β grains is not perpendicular to the build orientation. Due to heat distributions, an average angle between layer orientation and columnar grain direction between 90 - 115 degrees was measured. For both 90 - SR and 90 - HIP angles were measured which were respectively 106° and 104°. These specimens had cracks propagating normal to the applied load therefore, it is concluded that the crack did not follow the columnar β grains. However, still the hypothesis might be valid but would be visible for layer orientations between 80 and 85 degrees. This means that if the crack would follow the columnar beta grains and less energy is needed, it would be noticeable for layer orientations between 75 - 80 degrees. However, no data is available for these angles to confirm this line of thought.

Finally, from the DIC results, the HIPed specimens appear to have a lower yield stress, as could be seen in Figure 4.14. A lower yield stress would result in larger plastic zones which in its turn can result lower crack propagation rates. However, no differences were observed in crack propagation rates for stress relieved or HIPed specimens. As the real yield stress could not be measured, it is hard to say if larger plastic zones were present for HIPed specimens. Nevertheless, if this was the cases the difference in zone size was only limited as no remarkable differences in crack propagation results were observed.

5.4. Effect of build orientation and heat treatment on crack propagation direction

The crack path results showed some interesting effects. For specific combinations of build direction and heat treatment, cracks deflected from their original crack path. Therefore, it is hypothesized that the crack propagation direction is influenced by a specific combination of build direction and heat treatment.

In this hypothesis, the combination of build orientation and heat treatment is crucial. This makes it even more interesting since there was not a single build direction which showed crack deviations for both heat treatments. Depending on the heat treatments, different build orientations resulted in deflecting cracks. However, the results were repetitive which means that the material is causing this effect. This is proven again by Figures 5.4 & 5.5, where the mean and standard deviations are plotted for respectively stress relieved specimens and HIPed specimens.

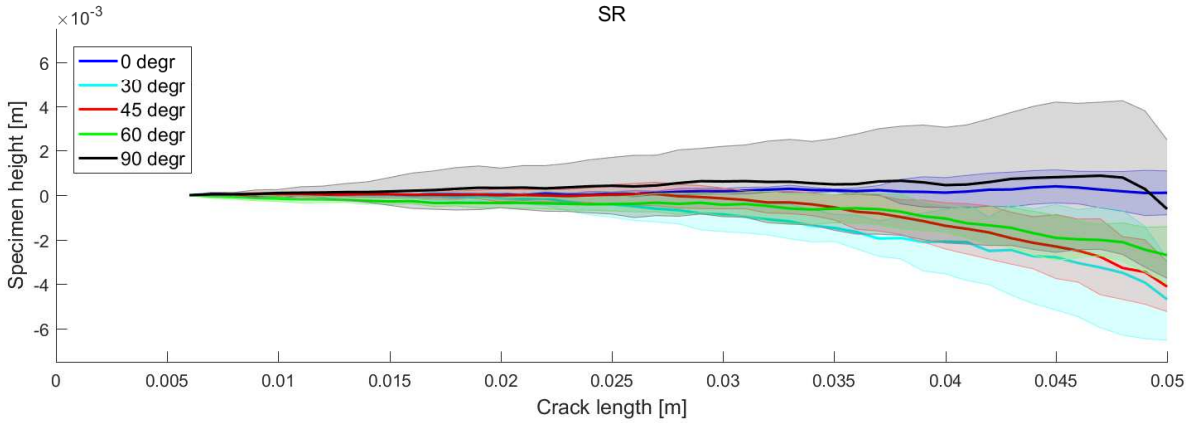

Figure 5.4: Mean and standard deviation - Crack path - Stress relieved

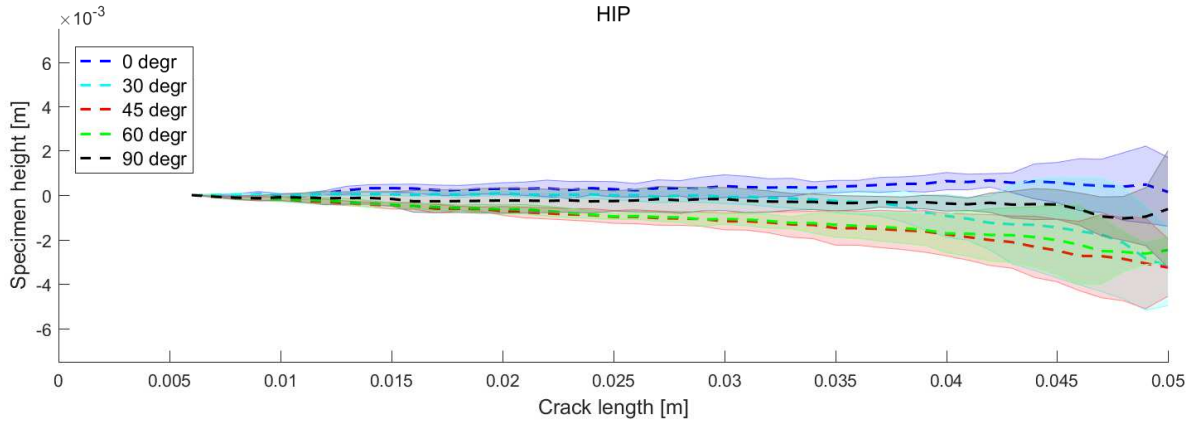

Figure 5.5: Mean and standard deviation - Crack path - HIP

Still, the question remains what causes the cracks to deviate from the original crack path, perpendicular to the applied load. In general, two factors can change the crack propagation direction, namely, the microstructure and the stress field. The influence of the microstructure on the crack direction is most dominant for microcracks, whereas, as the crack grows, the direction is more influenced by the applied stress.

Crack deviations were observed for 30° - SR and 45° & 60° - HIP. First, it is clear that these specimens are all printed off-axis, which suggests that the anisotropy of the material causes the crack deflections. When analysing the overall crack path, a second interesting observation can be made. For both heat treatments, the slope of the crack paths seems to be relative constant. However, the crack length at which they start to deviate is different. For HIPed specimens, crack deflection starts immediately whereas for 30° - SR the crack starts to deviate around 20 mm. This means that different aspects might be creating the change in crack propagation direction.

As this results is rather interesting, it is important to first eliminate possible human errors which could have created this result. Misalignment of the specimens in the fatigue machine can result in cracks not following the expected horizontal direction. Nevertheless, Figure 5.6, shows that this line of thought can be excluded.

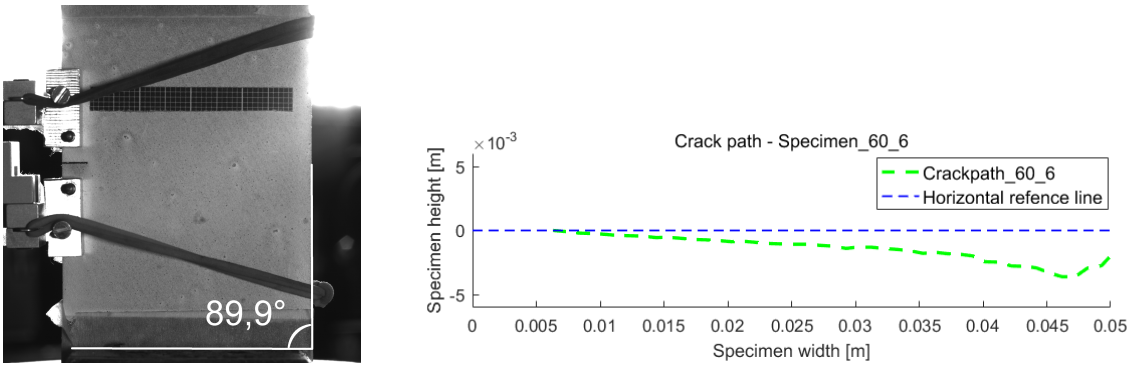

(a) Specimen position

(b) Crack path

Figure 5.6: Evidence against off-axis load initiation - Specimen_60_6

To eliminate any influence of the machine on the crack propagation direction, one set of specimens were flipped (placed upside down) in the fatigue machine. For flipped specimens, similar results were obtained which means that the influence of the fatigue machine could also be excluded.

As a result, the hypothesis can be made that crack path deflections are created by the material itself. As mentioned before, the cracks deviate only for off-axis printed specimens which means that the anisotropy of the material should be taken into account. As DIC results did not show large differences, it is assumed that residual stresses are relieved. Consequently, only the anisotropy of the microstructure remains. Three different areas of the effect of microstructure are taken into account; a direct influence of the microstructure on the crack direction, a change in the global strain field due to the anisotropic microstructure and finally a local effect of microstructure on the strain field near the crack tip.

A direct influence of the microstructure on the crack propagation direction is not very plausible. As the specimen is built out of separate layers, one might argue that the crack grows in between the different layers. Although the direction is correct, the slope is not. Crack deviations are much smaller compared to the build orientations. Furthermore, microstructural analysis showed no sign of the layer orientations which means that one solid material is created. Secondly, before this research, it was expected that the crack would follow the columnar prior beta grains. This hypothesis is both disproved and approved by the microstructural analysis. Figure 5.7 shows the microstructure of a 60° HIP specimen. All these specimens had cracks deflecting down with a constant slope. In the figure, the columnar prior beta grains are indicated in red. There is a clear mismatch in direction between the columnar grains and the crack path. Based on this picture, the hypothesis could be made that the crack does not follow the prior beta grains.

However, when looking to the microstructure near the crack for specimen_90_4, which was an outlier in the results, a different observation can be made. Out of all specimens, this specimens had the only crack path with a positive slope. When looking to Figure 5.8, it can be seen that the crack is running parallel to the columnar prior β grains. From which can be concluded that the crack is following the prior beta grains, which is the opposite of the hypothesis before. However, this effect was only visible for specimen_90_4. All other 90 degrees specimens propagate in a direction more or less normal to the applied stress. Literature showed that the columnar grains grow towards the heat source. A variation of angles between layer orientation and columnar grain direction were measured during the microstructural analysis. Therefore, it may be that the angle for specimen_90_4 was small enough (within 6°) to allow the crack to follow the columnar beta grains, where for all other specimens the angle was larger and the crack could not follow the columnar grains. Based on the fact that the crack does and doesn't follow the columnar grains for certain angles, the hypothesis can be made that there is a range of degrees in which the crack will follow the columnar prior beta grains. More research with smaller differences in layer orientation should be done to fully confirm this hypothesis.

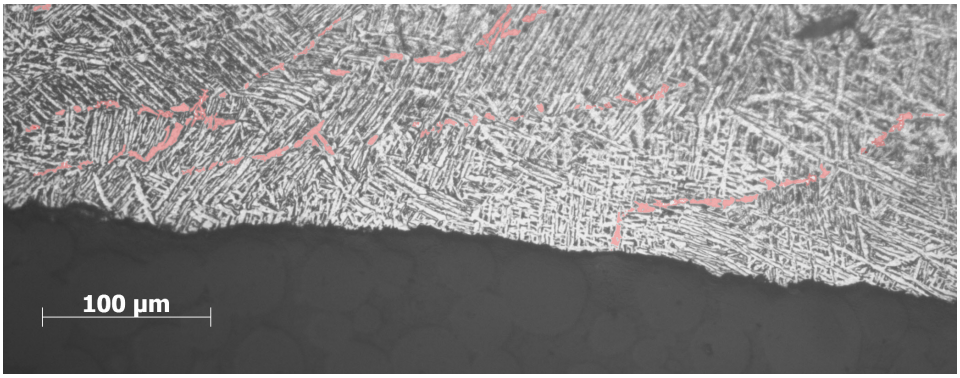

Figure 5.7: Crack path (60 HIP) - Prior beta grain in red

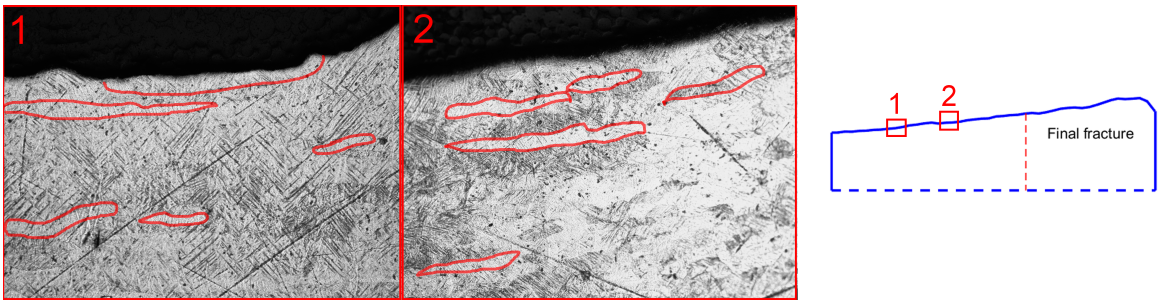

Figure 5.8: Crack path (90_4) - Prior beta grain in red

Finally, it is hard to believe that the microstructure has a direct influence on the crack propagation direction as the influence of the microstructure decreases with increasing crack length. Based on this fact, it is hard to explain why a crack would start deviating at a crack length of 20 mm (30° - SR), if the microstructure is the direct reason for crack deviations.

As crack deviations are observed for large crack lengths, it is more obvious to believe that a change in stress field would change the crack direction. Residual stresses were excluded by the DIC analysis. However, as anisotropic microstructures are tested off-axis, shear coupling might have happened. Long columnar grains run parallel to the specimens height. As these columnar grains are relatively long, slip can occur more easy. Such a shear coupling effect would force the crack path in the correct direction. However, the shear strain data for all specimens does not show any differences. Again, it is hard to believe that large slip occurred and changed the overall stress field which resulted in crack deviations.

This story changes when looking to the local effect of the microstructure. Near the crack tip, increased local stresses are present, when the energy in front of the crack tip is large enough a crack can grow. During this process, small plastic deformations are created at both side of the crack tip. These plastic deformations are concentrated along the slip zones in the planes of maximum shear, which are in general at 45° for Mode I fractures. During loading and unloading, the crack tip is symmetrically blunted and re-sharped respectively [30], creating the striations which were seen in the SEM. Due to anisotropic material properties, this symmetric behaviour might change. As the columnar grains are stretched out, slip can more easily occur at the grain boundaries. This would shift the angle at which the plastic deformation happens, resulting in asymmetric blunting and resharping. When this would happen, plastic zones will be created at different angles (for example at 40 and -60 degrees). As the crack will not propagate through plastically deformed zone it will grow in between them. This will eventually cause the crack to change its direction. The DIC results did not show any changes in plastic zone orientation. However, it is possible that the local plastic deformations may have been too small to be captured by the DIC cameras. Meaning that the accuracy of the DIC was too low to be able to observe this effect. This hypothesis may only explain the crack deflection for 45° & 60° - HIP. As yield stresses are lower for HIPed specimens and therefore plastic deformations will happen faster. To confirm this

hypothesis, more tests are required which will focus on the local strain field near the crack tip.

Overall, it is believed that two different causes for crack deflection are present. As the global stress field does not show any differences, it is believed that local strain fields cause the crack deviations due to the presence of the large columnar prior β grains. Nevertheless, more detailed research is needed to make strong conclusions in this field.

5.5. Effect of plane stress conditions on Paris curves

This study was the first in its kind to create Paris curves of SLM Ti-6Al-4V tested in plane stress conditions. Comparing the results to plane strain results from literature can give some valuable information.

Before discussing the results, one should keep in mind that the fatigue tests were performed with an h/w of 0.8. As the effect on the stress intensity factor was rather large, a correction factor was calculated in Appendix C. Applying this correction factor allows to compare the results with literature data. Below, in Figure 5.9, both the corrected and uncorrected results are shown to show the influence of the correction factor. When comparing to the literature, only the corrected results will be taken into account.

Figure 5.9 shows Paris curves for different situations. Both plane stress and plane strain results are shown for both SLM printed specimens as casted specimens from literature. Table 5.1, gives additional information about the data which was used to come up with these Paris curves.

Table 5.1: Additional information about Paris curve results

Description	Orientation	Heat treatment	Thickness	Reference
Plane stress - Raw	-	-	1.5 mm	[31]
Plane strain - Raw	-	Mill-annealed	6.35 mm	[4]
Plane stress - SLM	0°	735 ° - 1 hour	2.3 mm	-
Plane strain - SLM (Leuders)	0°	800 ° - 2 hours	6.25 mm	[5]
Plane strain - SLM (Cain)	0°	640 ° - 4 hour	6.25 mm	[15]

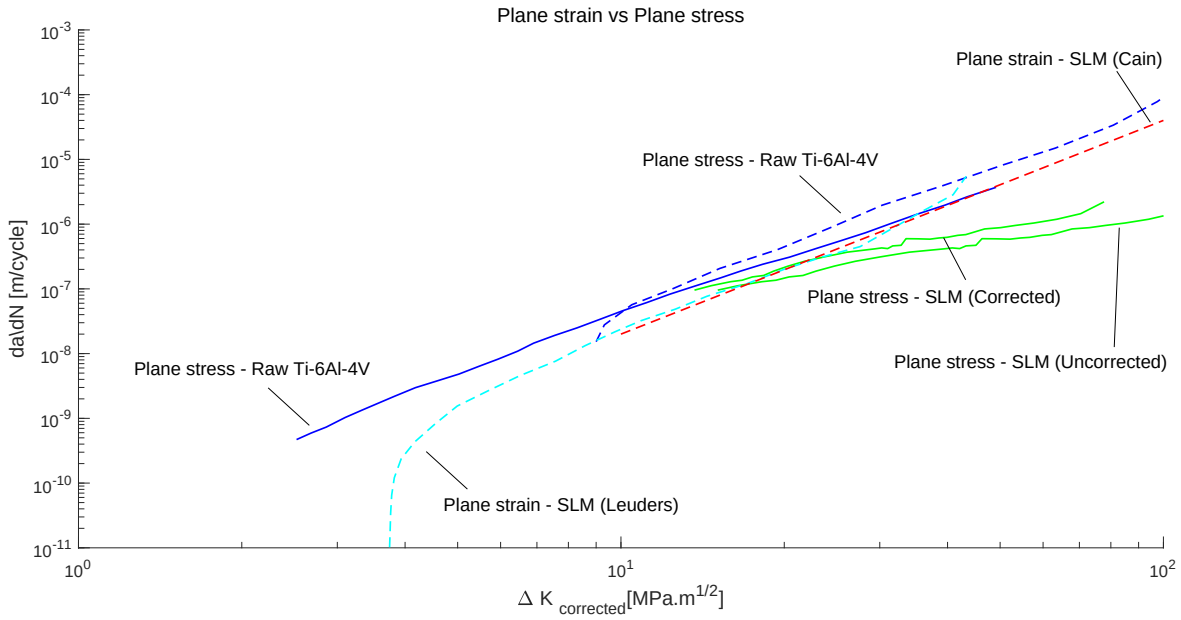

Figure 5.9: Plane strain vs Plane stress

As can be seen, all Paris curves act in a similar region, however some differences can be observed. First, it can be seen that the slope of SLM plane stress is less steep compared to the SLM plane strain results. The difference in slope can be attributed to the increased plastic zone which is present for plane stress specimens. As the crack length increases, the stress near the crack tip increases which means that the plastic zone will also increase. As a material can store more energy when it is plastically deformed, the crack propagation rate will be lower for increasing stress intensity factors. The same result can be observed when comparing raw plane stress specimens with their plane strain counterparts.

Small differences in the crack propagation rate can be caused by the microstructure present in the material. However, this microstructure is unknown for all specimens which makes it hard to directly compare the impact. Nevertheless, it seems that SLM specimens have slightly better crack propagation properties compared to these raw Ti-6Al-4V specimens. It is believed that this small difference comes from the difference in microstructure In terms of crack propagation properties, a coarse lamellar microstructure is preferred as it forces the crack to constantly change direction, which requires more energy. Both the raw and SLM specimens have those $\alpha + \beta$ lamellar microstructures, however there is a difference in the orientation of the α lamellae within the β grains. For raw Ti-6Al-4V, these α lamellae are organised in colonies, where the α lamellae for SLM specimens have a more random and chaotic distribution caused by the fast cooling during production. Therefore, it may be the case that more energy is required as the crack has to change direction more often. However, as the microstructure is not known for these specimens it is hard to give a conclusive conclusion.

From this comparison the hypothesis can be drawn that crack propagation properties improve when using SLM specimens in a plane stress conditions. This can be useful in future applications. However, more tests should be done to gain more confidence in this field. Currently, as more data is available for plane strain SLM specimens, plane strain crack propagation properties obtained by these studies can be used. Using these properties will result in conservative design choices which is often done in the aerospace industry. However, as structures may perform better when they are tested in plane stress conditions, there is a need to perform more tests and gather more data as this will result in more weight efficient structures.

6

Conclusion & Recommendations

The aim of this thesis was to investigate the effect of build direction and heat treatment on the crack propagation properties of SLM Ti-6Al-4V. By means of experiments, crack growth was measured and analysed. Based on the experimental data, interesting effects were observed, leading to some new conclusions in this field.

During this thesis, some assumptions were made in order to come up with the conclusions. In order to interpret the conclusions in the correct context, these assumptions should be taken into account when going through the results.

6.1. Assumptions & Limitations

Conclusions were drawn by analysing the effect of five different build orientation (0, 30, 45, 60 and 90°) and two different heat treatments (Stress relieved and Hot Isostatic Pressing).

Analysis of the Paris curves was performed in the stress intensity factor range between 10 and 100 $MPa\sqrt{m}$ which is in the second stage of the Paris curve for Ti-6Al-4V..

Paris curves were calculated by measuring the horizontal crack lengths for the crack propagation rate. Stress intensity factors were determined based on the general equation which assumes linear elastic fracture mechanics.

In the experiment, an h/w ratio was used which was lower than 1. Conclusions based on relative performance are based on the processed Paris curves, whereas a correction factor is used to make conclusions when comparing results to literature.

6.2. Conclusions

The main goal of this thesis was to investigate the influences on the crack propagation rate caused by a varying build direction or heat treatment. Based on the experimental data, some interesting conclusions were drawn which were not expected at the start of this thesis:

- Build direction has no or little effect on the crack propagation rate for SLM heat treated specimens. The microstructural anisotropy does not influence the crack propagation rate in SLM Ti-6Al-4V.

- Heat treating SLM specimens results in improved crack propagation rates compared to as-built. However, crack propagation rate is equal for both a stress relieved heat treatment with a hot isostatic pressing treatment. This means that the initial defects and higher treatment temperature (below β transus) have no effect on crack propagation rate.

- Different combinations of build direction and heat treatment result in similar crack propagation rates.

- Crack propagation rates improve for SLM specimens when loaded in a plane stress condition.

As a second research objective, the influence on the crack propagation direction was also investigated. Due to the presence of the anisotropic microstructure some interesting conclusions were drawn:

- Build direction influences the crack propagation direction for heat treated SLM specimens. Small but repetitive crack deviations are present for off-axis building directions.

- Orthogonal build directions result in crack paths perpendicular to the load direction for both heat treatments. Off-axis specimens show deviating crack paths but only in combination with specific heat treatments. Other off-axis printed specimens have cracks propagating normal to the applied stress.

- The largest crack path deviations were found for 30° when stress relieved and 45 & 60° with a HIP treatment. Crack deflection starts immediately for 45 & 60° specimen whereas the crack turns after 20mm for 30° .

- The anisotropic microstructure causes the crack deflection. Based on the gathered experimental data, no conclusive explanation for the crack deflections can be given.

With these conclusions in mind, it can be interesting to reflect back on the certification of SLM materials. By doing this, the impact of the results can be set into their perspective.

The main conclusion is that an off-axis build direction has only little impact on the crack propagation properties of SLM Ti-6Al-4V. No differences regarding the crack propagation rate could be seen while only small deviations of the crack path were seen for off-axis build directions. The same can be said for the different heat treatments. Both the stress relieved treatment and a stress relieved with HIP treatment, result in similar crack propagation rates.

This conclusion can be very useful for certification of SLM parts. This means that, although microstructural anisotropy was created by the process, it can be neglected for certification of the part. Which means that the material can be treated as isotropic, for crack propagation rate, in this plane of the material, which is a major advantages in the terms of certification.

Comparison to the literature results showed that SLM Ti-6Al-4V tested in a plane stress condition has better crack propagation properties than raw Ti-6Al-4V in both plane strain and plane stress, and SLM Ti-6Al-4V in plane strain. This result is also promising for certification of the material. Although more research is needed to confirm these observations, using the raw Ti-6Al-4V material properties for SLM Ti-6Al-4V design would mean that a conservative design is created. As the result is conservative, industry might be willing to faster use the material in applications, which will only increase the potential and research to the material.

However, the crack path showed small variations for different off-axis build directions. This effect can be interesting with respect to future design and certification of SLM parts. When the cause of crack turning is fully understood, it can be used to steer a crack in certain directions. Crack steering can lead to new possibilities in terms of certification. For example, the crack direction can be controlled so that it does not propagate towards critical areas. An other example could be that a crack could propagate towards a certain locations where it will trigger an 'alarm' for the maintenance department. These are all future applications but might change the way in which certification and maintenance is done.

6.3. Recommendations

This research gave a first inside in how crack propagation is influenced by an off-axis build direction. However, not everything is covered yet and still some knowledge gaps can be found. In this section, some recommendations are done with respect to future research.

Experiments were performed at relative high stress intensity factors. As described before, it is expected a more dominant effect of the build orientation will be visible at low stress intensity factors, as the microstructure has more influence at low stress intensity factors. This means that is can be interesting to see what happens at a lower stress intensity factors. Differences in crack propagation rate at low stress intensity factors or different threshold values can eventually result in large difference variations in lifetime.

The amount of data and tests performed were not sufficient to fully explain the cause of crack deflections. Further research is needed with new tests to analyse this effect in more detail. As the hypothesis stated that an asymmetric plastic zone near the crack tip may be creating this effect, a more detailed DIC analysis is advised

Furthermore, more tests should be performed for build orientation between 60 and 90° to investigate in which range the crack will follow the columnar prior β grains. This can be interesting for both the crack propagation direction and rate, as it may be that larger crack propagation rates are measured when the crack follows the columnar prior beta grains.

Comparison to the literature showed that crack propagation properties are improved for SLM Ti-6Al-4V in plane stress conditions compared to raw Ti-6Al-4V and plane strain SLM Ti-6Al-4V. As this thesis, was the first in its kind to test in plane stress conditions, more tests are required to confirm this observation. If indeed SLM Ti-6Al-4V has better crack propagation properties compared to the current Ti-6Al-4V, the next step towards more weight efficient structures can be made.

This research investigated the effect of an off-axis build direction in the plane perpendicular to the thickness (XZ - plane). However, Cain ([15]) showed that when loading a part in the XY direction, different crack propagation rates are found. Therefore, it might by interesting to look what causes the difference in crack propagation in this plane. Off-axis build direction might reveal differences in crack propagation which would mean that the material cannot be treated as isotropic in this plane.

A

Load selection approach

As described before, a fatigue test with constant load amplitude had to be set up to measure the crack propagation rate. However, due to the uncertainty of the material properties and the large scatter in literature data (Paris curves), it was unknown which load should be used. Therefore, preliminary tests were performed to determine the load cycle which should be used in this experiment.

This preliminary test had two goals. First, it should find a correct load cycle which forces a crack to propagate but allows the specimen to make a large amount of cycles (around 200000 cycles). As a second objective, the preliminary test should give a first indication if large differences in the fatigue properties are present. This is important when deciding if one load should be used or a different load cycle for SR or HIPed specimens.

In order to reach these goals a test procedure was designed which would increase the load every amount of cycles. By doing this it would be clear for which loads the crack would propagate and how fast. To come up with the load step up procedure, three critical parameters should be determined, namely, starting load, load increase and the amount of cycles between load increases.

The starting load was set equal to 10kN and is calculated based on the stress intensity factor (Δ K). A load of 10 kN results in a stress intensity factor of 11.61 $MPa\sqrt{m}$, which is higher than threshold values found in literature (between 2 and 5$MPa\sqrt{m}$). However, the difference between 11.61 and 5 $MPa\sqrt{m}$ is quite significant. Still this stress intensity factor was chosen based on some tests which were performed using plane stress specimens (same dimensions) printed by Layerwise. During these tests no crack growth was observed below 10 kN.

The load increase was set equal to 10%. This means that after a certain amount of cycles, the load would be increased by 10%. This parameter was determined based on the Paris curve data in literature. When a load is increased, the lifetime (amount of cycles left) will decrease. Consequently, a load increase should be selected which is large enough to propagate the crack but should be small enough to maintain enough cycles. Paris curve data from literature was used to determine the effect of a change in the m-value on the lifetime of the specimen. The minimum and maximum m-value found in literature was used for this selection. Table A.1 shows what the effect is of increasing the load by a certain factor on the lifetime of the specimen. Based on this data, is was decided that an increase of 10% will be used as it does not change the lifetime to much.

Finally, an interval between each load increase of 50000 cycles was selected. 50000 cycles gives 50 pictures which means that a change in crack length should be noticeable but still would increase the load fast enough to reach high stresses if required.

Combining these parameters results in the load procedure shown in Figure A.1.

Following this load procedure the following results were obtained. Instead of calculating the Paris curve, the crack length over number of cycles were plotted. This would show in which interval the first changes in crack length were measured and where large crack propagation rate would be measured.

Table A.1: Effect of load increase on the lifetime of the specimen

Increasing load by factor:	**Decreases lifetime by factor:**	
	for m = 5.84	**for m = 2.366**
5	12077.7	45.1
2	57.3	5.3
1.5	10.7	2.6
1.25	3.7	1.7
1.1	1.7	1.3

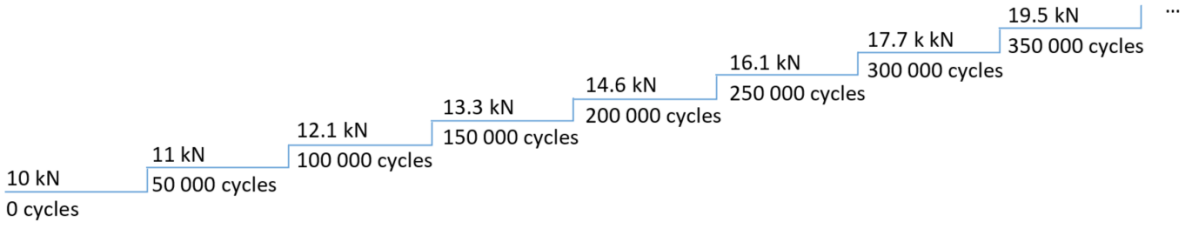

Figure A.1: Load procedure

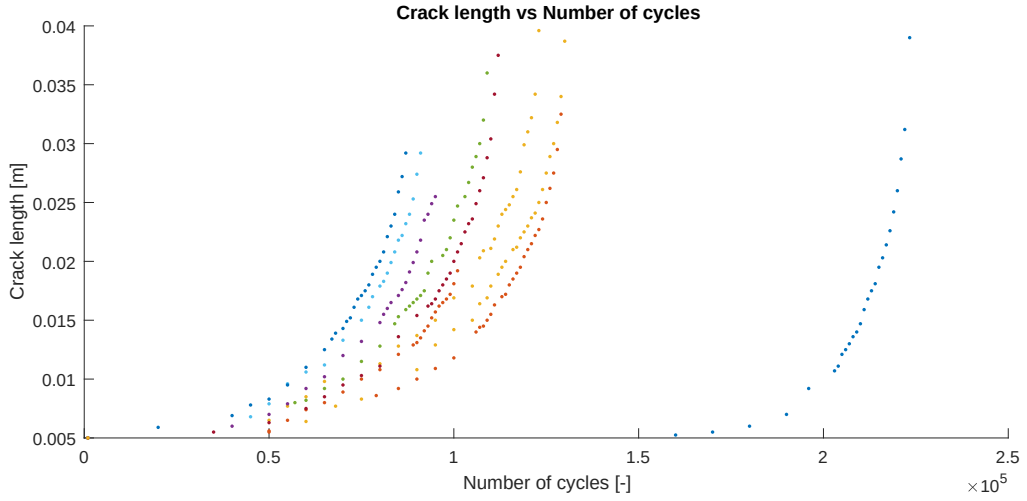

Figure A.2: Results of step up phase

Observation of the results showed that for almost all specimens, first changes in crack length were measured were observed around 50000 cycles but quickly increased afterwards. The reason for one outlier was not investigated as this is not required to select the ideal constant load.

In the end, the conclusion was made that 10 kN will be used as a maximum applied load during the experiment. Lower stress intensity factors may have been possible as well however due to the limited amount of specimens available, it was decided not to try a lower load case as 10 kN would give a sufficient amount of data points.

B

Additional results

This appendix provides some additional results which were not shown in the report.

B.1. Crack propagation rate

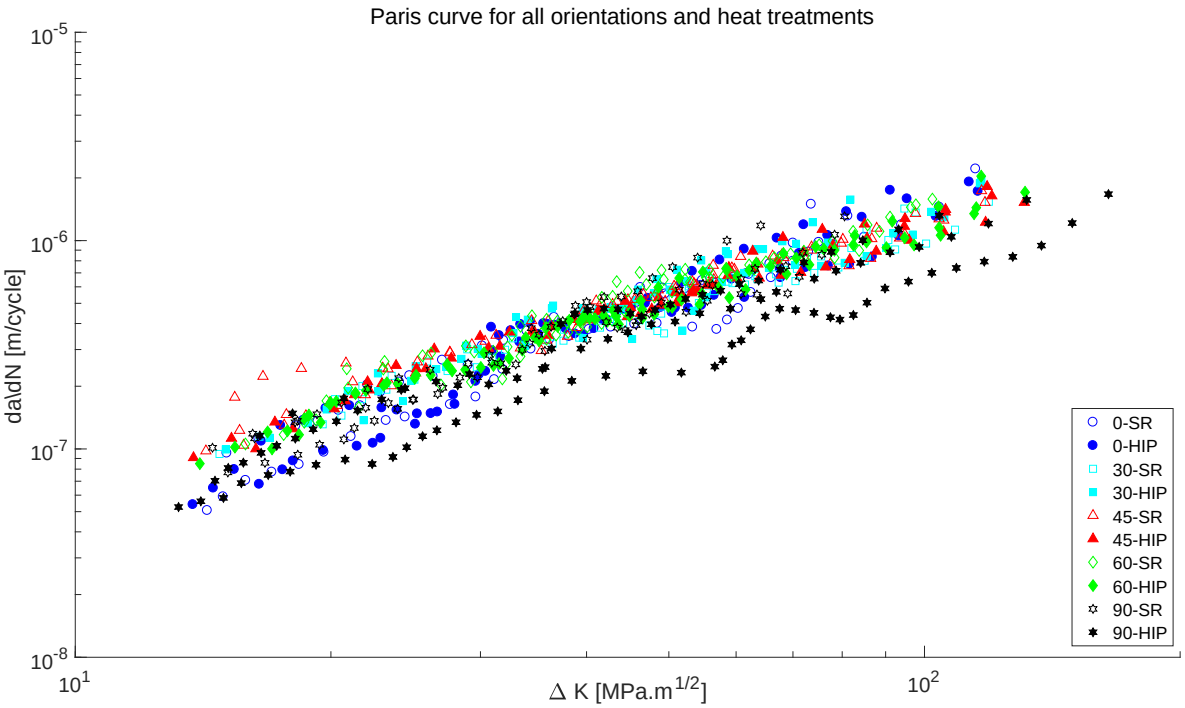

Figure B.1: All Paris curves

B.2. Crack path

Effect of heat treatment

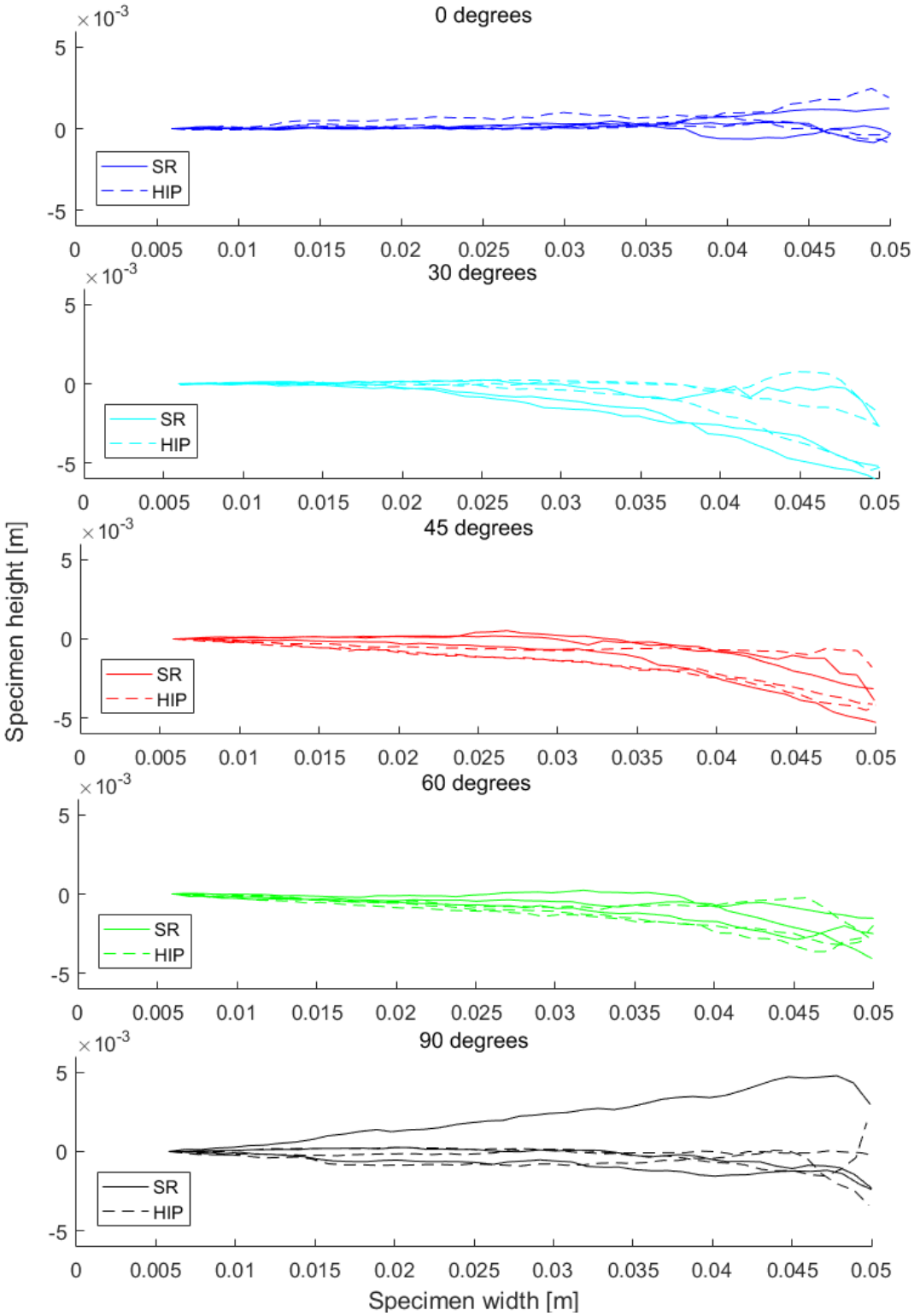

Figure B.2: Crack path - Effect of heat treatment

All crack paths

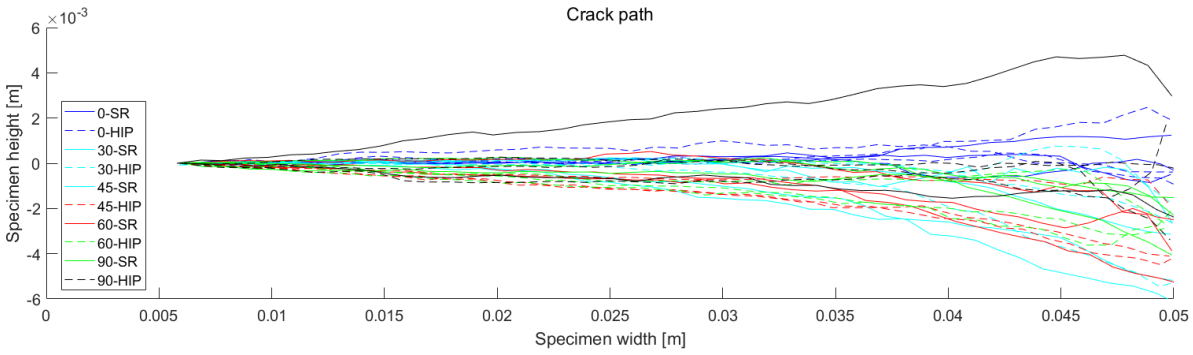

Figure B.3: Crack path - All specimens

B.3. DIC

In this appendix, all the contour plots obtained by the DIC are shown.

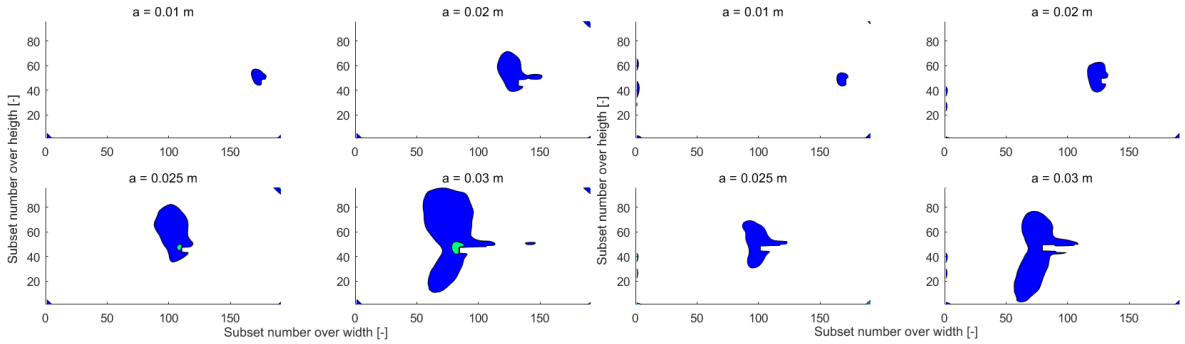

(a) Specimen_0_4 (b) Specimen_0_8

Figure B.4: Strain field - White: VM < 0.0025; Blue: 0.0025 < VM > 0.0075; Green: VM > 0.0075

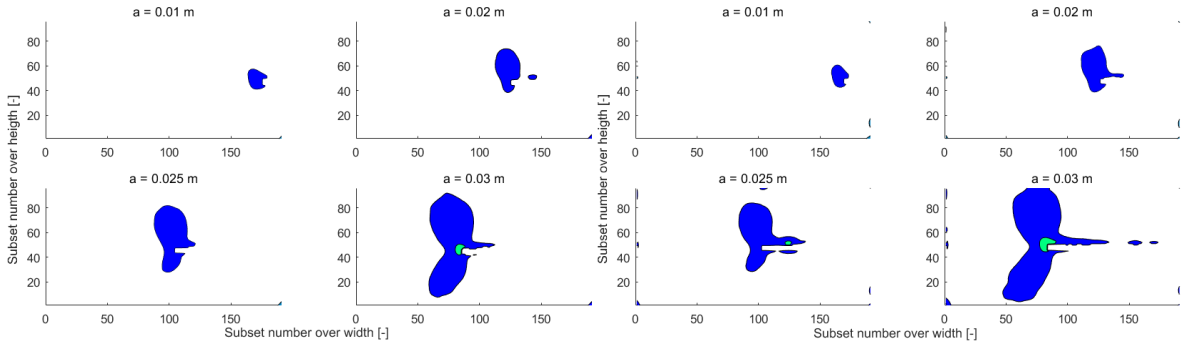

(a) Specimen_30_4 (b) Specimen_30_8

Figure B.5: Strain field - White: VM < 0.0025; Blue: 0.0025 < VM > 0.0075; Green: VM > 0.0075

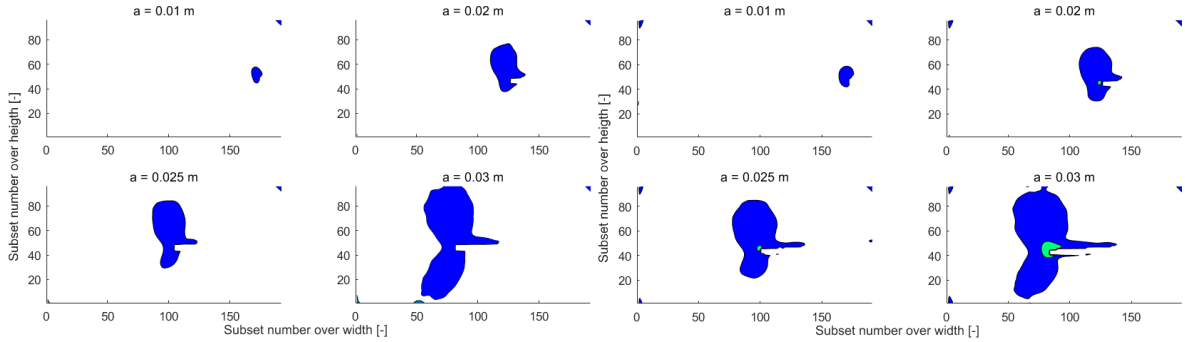

(a) Specimen_45_4 (b) Specimen_45_6

Figure B.6: Strain field - White: VM < 0.0025; Blue: 0.0025 < VM > 0.0075; Green: VM > 0.0075

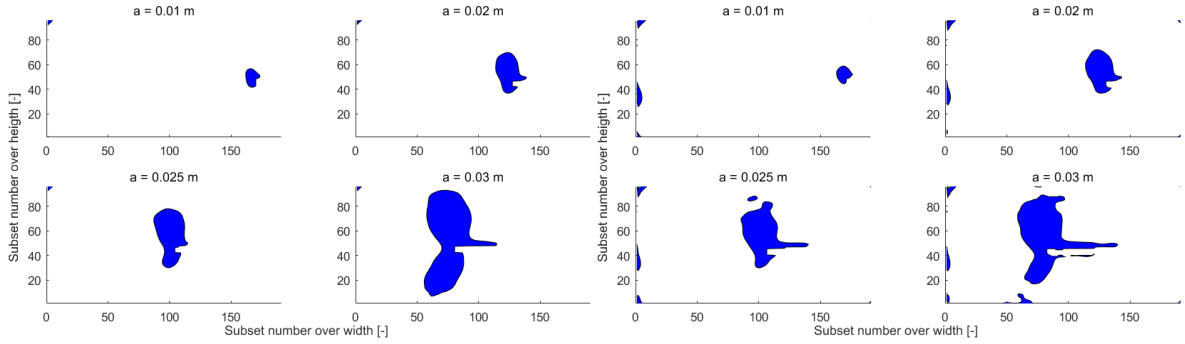

(a) Specimen_60_2 (b) Specimen_60_8

Figure B.7: Strain field - White: VM < 0.0025; Blue: 0.0025 < VM > 0.0075; Green: VM > 0.0075

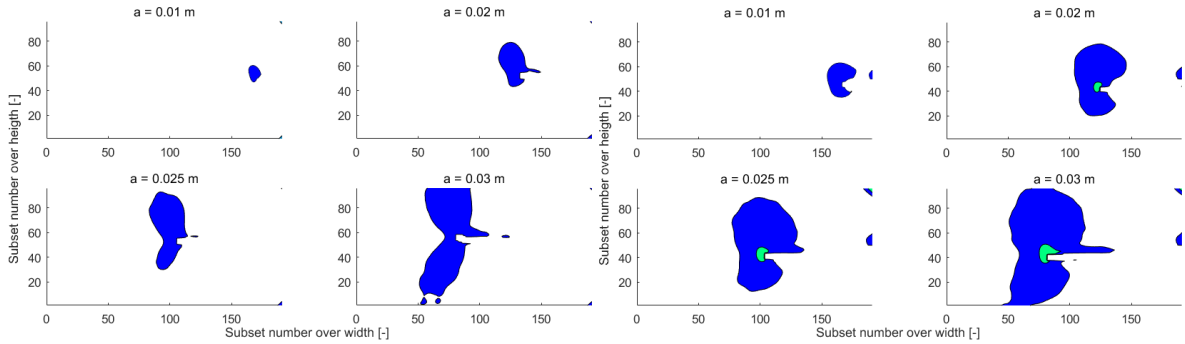

(a) Specimen_90_4 (b) Specimen_90_6

Figure B.8: Strain field - White: VM < 0.0025; Blue: 0.0025 < VM > 0.0075; Green: VM > 0.0075

B.4. Microstructure orientations

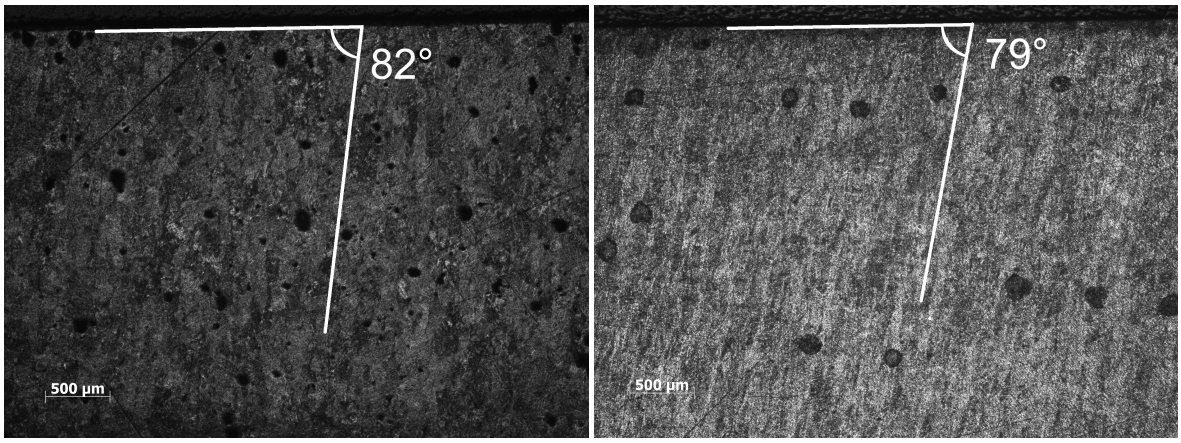

(a) 0° SR (b) 0° HIP

Figure B.9: Orientation of columnar grains

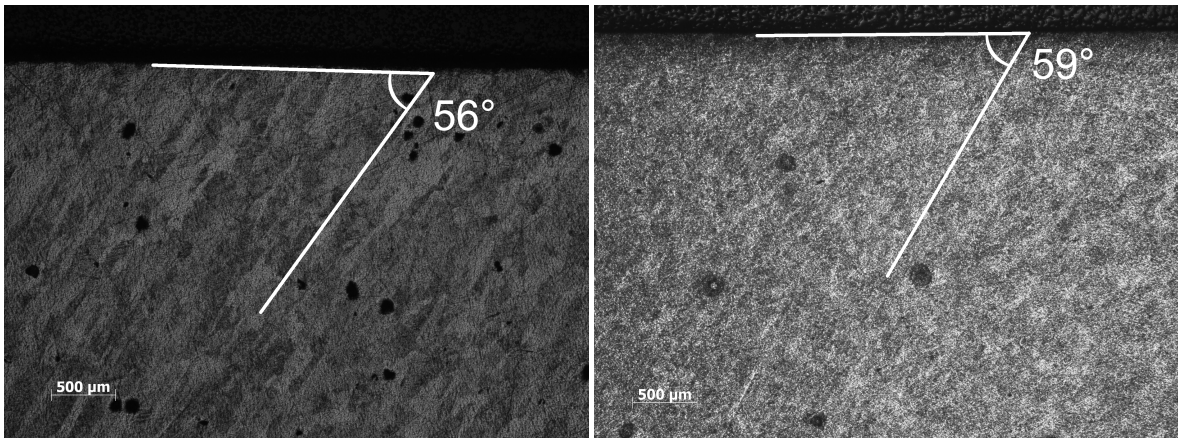

(a) 30° SR (b) 30° HIP

Figure B.10: Orientation of columnar grains

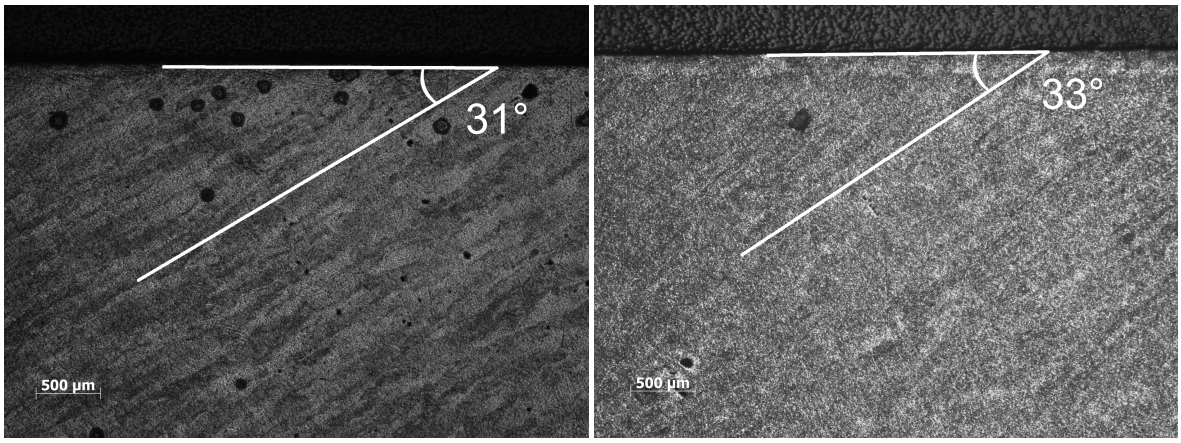

(a) 45° SR (b) 45° HIP

Figure B.11: Orientation of columnar grains

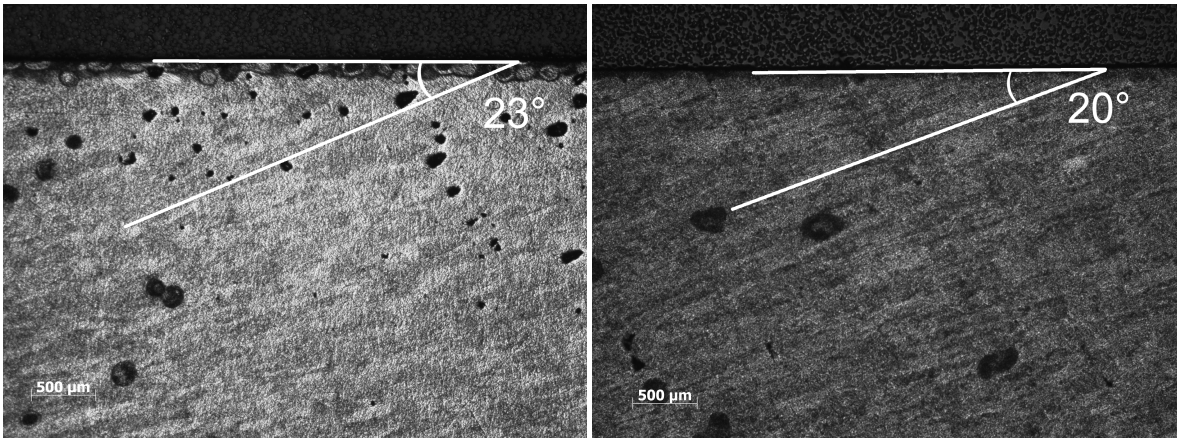

(a) 60° SR (b) 60° HIP

Figure B.12: Orientation of columnar grains

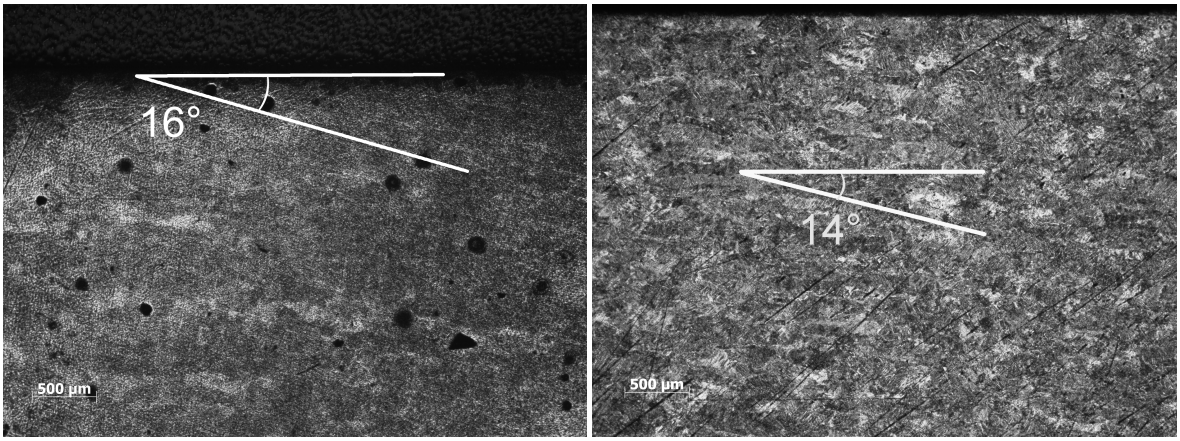

(a) 90° SR (b) 90° HIP

Figure B.13: Orientation of columnar grains

C

Δ K - Correction factor

A major limitation during this thesis, is the use of an h/w ratio which is below the recommended value in the test standard. In Section 5.1, the effect of this lower h/w ratio was shortly discussed and concluded that the stress intensity factor was calculated wrong based on the research of John [7]. Due to this limitations, Paris curves calculated in this thesis cannot be directly compared to the Paris curves found in literature. Therefore, a correction factor is calculated which eliminates the effect of the smaller h/w value.

The research of John [7] focussed on the effect of a change in h/w on the stress intensity factor. Using a Finite Element Method (FEM), he showed that the stress intensity factor increases with an increasing h/w ratio, in the range for h/w between 1 and 5. In this thesis, an h/w ratio of 0.8 which is out of the range investigated by John. Therefore, a FEM is created, in Abaqus, which is verified by the results of John. This model is used to calculate an accurate correction factor and come with correct Paris curves which can be compared to literature.

Results obtained by John

Figure C.1 describes the effect of H/W on the normalised stress intensity factor. This normalised stress intensity factor is equal to the geometry term β. The experiment performed by John uses $2 \leqslant \frac{H}{W} \leqslant 10$, however due to a difference in annotation this is equal to $1 \leqslant \frac{H}{W} \leqslant 5$.

When looking at the graph (C.1) it can be seen that the normalised stress intensity factor is similar for all ratios at small crack lengths. When the crack length increases the difference in K also increases. Small height over width ratios result in lower stress intensity factors.

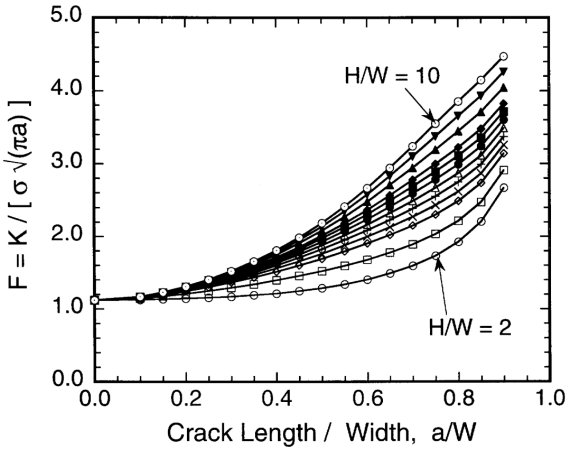

Figure C.1: Effect of H/W on normalized stress intensity factor [7]

When extrapolating this trend, it can be said that a h/b of 0.8, will result in a smaller stress intensity factor. However, the stress intensity factors in this thesis are calculated with the assumption of h/b is equal to 1. This means that the calculated Paris curves are too optimistic. A correction factor is calculated based on a Finite Element Model created in Abaqus.

Finite Element Model

A finite element model was created in Abaqus to be able to measure the real stress intensity factors in front of the crack tip for specimens with a h/w ratio of 0.8. This was done using a 3D deformable planar shell which represents half a specimen. All real specimen dimensions were used. The model is shown in Figure C.2.

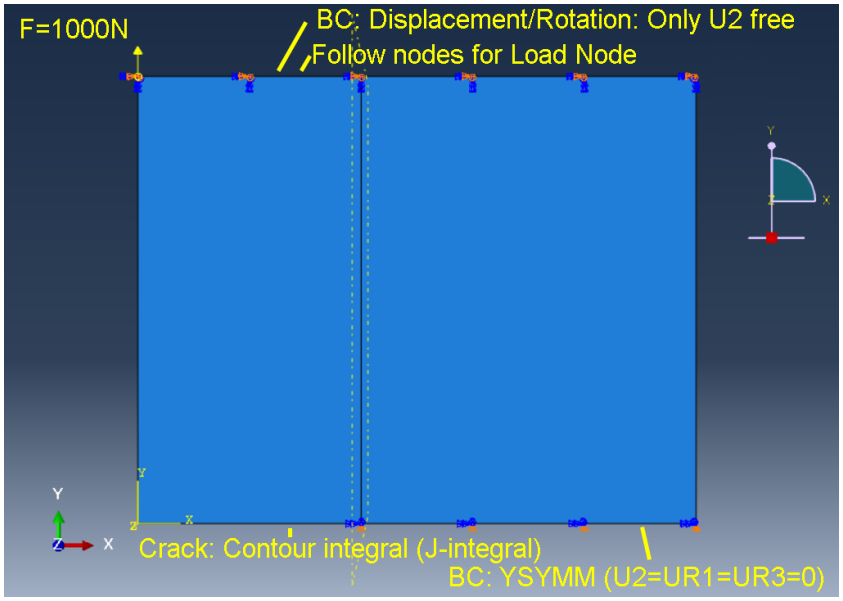

Figure C.2: Abaqus model

As can be seen only half of the specimen is modelled with symmetry, to simulate a crack. At the intersection, a crack is modelled which is a 'contour integral' type. Using this, the strain energy release rate can be measured by measuring the J-integral. As a straight crack is modelled and an isotropic linear elastic material is assumed, the stress intensity factor can be calculated from this J-integral using the following equation [32]:

$$J = \frac{K_i^2}{E'} => K_i = \sqrt{J.E'} \tag{C.1}$$

In this equation, E' is equal to the stiffness, E, as the specimen fails in plane stress conditions. In the end this stress intensity factor can be normalised using equation C.2, which is in fact equal to the β factor.

$$\beta = \frac{K_i}{\sigma\sqrt{\pi a}} \tag{C.2}$$

With a finite element model and a method to calculate the normalised stress intensity, the model can be verified using the results of the research of John.

Verification of the model

Verification of the model is important to know if the results of the model can be trusted. Figure C.3 and Table C.1 shows a good correlation between the created model and the results of John. As these results were validated with experimental tests, it can be concluded that the Abaqus model gives accurate results and can be used to define a correction factor for h/w is 0.8.

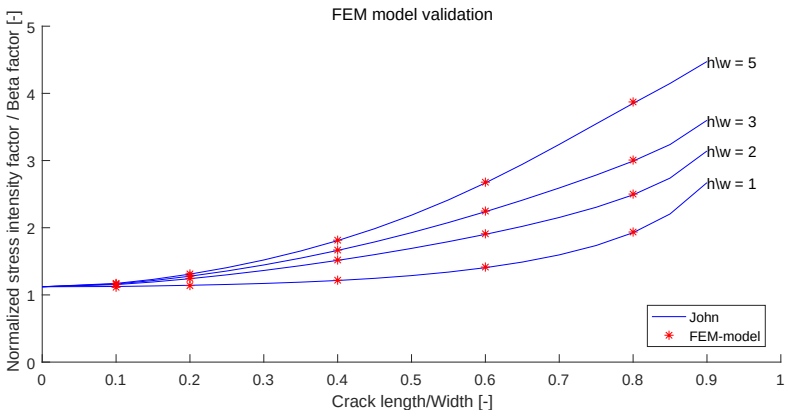

Figure C.3: Model verification with results of John

Table C.1: Normalised verification error [%]

Crack length	**Height over Width**			
	1	**2**	**3**	**5**
0.1	0.96	0.08	0.05	0.04
0.2	0.43	0.28	0.25	0.24
0.4	0.35	0.38	0.36	0.35
0.6	0.66	0.43	0.43	0.42
0.8	0.51	0.46	0.52	0.56

Correction factor

Throughout the thesis, Equation 2.1 was used to calculate the stress intensity factor. However, this equation assumes a h/w equal to 1 which is not the case for the experiment performed. Using the Abaqus model explained before the difference in normalised stress intensity factor for h/w equal to 1 and 0.8 is calculated and shown in Figure C.4.

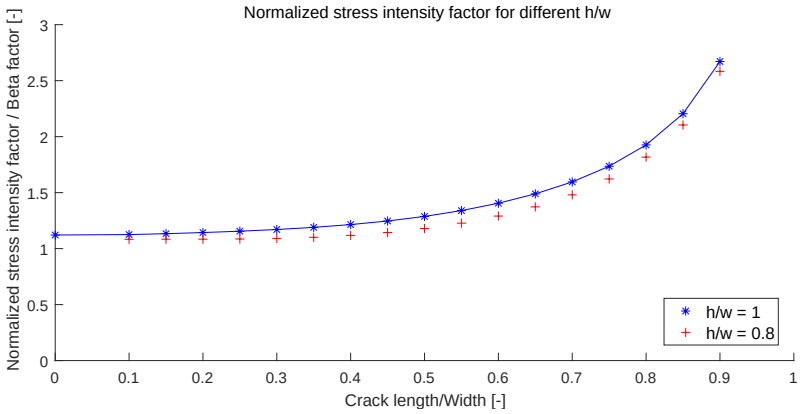

Figure C.4: Normalised stress intensity factor for h/w = 1 & 0.8

When dividing the β for h/w = 0.8 by the old β factor, a correction factor is calculated. The correction factor over the whole crack length range is shown in Figure C.5 where a 4th-order polynomial fit is used to fit the data.

Finally, this correction factor can be applied to the stress intensity factors calculated before. The difference in Paris curve is shown in Figure C.6 where it can be seen that the crack propagation properties are worse

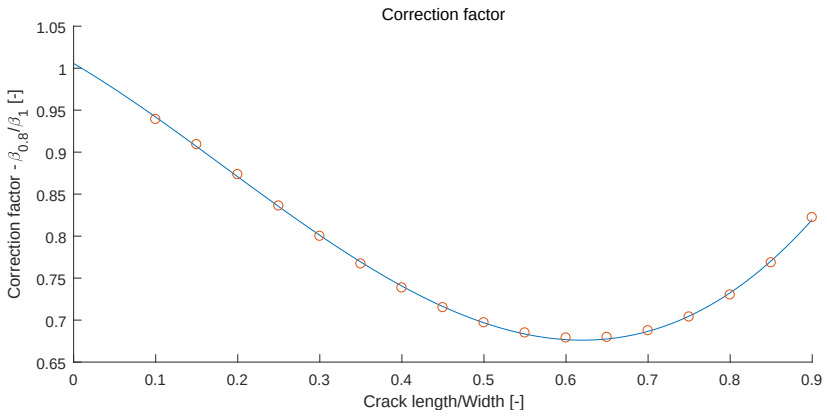

Figure C.5: Correction factor over the whole crack length range

for h/w of 0.8, as was expected.

In general, this correction factor will be used when comparing the results to the literature. For conclusions based on relative performance, the correction factor will not be used.

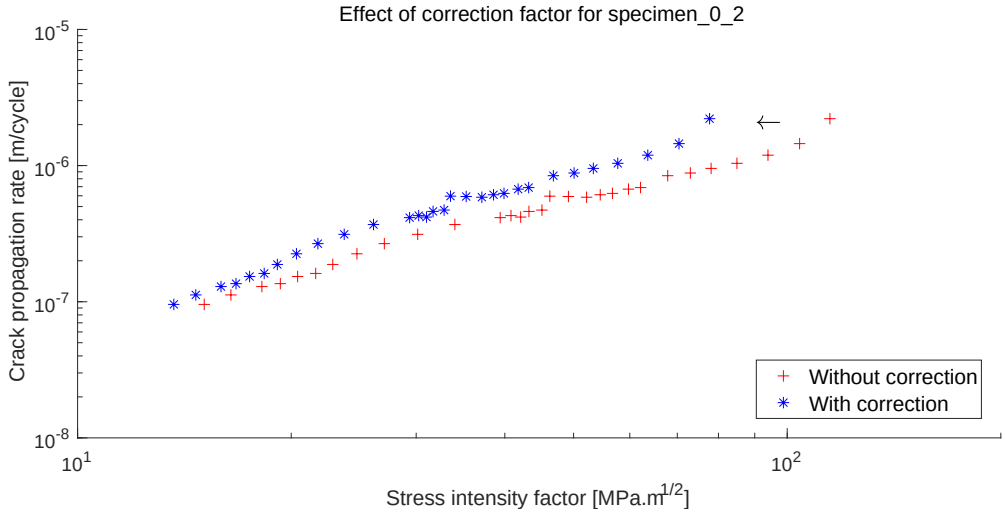

Figure C.6: Effect of correction factor on specimen_0_2

Bibliography

[1] Riemer, A., Richard, H.A., Bruggemann, J.P., Wesendahl, J.N.: Fatigue crack growth in additive manufactured products. Frattura ed Integrita Strutturale **9**(34) (2015) 437–446

[2] Rangaswamy, P., Griffith, M.L., Prime, M.B., Holden, T.M., Rogge, R.B., Edwards, J.M., Sebring, R.J.: Residual stresses in LENS components using neutron diffraction and contour method. Materials Science and Engineering A **399**(1-2) (2005) 72–83

[3] Vilaro, T., Colin, C., Bartout, J.D.: As-fabricated and heat-treated microstructures of the Ti-6Al-4V alloy processed by selective laser melting. Metallurgical and Materials Transactions A: Physical Metallurgy and Materials Science **42**(10) (2011) 3190–3199

[4] Mil-hdbk, S.: Handbook Metallic Materials and Elements for. October (January) (2003) 8–106, 8–109

[5] Leuders, S., Thone, M., Riemer, A., Niendorf, T., Troster, T., Richard, H.A., Maier, H.J.: On the mechanical behaviour of titanium alloy TiAl6V4 manufactured by selective laser melting: Fatigue resistance and crack growth performance. International Journal of Fatigue **48** (2013) 300–307

[6] Vrancken, B., Cain, V., Knutsen, R., Van Humbeeck, J.: Residual stress via the contour method in compact tension specimens produced via selective laser melting. Scripta Materialia **87** (2014) 29–32

[7] John, R., Rigling, B.: Effect of height to width ratio on K and CMOD solutions for a single edge cracked geometry with clamped ends. Engineering Fracture Mechanics **60**(2) (1998) 147–156

[8] Gibson, Ian, David W. Rosen, Stucker, B.: Additive Manufacturing Technologies. (2010) 400–414

[9] Gibson, Ian, David W. Rosen, Stucker, B.: Additive Manufacturing Technologies - 3D Printing, Rapid Prototyping, and Direct Digital Manufacturing. (2013)

[10] Strantza, M., Vafadari, R., De Baere, D., Vrancken, B., Van Paepegem, W., Vandendael, I., Terryn, H., Guillaume, P., Van Hemelrijck, D.: Fatigue of Ti6Al4V structural health monitoring systems produced by selective laser melting. Materials **9**(2) (2016) 1–15

[11] Inagaki, I.: Application and Features of Titanium for the Aerospace Industry. (106) (2014) 22–27

[12] Leyens, C., Peters, M.: Titanium an Titanium Alloys. (2003)

[13] Thijs, L., Verhaeghe, F., Craeghs, T., Humbeeck, J.V., Kruth, J.P.: A study of the microstructural evolution during selective laser melting of Ti-6Al-4V. Acta Materialia **58**(9) (2010) 3303–3312

[14] Schijve, J.: Fatigue specimens for sheet and plate material. Fatigue & Fracture of Engineering Materials & Structures **21**(3) (1998) 347–357

[15] Cain, V., Thijs, L., Van Humbeeck, J., Van Hooreweder, B., Knutsen, R.: Crack propagation and fracture toughness of Ti6Al4V alloy produced by selective laser melting. Additive Manufacturing **5** (2015) 68–76

[16] Yadroitsava, I., Grewar, S., Hattingh, D., Yadroitsev, I.: Residual Stress in SLM Ti6Al4V Alloy Specimens. Materials Science Forum **828-829** (2015) 305–310

[17] Edwards, P., Ramulu, M.: Fatigue performance evaluation of selective laser melted Ti-6Al-4V. Materials Science and Engineering A **598** (2014) 327–337

[18] Leuders, S., Lieneke, T., Lammers, S., Tröster, T., Niendorf, T.: On the fatigue properties of metals manufactured by selective laser melting – The role of ductility. Journal of Materials Research **29**(17) (2014) 1911–1919

[19] Qiu, C., Adkins, N.J.E., Attallah, M.M.: Microstructure and tensile properties of selectively laser-melted and of HIPed laser-melted Ti-6Al-4V. Materials Science and Engineering A **578** (2013) 230–239

[20] Atkinson, H., Davies, S.: Fundamental aspects of hot isostatic pressing: an overview. Metallurgical and Materials Transactions A **31A**(December) (2000) 2981–3000

[21] Song, B., Dong, S., Zhang, B., Liao, H., Coddet, C.: Effects of processing parameters on microstructure and mechanical property of selective laser melted Ti6Al4V. Materials and Design **35** (2012) 120–125

[22] ASTM: Standard Test Method for Measurement of Fatigue Crack Growth Rates 1. **03**(July) (1999) 1–43

[23] Edwards, P., Ramulu, M.: Effect of build direction on the fracture toughness and fatigue crack growth in selective laser melted Ti-6Al-4V. Fatigue and Fracture of Engineering Materials and Structures **38**(10) (2015) 1228–1236

[24] Simonelli, M., Tse, Y.Y., Tuck, C.: Effect of the build orientation on the mechanical properties and fracture modes of SLM Ti-6Al-4V. Materials Science and Engineering A **616** (2014) 1–11

[25] Vrancken, B., Thijs, L., Kruth, J.p., Humbeeck, J.V., Van Humbeeck, J.: Heat treatment of Ti6Al4V produced by Selective Laser Melting : Microstructure and Mechanical properties. Journal of Alloy and Compounds **541**(0) (2012) 177–185

[26] Dhansay, N.M., Tait, R., Becker, T.: Fatigue and Fracture Toughness of Ti-6Al-4V Titanium Alloy Manufactured by Selective Laser Melting. Advanced Materials Research **1019** (2014) 248–253

[27] Van Hooreweder, B., Moens, D., Boonen, R., Kruth, J.P., Sas, P.: Analysis of Fracture Toughness and Crack Propagation of Ti6Al4V Produced by Selective Laser Melting. Advanced Engineering Materials **14**(1-2) (2012) 92–97

[28] Tada, H., Paris, P.C., Irwin, G.R.: The Stress Analysis of Cracks Handbook. Third edn. (2000)

[29] Rafi, H.K., Starr, T.L., Stucker, B.E.: A comparison of the tensile, fatigue, and fracture behavior of Ti-6Al-4V and 15-5 PH stainless steel parts made by selective laser melting. International Journal of Advanced Manufacturing Technology **69**(5-8) (2013) 1299–1309

[30] Laird, C., Smith, G.C.: Crack propagation in high stress fatigue. Philosophical Magazine **7**(March) (1962) 847–857

[31] Stephen W., S., Robert S., P.: Fatigue Crack Growth Characteristics of Thin Sheet Titanium Alloy Ti 6-2-2-2-2. (March) (2001)

[32] Zhu, X.K., Joyce, J.A.: Review of fracture toughness (G, K, J, CTOD, CTOA) testing and standardization. Engineering Fracture Mechanics **85** (2012) 1–46